ACCESS AND STABILITY ISSUES IN SPECTRUM COMMONS

JIANGBIN LU

NATIONAL UNIVERSITY OF SINGAPORE

2015

ACCESS AND STABILITY ISSUES IN SPECTRUM COMMONS

JIANGBIN LU

(*B.Eng. (Hons), Zhejiang University, China*)

A THESIS SUBMITTED

FOR THE DEGREE OF DOCTOR OF PHILOSOPHY

NUS GRADUATE SCHOOL FOR INTEGRATIVE SCIENCES
AND ENGINEERING
NATIONAL UNIVERSITY OF SINGAPORE

2015

Declaration

I hereby declare that this thesis is my original work and it has been written by me in its entirety. I have duly acknowledged all the sources of information which have been used in the thesis.

This thesis has also not been submitted for any degree in any university previously.

Jiangbin Lu

November 18, 2015

To my loving parents: Tengfei and Mianhua.

Acknowledgement

I would like to express my sincere gratitude to my supervisor, Prof. Lawrence Wong Wai-Choong, for his guidance, support, and many opportunities he has provided to me through the years. I am very grateful for his mentoring and sharing of experiences, which have opened doors for me, helped me grow both in technical skills and intuition. I have benefited from his insights and advice during our discussions, which have motivated many ideas in my research.

I would like to express my heartfelt appreciation to my co-supervisor, Dr. Chew Yong Huat, for his mentorship and encouragement throughout my PhD candidature. His breadth of knowledge, his motivational thoughts, and the continuous rigor and effort he puts into our work, have always inspired me to move forward. His kindness, patience and enthusiasm are essential to my progress.

I thank Prof. Lee Tong Heng and Prof. Tham Chen Khong for serving on my thesis advisory committee, and for their interest and invaluable suggestions on my research. Prof. Lee has also taught me a lively course on adaptive control.

I thank Prof. Chen Jiming, Prof. Dai Liankui, Prof. Wang Hui and Prof. Ye Wei from Zhejiang University, for their teaching, advice, and kindest help in my undergraduate studies. I thank my beloved teachers in my hometown Xiamen, whose patient teaching and selfless caring have helped me grow up.

I would like to express my deepest gratitude to my parents. It is their love, care, support and encouragement that raised me up from a poor village and offered me the opportunities to receive better education. I am also grateful to my elder brother and sister-in-law, who accompany our parents when I am away from home.

I thank the lab officers, Song Xianlin, Guo Jie and Ang Kian Sin for providing assistance in carrying out my research. I also thank the alumni Lu Yu, Wang Lei, Chen Penghe, Wang Ke and Yu Jinqiang for helpful discussions and advice.

I thank my host family Ip Pik-Ching and Hui Yew-Foong, and other friends in Singapore, for the happy times together.

Last but not least, I would like to thank Singapore, and NGS in particular, for providing me scholarship to pursue my PhD degree.

Contents

Summary

This thesis studies the shared access and stability issues in a spectrum commons among a group of spatially distributed transmit-receive (Tx-Rx) user pairs. These users with built-in intelligence are able to learn the local spectrum dynamics and other users' decisions, and then dynamically adapt their transmission parameters to exploit the spatial and temporal spectrum opportunities. As a result of their selfish nature, the built-in intelligence should jointly consider the stability issues concerning whether the whole network converges to an equilibrium solution during interactions, which also provides efficiency and fairness for the users. We study how to manage the spectrum access problem for such autonomous and spatially distributed Tx-Rx pairs with the objective to achieve efficient spectrum sharing with fairness and scalability.

Chapter 1 gives some background of the thesis, including dynamic spectrum access, multi-agent systems, Aloha-type and CSMA-type random access games, device-to-device communications, etc. The motivations and contributions of the thesis are also outlined.

In Chapter 2 we introduce the spatial Aloha model in single channel and multi-channel scenarios, and state the problems to be solved. Then we introduce the ideal CSMA network (ICN) model which is the basis for our study in Chapter 7.

As an initial attempt to address the shared access and stability issues in a spectrum commons, we first investigate slotted Aloha type of random access with spatial reuse in Chapter 3. We propose the generalized Aloha games and obtain the stability conditions for the unique Nash equilibrium (NE) in terms of medium access probability (MAP), as a result of the users' autonomous and selfish strategic interactions.

Based on the stability conditions, we develop a heuristic algorithm in Chapter 4 to approach the Pareto front in spatial Aloha networks. Each user repeatedly measures its current throughput and adjusts its target rate based on a set of pre-installed rules, so that a fair and close-to-Pareto-front operating point can be found. The algorithm is implemented in a fully ditributed manner, which requires no information exchange among the users.

The drawback of the heuristic algorithm is the transient fluctuations and long convergence time. To provide faster and more smooth convergence to a stable operating point, we apply the control theoretic approach to spatial Aloha networks

in Chapter 5. Based on a sufficient stability condition in Chapter 3, we define a local parameter R which indicates the cumulative radio intensity level within each user's one-hop communication range. The users first self-organize into several non-overlapping neighborhoods, each of which elects the user with the highest node degree as the local leader. By ensuring $R \leq 2$ at the local leaders, the stability of network can be guaranteed even when each user has only local information. We propose each local leader to use $R = 2$ as the constant reference signal to its built-in proportional and integral (PI) controller. The PI parameters are adaptively tuned to provide fast and smooth convergence, regardless of the network size or user densities. We validate through simulations that the proposed scheme achieves fair and close-to-Pareto-front throughputs.

After investigating the single-channel scenario, we then extend to multi-channel spatial Aloha networks in Chapter 6. We propose a multi-leader Stackelberg game to solve the joint MAP tuning and spatial channel selection problem. Compared to existing method of pre-allocating MAPs, the proposed game further improves the overall network throughput by iteratively tuning the MAPs toward max-min fair throughputs in each sub-network.

Finally, we leverage on the ICN model in the context of overlay D2D communications in Chapter 7, and investigate how the commons spectrum can be efficiently and fairly shared among the self-interested spatial CSMA users with heterogeneous rate requirements. A Stackelberg game is proposed in which the base station acts as the Stackelberg leader to regulate the individual payoff by modifying the service price, so that the total D2D throughput can be maximized.

In summary, this thesis provides theoretical guidance for managing the shared access to a spectrum commons, with insights into how the spatially distributed Tx-Rx pairs can share the commons spectrum with stability, efficiency, fairness and scalability. Some future directions are discussed in Chapter 8.

List of Tables

List of Figures

List of Symbols

Symbol	Meaning
$\mathbf{A}$	interference matrix
a_{ij}	element in the interference matrix, i.e., $a_{ij} = [\mathbf{A}]_{ij}$
N	number of users
$\mathcal{N}$	set of users: $\{1, 2, \cdots, N\}$
N_i	number of neighbors for user i, i.e., $N_i = \sum_j a_{ij}$
$\mathbb{R}^N$	N-dimensional real space
Γ	N-dimensional real subspace $\Gamma \subset \mathbb{R}^N$
q_i	medium access probability (MAP) of user i
$\underline{q}$	vector of MAPs for N users
θ_i	normalized throughput of user i
$\underline{\theta}$	vector of throughputs for N users
y_i	target rate of user i
$\underline{y}$	vector of target rates for N users
$\preceq$	component-wise less than or equal to
$\mathbf{J}$	Jacobian matrix
$\det(\mathbf{J})$	determinant of Jacobian matrix
Ψ	neighborhood region $\Psi \subset \mathbb{R}^N$ of the NE in generalized Aloha games
I	region of the initial iteration point $\underline{q}^{(0)}$ in generalized Aloha games
$\Lambda(\underline{q})$	Lyapunov function in generalized Aloha games
Ω	set of elected leaders in the SALE scheme
R_l	Radio Intensity Metric (RIM) of user l
$R_{l,sp}$	set-point or the desired RIM value of user l
H_l	height of a tree l in the interference graph
$\{K_{P,l}, K_{I,l}\}$	proportional and integral parameters for the PI controller in user l
d_{Pareto}	distance of the current throughput to the Pareto front
L_S	number of bits in a packet of slotted Aloha

L_F	number of time slots in a frame in the SALE scheme
L_{ND}	number of time slots to estimate node degree in the SALE scheme
G	number of mutually disconnected subnets
$\mathcal{G}$	set of mutually disconnected subnets: $\{1, 2, \cdots, G\}$
$\mathcal{M}_g$	set of users in the subnet $g \in \mathcal{G}$
l_g	ID of elected leader in subnet $g \in \mathcal{G}$
K	number of available orthogonal channels
$\mathcal{K}$	set of available channels, i.e., $\mathcal{K} = \{1, 2, \cdots, K\}$
c_i	$c_i \in \mathcal{K}$ is the channel selected by user i
t_{cd}	countdown (backoff) time
t_{tr}	transmission time
λ	rate of transition from backoff to transmission: $\lambda = 1/E[t_{cd}]$
μ	rate of transition from transmission to backoff: $\mu = 1/E[t_{tr}]$
ρ	access intensity, i.e., ratio of mean transmission time to mean countdown time: $\rho = E[t_{tr}]/E[t_{cd}] = \lambda/\mu$
$\underline{\rho}$	access intensity of N links: $\underline{\rho} = [\rho_1, \rho_2, \cdots, \rho_N]$
r	transmission aggressiveness: the natural logarithm of ρ, i.e., $r = \log_e \rho$
r_{max}	upper limit on transmission aggressiveness
$\underline{r}$	transmission aggressiveness of N links: $\underline{r} = [r_1, r_2, \cdots, r_N] = \log_e \underline{\rho}$
s_i	state of link i: $s_i = 1$ if link i is transmitting and $s_i = 0$ otherwise
$\underline{s}$	system state of N links: $\underline{s} = [s_1, s_2, \cdots, s_N]$ or simply a string $\underline{s} = s_1 s_2 \cdots s_N$
$\mathcal{S}$	set of feasible system states
$p_{\underline{s}}$	probability of the system state $\underline{s} \in \mathcal{S}$
$\bar{\mathcal{C}}$	feasible throughput region in the ICN model
$\mathcal{C}$	strictly feasible throughput region in the ICN model
M	network price per service rate

List of Abbreviations

Abbreviation	Meaning
AI	access intensity
BS	base station
CDMA	code division multiple access
CR	cognitive radio
CSMA	carrier sense multiple access
D2D	device-to-device
DCF	distributed coordination function
DOS	Distributed Opportunistic Scheduling
eNB	evolved node B
FDMA	frequency division multiple access
FIP	finite improvement property
ICN	ideal CSMA network
ID	identity number
ISM	industrial, scientific and medical
LFP	least fixed point
MAC	medium access control
MANET	Mobile Ad-hoc NETworks
MAP	medium access probability
MDP	Markov decision process
MINLP	mixed integer nonlinear programming
MLSG	Multi-Leader Stackelberg Game
MPE	Markov perfect equilibrium
MPR	multi-packet reception
NE	Nash equilibrium
NP-hard	Non-deterministic Polynomial-time hard
ORM	Oscillation Resolving Mechanism

P2P	peer-to-peer
PHY	physical
PI	proportional and integral
PLAN	Physical confLict grAph geNerator
RF	radio frequency
RIM	Radio Intensity Metric
RoA	Region of Attraction
RTS/CTS	request-to-send / clear-to-send
SALE	Spatial Aloha via local Leader Election
SINR	signal to interference and noise ratio
TA	transmission aggressiveness
TCP	Transmission Control Protocol
TDMA	time division multiple access
Tx-Rx	transmit-receive
UWB	ultra-wide band
WLAN	wireless local area network

Chapter 1

Introduction

1.1 Dynamic Spectrum Access

The increasing demand for wireless communication, along with the poor utilization efficiency in the conventional static spectrum allocation scheme, has triggered the development of dynamic spectrum access schemes [1]. One of the critical enabling technologies for a dynamic spectrum access network is *cognitive radios* (CRs). By properly designing the built-in intelligence, CRs will discipline themselves and be able to make dynamic adaptations when accessing the spectrum to improve overall system performance.

1.1.1 Cognitive Radios

According to Simon Haykin's definition [3], a CR is an intelligent wireless communication device which is capable in using the understanding-by-building methodology to learn from its surrounding radio environment and adapt its internal system states according to the learned statistical behaviors observed in the incoming radio frequency (RF) stimuli. In other words, by sensing the RF stimuli or monitoring the transmission outcomes, a newly arrived CR can learn from its surrounding environment and gather necessary information such as transmission frequency, bandwidth, interference level, etc. After a CR gathers its needed information from the radio environment, it can dynamically adapt its transmission parameters to exploit the spatial and temporal spectrum opportunities, hopefully without significant degradation to the performance of existing users. The design of CRs bears two primary objectives: 1) highly reliable communications whenever and wherever needed; 2) efficient utilization of the radio spectrum.

This thesis focuses on the spectrum sharing problems among a group of spatially

distributed transmit-receive (Tx-Rx) user pairs. We use the concept of CRs in the broadest sense and refer them as intelligent wireless communication users, which are able to learn from RF environment and other users' behaviors before adapting their transmission parameters to achieve a certain performance objective. If such intelligent users participate in sharing a common spectrum for transmission, they should be able to make intelligent decisions on spectrum access and choose transmission parameters based on learned spectrum dynamics and their competitors' decisions. As a result of their autonomous behaviors and interactions, stability issues arise concerning whether the whole network converges to an equilibrium solution which also provides efficiency and fairness for the users. We therefore study how to manage the spectrum access problem for such autonomous and spatially distributed Tx-Rx pairs with the objective to achieve efficient spectrum sharing with fairness and scalability.

1.1.2 Dynamic Spectrum Access Models

As opposed to the current static spectrum management policy, the term *dynamic spectrum access* has broad connotations that encompass various approaches to spectrum reforms that try to improve spectrum utilization [1]. As shown in Fig. 1.1, dynamic spectrum access strategies can be broadly categorized under three models: dynamic exclusive use model, hierarchical access model, and open sharing model [1].

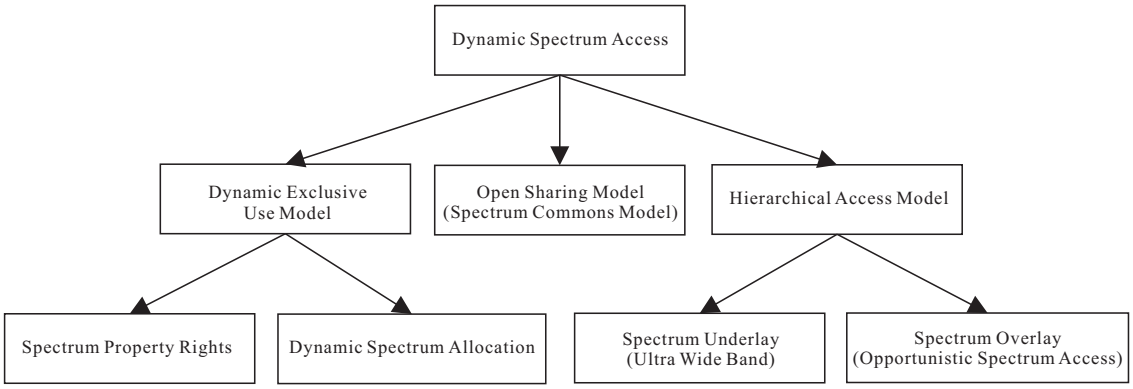

Figure 1.1: A Taxonomy of Dynamic Spectrum Access [1]

In the dynamic exclusive use model, spectrum bands are licensed to services for exclusive use, which maintains the basic structure of the current spectrum management policy. What is different is the additional flexibility in dynamically allocating spectrum to improve spectrum efficiency. Specifically, spectrum property rights [4] and dynamic spectrum allocation [5] are proposed under this model. Spectrum

property rights allow the license holders to trade spectrum and freely adopt technologies to provide services. The spectrum resource utilization is thus regulated by economy and market and driven toward the most profitable use. In the other approach known as dynamic spectrum allocation, improvement of spectrum efficiency is achieved through dynamically assigning the spectrum according to the spatial and temporal traffic statistics of different services [1].

The hierarchical access model consists of both primary users (licensees) and secondary users (unlicensed users), with the secondary users having a lower access priority. In this model, the licensed spectrum is opened to the secondary users with restrictions on the interference caused to the primary users. Spectrum underlay and spectrum overlay are considered for spectrum sharing between primary users and secondary users [6]. Spectrum underlay restricts the transmission power of secondary users such that they operate below the noise floor of primary users [7]. Transmission with extremely low power is possible for the secondary users by spreading the transmitted signal over a wide frequency band (UWB) [8]. On the other hand, spectrum overlay, also known as opportunistic spectrum access, does not restrict the transmission power of the secondary users, but rather restricting when and where they may transmit [1]. This approach exploits the spatial and temporal spectrum opportunities by enabling the secondary users to identify and access the spectrum white space in an opportunistic manner. Therefore, there exists a trade-off between the services provided to the secondary users and the protection provided to the primary users from secondary interference.

The open sharing model will be discussed in the next subsection.

1.1.3 Spectrum Commons

The open sharing model, also known as *spectrum commons* [9–13], treats the spectrum as an open resource for peer users to share among themselves. An example of this model is the unlicensed industrial, scientific and medical (ISM) radio band, which brings up the success of wireless operating systems such as WiFi, Bluetooth, RFID, ZigBee, etc [14]. However, open sharing without regulations may lead to the overuse of the time, frequency and power units, and eventually the users would suffer from a "tragedy of the commons" [15] due to increasing interference.

Actually, there are distinctions between the ideas of "open access" and "commons", although they are often used interchangeably. A commons is a resource that is owned or controlled jointly by a group of individuals [16]. It is characterized

by the restrictions on who uses the resource, and when and how. The owner or controller of the commons is the person or group of persons that establishes and enforces these restrictions. On the other hand, open access is a regime in which anyone has access to an unowned resource without limitations; no one controls access to the resource under open access [16]. Therefore, open access is subject to over-exploitation and degradation of a finite resource if the users have no incentive to preserve. Based on the above discussion, the tragedy does not befall commons generally but rather "unmanaged commons" [17].

To improve the efficiency of the spectrum usage, [13] suggests basic protocols/etiquettes to be set by either government or industry standardization, and the commons spectrum should only be shared among those wireless users which conform to these protocols/etiquettes. The design of such protocols/etiquettes should follow three general principles: efficiency, fairness, and incentive compatibility [18]. A resource allocation is *efficient* if it is impossible to improve the performance of a user without degrading the performance of some other users (also known as *Pareto optimality* [19]). Usually many efficient operating points exist, each representing a different performance trade-off among the users. *Fairness* is related to the relative performance among the users, based on different criteria such as max-min fairness, proportional fairness, etc [20, 21]. Finally, an allocation is *incentive compatible* or *self-enforcing* if no user has incentive to deviate from such an operating point, which means that no intervention from an external authority is needed [18]. This is particularly important for new technologies such as CRs, which equip users with cognitive capability and self-adaptivity to make autonomous decisions about spectrum usage based on learned environment characteristics and interactions among the users. Both centralized [22, 23] and decentralized [18, 24–27] spectrum sharing approaches have been proposed under the spectrum commons model.

1.2 Multi-Agent Systems

The key component of dynamic spectrum access is how to provide efficient and fair spectrum allocation or scheduling solutions for the users [28]. For autonomous Tx-Rx pairs which are participating in sharing a commons spectrum for transmission, they should be able to make intelligent decisions on spectrum usage and choose transmission parameters based on learned spectrum dynamics and their competitors' decisions. We therefore study how to manage the spectrum access problem for such autonomous and spatially distributed Tx-Rx pairs with the objective to

achieve efficient spectrum sharing with fairness and scalability.

A network consisting of autonomous and spatially distributed Tx-Rx user pairs is essentially a multi-agent system [29]. The users are said to be autonomous if they are capable of making independent decisions about what to do in order to satisfy their design objectives. In reality, the spatially distributed users only possess local views, i.e., no user has a full global view of the network, or the network is too large for a user to gather all information and make practical use of such knowledge. How each individual can make a decision on the transmission parameters with partial network knowledge so as to approach the design objective, and how much partial knowledge is required are the two main design challenges.

A multi-agent system may target at a global objective but solve it distributively [30]. In such settings there is no concern about the individual preferences, but rather it may be advantageous to distribute the task among multiple users, whose actions may require coordination. Examples of such problems can be found in [20, 21, 31]. The effective mathematical tool in use is the distributed optimization techniques [30, 32].

On the other hand, a multi-agent system may also embrace issues of competition as well as coordination. The key mathematical tool to model the problems is game theory, which models strategic interactions among the users using formalized incentive structures. Game theory provides models for efficient self-enforcing distributed design. The formulated game model should also be able to derive well defined equilibrium criteria to study the optimality of game outcomes under various game settings (static versus dynamic, complete versus incomplete information, non-cooperative versus cooperative, etc) [28]. More details will be reviewed in the next subsection.

1.2.1 Game Theory

Game theory is often described as a branch of applied mathematics and economics that studies situations where multiple players (self-interested agents) interact and make decisions in an attempt to maximize their own benefits. The essential feature is that game theory provides a formal mathematical approach to modeling these social situations in which all agents participate and interact. A game consists of a set of players, a set of moves (or strategies) available to those players and a complete set of payoffs for every combination of strategies available. All possible outcomes are thus encapsulated in the mathematical model of the game.

To enable efficient dynamic spectrum sharing, the behaviors and interactions among network users have to be thoroughly investigated and analyzed. Game theory has been used to study the competition and cooperation among rational decision makers, and thus has excellent match when applied to dynamic spectrum sharing problems [28].

The advantages of using game theoretical framework to analyze dynamic spectum sharing are multifold [28]. First of all, by modelling dynamic spectrum sharing as games, the strategic interactions among network users can be expressed in a formal game structure, by which the theoretical results from game theory can be fully utilized. Moreover, since the optimization for heterogeneous network users is a distributed multi-objective optimization problem with each individual user having its own objective and constraints, the problem is difficult to analyze and solve. Game theory equips us with well defined equilibrium solutions to evaluate the system optimality under various network scenarios. Finally, non-cooperative games [33] can be used to analyze the selfish behaviors of network users, which inspires us to look for ways to design incentive compatible or self-enforcing protocols to achieve efficient and fair spectrum sharing.

1.2.2 Nash Equilibrium

An important solution concept to non-cooperative games is the *Nash equilibrium* (NE) [34]. A NE, named after John Nash, is a set of strategies, one for each player, such that no player has an incentive to change its action unilaterally. If each player has chosen a strategy and no player can benefit by changing its strategy while the other players keep theirs unchanged, then the current set of strategies and payoffs constitute a NE.

Formally, we can define $s_{-i} = (s_1, \cdots, s_{i-1}, s_{i+1}, \cdots, s_N)$ as a strategy profile of N players without player i (also known as the opponent of i). Thus we can write $\underline{s} = (s_i, s_{-i})$ as the strategy profile of all N players. If the players other than i (whom we denote as -i) were to commit to play s_{-i}, a player who is intent on maximizing its own payoff u_i would be faced with the problem of determining its best strategy from its strategy set $\mathcal{S}_i$ in response to s_{-i}, or best response. Therefore we have the following definitions.

Definition 1.1. ***(Best response)*** *Player i's best response to other players' strategy s_{-i} is a strategy $s_i^* \in \mathcal{S}_i$ such that $u_i(s_i^*, s_{-i}) \geq u_i(s_i, s_{-i})$ for all strategies $s_i \in \mathcal{S}_i$.*

Definition 1.2. ***(Nash equilibrium)*** *A strategy profile* $\underline{s} = (s_1, \cdots, s_N)$ *is a Nash equilibrium if, for all players* i, s_i *is a best response to* s_{-i}.

In the above definitions, a NE is defined as a strategy profile (i.e., vector of players' strategies) in which each player's strategy is the best response to the strategies of all the other players. Based on this definition, no selfish player has incentive to unilaterally change its strategy when operating at the NE. However, this solution concept for a non-cooperative game is essentially confined to searching for an equilibrium condition. It does not teach us about the underlying dynamics involved in establishing that equilibrium, or whether such dynamics are converging or diverging at the equilibrium due to disturbances (e.g., introduced by parameter estimation errors) [3]. The following subsection will review existing work on the dynamic stability of the NEs in non-cooperative spectrum access games.

1.2.3 Stability Issues

Existing game models in communication networks have adopted various game dynamics and stability concepts such as Markov decision process (MDP) and stochastic stability [35,36], which appear in a Markov game or stochastic game introduced by Shapley in [37]. A stochastic game is played in a sequence of stages. At the beginning of each stage, the game is in a certain state which follows a Markov process, i.e., in the next stage the game would move to a new random state whose distribution depends on the previous state and the actions chosen by the players. The procedure is repeated at the new state and play continues for a finite or infinite number of stages. The payoffs obtained in each stage depend on the state and the current actions of the players. The total payoff of a player is often taken to be the discounted sum of the stage payoffs or the limit inferior of the averages of the stage payoffs [35]. The corresponding equilibrium concept is the Markov perfect equilibrium (MPE) in which each player's chosen action depends only on the current state [33].

For example, in [38] [39], MacKenzie and Wicker consider the slotted Aloha protocol as a stochastic game between users contending for a conventional collision channel where no two or more users are allowed to transmit simultaneously. In their work, an infinite users' model is adopted with a finite packet arrival rate, and all users are assumed to be indistinguishable. In this game, the state represents the number of users currently contending for the channel, and this information is assumed to be known to all users. A strategy in this game is a mapping from

the number of backlogged users to a medium access probability (MAP). The total payoff of a user is the discounted sum of the stage payoffs. The authors then prove the existence of an MPE in such a game using the Glicksberg-Fan fixed point theorem [40, 41]. The stability of the equilibrium is analyzed based on the drift analysis of a Markov chain and the selfish behavior of users when the number of backlogged users goes to infinity. The authors conclude that, the equilibrium strategy is stable given that the total packet arrival rate of the Aloha system is less than a certain value determined by the cost parameter. Moreover, for the optimal value of the cost parameter, the throughput of a slotted-Aloha system with non-cooperative users can be as high as the throughput of a centrally controlled system. This result is generalized in [42] to show that the same result holds for multi-packet reception channels that allow more than one packet to be successfully received simultaneously.

Besides MDP and its stochastic stability, some other game models in communication networks have formulated the game as a nonlinear system and studied its asymptotic stability using Lyapunov functions [43,44]. The authors in [45] formulate a random access game consisting of N wireless nodes in a wireless local area network (WLAN) [14] with contention-based medium access. Three types of repeated play have been considered for the distributed strategy update mechanism to achieve the NE, namely, best response, gradient play, and Jacobi play. The simplest update mechanism is the best response strategy: at each iteration, every player chooses the best response to the actions of other players in the previous iteration. The authors restrict the discussion to supermodular games [46] with the problem-specific payoff function and prove its convergence. Another dynamic is the gradient play [47], i.e., each player adjusts its strategy gradually in a gradient direction that improves its current payoff. In gradient play, nobody must know the game, his rivals, their preferences or actions; no one looks for large size improvements, i.e., nobody makes a great leap towards a best response. Each player simply observes its marginal payoff persistently and use restricted stepsize to update its strategy. Despite that players know little and update slowly, the gradient play does enjoy remarkable stability (see [47] for more details). The third update scheme is Jacobi play [48]. In Jacobi play, each player adjusts its current strategy gradually towards the best response strategy, i.e., the player does not make a great leap towards a best response within one single iteration, but instead applies a discount factor $\epsilon \leq 1$ to the stepsize. Another example that uses the Jacobi play is the Aloha game model proposed by Jin and Kesidis [49]. The dynamics of the Jacobi play is approximated by a continuous-

time nonlinear system whose asymptotic stability at the equilibrium is studied by constructing a Lyapunov function [43, 44].

The next two sections review some types of random access games which are based on the Lyapunov stability concept.

1.3 Aloha-Type Random Access Games

Game theoretic approaches have been widely used to design multiple access protocols in wireless networks. In [50], the authors provide a comprehensive review of the game models developed for different multiple access schemes, including both contention-free and random access schemes. For contention-free schemes, time-division multiple access (TDMA) [51–53], frequency-division multiple access (FDMA) [54–56], and code-division multiple access (CDMA) [57–59] are reviewed. For contention-based channel access, Aloha and carrier sense multiple access (CSMA)-based game models are discussed.

This thesis focuses on random access based game models in wireless networks. In the following subsections, we would review certain classes of Aloha games and channel selection games in Aloha-type of random access networks. CSMA-type random access games will be reviewed in Section 1.4.

1.3.1 Aloha Games

In [50], several channel access games in ALOHA-like protocols are presented. A good example is the Aloha games proposed by MacKenzie and Wicker in [38, 39]. An alternative Aloha game model is proposed by Jin and Kesidis [49], whereby a group of heterogeneous users in a fully connected network share a conventional collision channel and transmit via slotted Aloha. Each user in this game attempts to obtain a target rate by updating its MAP in response to observed activities. The authors further assume in [60] that, for users with inelastic bandwidth requirements, each user's target rate depends on its utility function and its willingness to pay, and they propose a pricing strategy to control the behavior of the users (in order to bring their target rates within the feasible region). This Aloha game model is further investigated in [61–63]. In [61], the authors investigate the effects of altruistic behavior on the stability of equilibrium points in a two-player game. In [62], the authors generalize the model and propose a generic networking game with applications to circuit-switched networks. In [63], Menache and Shimkin extend the

model by incorporating time-varying channel conditions to the channel model.

The conditions for the existence and stability of the equilibrium solutions have been well studied in these works. However, the results of these studies are more suitably applied to the fully connected uplink random access channel. In the context of spatially distributed Tx-Rx pairs, it is likely that not all players will interfere with each other. In these scenarios, we normally have to deal with a non-fully connected network, where the presence of a connected edge means that the two players are not allowed to transmit together. There also remain fundamental issues for such partially connected networks which are not addressed. For example, among all equilibrium solutions, does there exist an equilibrium point which is optimal to all players, or a solution which always favors different subgroups of players? Furthermore, if a global optimal solution does exist for all players, how to converge to that equilibrium point during implementation?

An important concept associated with partially connected networks is spatial reuse. Spatial reuse, also known as frequency reuse, is a powerful technique to improve the area spectral efficiency of multi-user communication systems. Cellular systems are examples whereby radios exploit the power falloff with distance and reuse the same frequency for transmission at spatially separated locations [64, 65]. Similar ideas can be applied to users in a distributed wireless network, where different transmit-receive pairs at a distance away are allowed to transmit simultaneously, with the objective to maximize system capacity whilst still meeting all the transmission quality requirements [66–69]. When spatial reuse is considered in a distributed wireless network where the autonomous Tx-Rx user pairs compete for transmission in the common collision channel using slotted Aloha, how to model the interactions and competitions among the users? Does there exist a stable equilibrium operating point? What about the efficiency and fairness of such an equilibrium, if they exist? How to approach the Pareto-front throughput solution using only limited local information?

The above challenges motivate our design of Aloha games with spatial reuse in Chapter 3, as well as a heuristic algorithm (Chapter 4) and a control theoretic method (Chapter 5) to approach the Pareto optimal throughput solution in the proposed games.

1.3.2 Channel Selection Games in Multi-Channel Aloha Networks with Spatial Reuse

To further improve network performance, multiple collision channels can be considered in Aloha networks with spatial reuse. Chen and Huang in [70] study the random access based distributed spectrum sharing problem with spatial reuse. Each user is allowed to access only one channel in each slot, under the assumption that the MAPs are fixed and pre-allocated. The problem is formulated as a spatial channel selection game, in which each user is a player who chooses one channel to access in order to maximize its own expected throughput. The game is shown to be a potential game [71] and thus possesses a NE and the finite improvement property (FIP). A game is said to be a potential game if the incentive of all players to change their strategy can be expressed using a single global function called the potential function, which is a special form of the Lyapunov function [72]. The FIP refers to the property that asynchronous player updating (where players switch channels to increase payoffs) always converges to a NE.

However, the method in [70] relies on the assumption that the MAPs are fixed and pre-allocated, but the efficiency and fairness of such allocations are not discussed. A better design is to let the users jointly optimize the MAPs and channel selection to maximize individual user throughput. This is a highly non-trivial problem since the setting of the MAPs would affect each user's expected throughput, intertwine with the channel selection decisions and thus affect the final location of the NE.

This challenging problem has been partially solved by Cohen *et al.* in [73], although no spatial reuse has been considered. The sub-game of channel selection under fixed MAP constraints is also shown to be a potential game, and thus the convergence to a NE is guaranteed. The authors then formulate the problem of choosing the MAPs as a single-leader Stackelberg game [33]. The classic Stackelberg games are a class of non-cooperative games in which a single "leader", who makes the first move in the game, anticipates the actions of the "follower" based on a model of how the follower would respond to the actions of the leader. Since no spatial reuse is considered, the users are homogeneous in the sense that each user's transmission will affect all remaining users in the network. Therefore, a single elected leader is sufficient to manage the network, which mandates all MAPs to be the same and sets this common MAP value to maximize the sum-rate at the NE of the sub-game.

When spatial reuse is considered, heterogeneous MAPs are generally observed

due to the *non-uniform* node degrees. Therefore, multiple leaders at different spatial locations might be a proper extension to better manage the network and handle the joint MAP tuning and channel selection problem in a local region. This motivates our design of a multi-leader Stackelberg game [74] in Chapter 6, which jointly considers the MAP tuning and channel selection problem in multi-channel Aloha networks with spatial reuse.

1.4 CSMA-Type Random Access Games

1.4.1 CSMA Games

In random access games, wireless users share a common channel and want to maximize their payoffs independently. A recent survey on applying game theory to CSMA can be found in [75], where several non-cooperative contention control games in CSMA methods are presented. Using game theory and the NE concept, it is shown in [76] that the current IEEE 802.11 standard does not work well if there are selfish users trying to maximize their performance by unfairly accessing the channel, as this reduces the ability of other users to access it. Besides fairness, the stability of strategic interactions among the self-interested users is also an important issue. The authors in [77, 78] model the exponential backoff protocol in 802.11 standards as a non-cooperative game in which links try to maximize their payoff function in the form of reward for successful transmission. After proving the existence of the NE, it has been shown that the obtained NE may not be unique and steady. Therefore, it becomes a motivation for designing medium access mechanisms so that the strategic interactions among the self-interested users would finally converge to a stable steady-state operating point.

The game presented in [79] is one of the first research works proposing a fair non-cooperative game model for 802.11 distributed coordination function (DCF) [80] mechanism. Authors of [45, 81–83] define a general game-theoretic model to capture the distributed nature of contention control and wireless users' interactions in CSMA. In these games, the strategy of a player is usually the MAP or equivalently the size of the contention window, and the payoff function is a combination of the channel access gain and the packet collision cost. The wireless users estimate their collision probabilities through observing idle time slots between transmissions as well as unsuccessful transmissions, and then accordingly adjust their MAPs. The utility functions of the users are designed to achieve a good trade-off between

efficiency and fairness. Gradient play is adopted as the game dynamics whose convergence to the steady-state NE is proved by constructing a proper Lyapunov function. In another CSMA game model, Jin and Kesidis [84] analyze the non-cooperative user behaviors in CSMA wireless networks where users have the freedom to choose the contention window sizes according to the network congestion level. The existence and uniqueness of the equilibrium point are investigated, as well as a distributed iterative method to converge to the equilibrium.

However, as commented by [75], most of the proposed CSMA games assume all-inclusive carrier sensing, i.e., each user hears transmissions of all the other users. The analysis in the above game models cannot be directly applied in the presence of spatial reuse.

1.4.2 Spatial CSMA Networks

When spatial reuse is considered in CSMA methods, the carrier-sense relationships among the CSMA users become *non-all-inclusive*, i.e., each CSMA user may only sense a subset, but not all other users. In [85], Bianchi proposes a simple model that accounts for all exponential backoff protocol details and allows computation of saturation throughput of IEEE 802.11 DCF [80]. Although simulations in [85] demonstrate high accuracy, the model does not consider the network topology and could not characterize the collisions that result from the other active nodes in the neighborhood of the transmitter. As commented by Liew *et al.* [86], it is extremely difficult to extend the analytic methods for all-inclusive carrier-sense networks (e.g., [85, 87–89]) to the non-all-inclusive case because of the inhomogeneity in the state spaces of the CSMA users. In fact, the problem of computing user throughputs in a spatial CSMA network is shown to be NP-hard [86].

In order to perform tractable analysis, existing literature [86,90–92] have adopted an *ideal CSMA network (ICN)* model to capture the essence of the CSMA mechanism under spatial reuse. Boorstyn *et al.* in [90] first consider the spatial CSMA network model with exponential idle and transmission times. They use a Markov model to efficiently analyze the throughput of CSMA networks with arbitrary topology. Wang and Kar in [91] model the throughput of the CSMA network using the same line of analysis, but they further take into account the RTS/CTS exchange in the CSMA network and their result is readily extended to the throughput analysis of the IEEE 802.11 DCF. The effectiveness of the throughput analysis is verified by simulation investigations.

The throughput analysis in [90, 91] corresponds to a subclass of the ICN model, which models the backoff and transmission processes with exponential distributions so that backoff and transmission processes are memory-less and can be analyzed using a continuous time-reversible Markov chain. In practical CSMA protocols, the backoff process is controlled by a counter and has "memory". The general ICN model in [86] takes this memory effect into account. It is proved that the link throughputs in ICN are insensitive to this memory effect and to the detailed distributions of the backoff countdown and transmission times given the ratio of their means. This result enables the use of ICN in practical CSMA networks.

Backoff collisions are unavoidable in practical networks, especially when the network is highly populated. The ICN model is an idealized model that removes such collisions by adopting a continuous-time countdown process [93]. In other words, it models a system in which the "minislot" used in the countdown backoff process is very small, and that carrier sensing is instantaneous. In [94], Kai and Liew propose a generalized ICN model for a perturbation analysis that tries to capture the effects of backoff collisions. However, as is pointed out in [94, Section V], the effects of collisions are not significant as far as the link throughputs are concerned. More specifically, the original ICN model already yields good approximations with errors within 10% even though it does not incorporate the collision effects. Jiang and Walrand in [95] extend the ICN model to an "almost" time-reversible Markov chain which takes into account the cost of collisions and overheads. The idea is to use RTS/CTS handshaking so that the collision period will be comparatively small under a sufficiently large holding time.

In summary, ICN is a proper mathematical model for the throughput analysis in spatial CSMA networks. The ICN model will be formally introduced in Section 2.4.

1.4.3 Managing Spatial CSMA Users with Heterogeneous Rate Requirements

Based on the ICN model, people are interested in the resource allocation problem in spatial CSMA networks for efficient spectrum sharing. In particular, Jiang and Walrand [92] develop an elegant distributed CSMA algorithm for throughput and total utility maximization based on the ICN model after making assumptions about concavity and monotonicity of the user utility functions. Their work removes the need for knowledge of the underlying link topology and their transmission param-

eters can be updated distributively. However, the approach implicitly assumes a best effort transmission to achieve total utility maximization and there is no explicit treatment if users have heterogeneous rate requirements and different willingness to pay. In other words, while optimizing the sum-rate, there is no mechanism to weigh the individual user utility so as to differentiate the services. Moreover, the global optimization approach does not reflect the fact that users are selfish and behave non-altruistically in maximizing their own payoff. In fact, Cagalj *et al.* have shown that even the presence of a few selfish users may lead such a CSMA network to collapse [96], while proper pricing or penalty mechanisms lead to overall improvement [97]. Indeed, when users with heterogeneous rate requirements coexist in the network and the collective target rates are outside the feasible throughput region, the self-interested actions by the CSMA users would lead the network into heavily congested status.

In Chapter 7 we incorporate a game theoretic framework into the ICN model to harness the selfish behaviors of a group of non-cooperative spatially distributed CSMA users with heterogeneous rate requirements.

1.5 Device-to-Device Communication

A prospective application background of the spatial CSMA network is overlay Device-to-Device (D2D) communication. In this section we give a brief introduction on D2D communication, and discussed the settings used in our work in Chapter 7.

The growing popularity of smartphones and tablets has resulted in the increasing demand for high data rate services, and a huge amount of data traffic normally needs to be transmitted through cellular networks, which in turn leads to severe traffic overload problems. Recently, D2D communication has emerged as a new data-offloading solution by enabling direct communication between two mobile users without traversing the base station (BS) or core network [98].

D2D communication can be implemented over the cellular spectrum (i.e. inband) or the unlicensed spectrum (i.e. outband). Inband D2D can be further classified into spectrum overlay and spectrum underlay. In the overlay scenario, the cellular and D2D transmitters use orthogonal time/frequency resources or alternate channels, while in the underlay scenario the D2D transmitters opportunistically access the time/frequency resources occupied by cellular users. The rate performance is evaluated in [99] for both overlay and underlay scenarios. It is observed that D2D mobiles in both scenarios can enjoy much higher data rate than regular cellular mo-

biles. As for cellular mobiles in the overlay scenario, their rate performance also improves due to the offloading capability of D2D communication. Besides performance improvement over the pure cellular mode, inband overlay D2D is also more tractable in analysis since it does not interfere with regular cellular mobiles or suffer from random interference from unlicensed band.

In the licensed spectrum, a potential D2D pair can communicate through conventional cellular mode (relay through the BS), dedicated D2D mode (spectrum overlay), or underlay sharing mode (share with cellular users). Game theoretic approaches have been applied in D2D communications for mode selection and resource management [100]. In particular, Cai *et al.* [101] model the spectrum sharing mode selection as a coalition formation game, and propose a distributed coalition formation algorithm to improve the total achievable rate. Wu *et al.* [102] study the underlay spectrum sharing problem among potential D2D pairs and cellular users with quality-of-service requirements. A coalition formation game and a distributed coalition formation algorithm are proposed to decide for the most energy-efficient spectrum sharing strategy. The focus of these works is to look for efficient spectrum sharing solutions among the D2D pairs and cellular users, and spectrum underlay is adopted in the sharing mode under the constraints on the amount of mutual interference. Our work focuses on spectrum overlay mode, in which the number of orthogonal channels is limited and there are multiple D2D pairs sharing a common channel via distributed transmission scheduling.

In [99] the authors use a simple spatial Aloha access scheme to support D2D scheduling. In Chapter 7 we assume that all D2D links use CSMA as the multiple access scheme to share a dedicated inband overlay channel. Spatial reuse is considered, i.e., different transmit-receive (Tx-Rx) pairs at a sufficient distance away that do not cause interference are allowed to transmit simultaneously [86], with the objective to achieve higher throughput while still meeting all the transmission quality requirements for the channel access of the individual link. Although D2D communication does not route the data traffic through the cellular network, the available network infrastructure can still be an effective means to exert light control over all the D2D links when performing resource allocation. In our model in Chapter 7, the D2D links have heterogeneous service requirements and different willingness to pay, and the central entity (e.g., evolved node B (eNB)) [98] controls the transmission behaviors of all links by modifying the price per unit service rate.

A simple example is given in Fig. 1.2, where there are three D2D links and a single BS oversees/controls them in the control plane. Each D2D link consists of

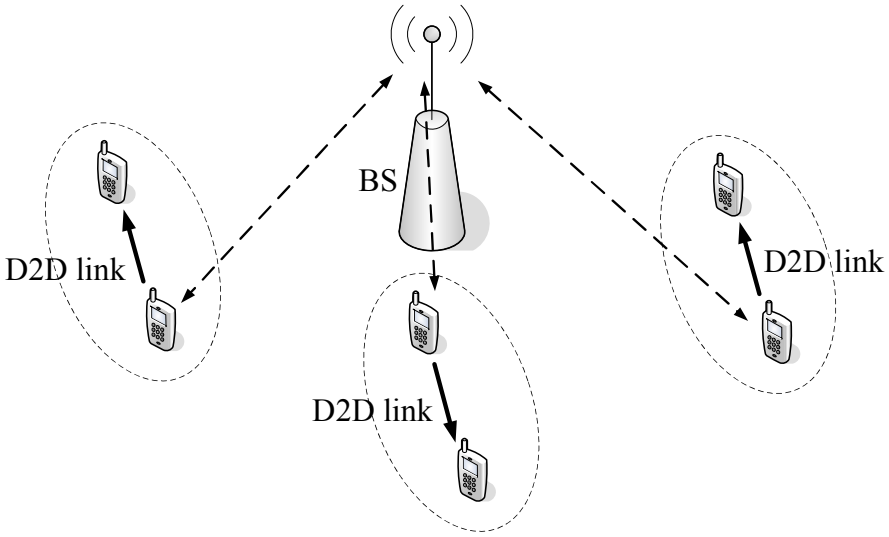

Figure 1.2: An Example of Overlay D2D Communications. The solid arrow represents the data communication of a D2D link; the dashed arrow represents the control information exchange between a D2D transmitter and the BS.

a Tx-Rx pair, and hence the D2D links resemble the situation where distributed pairs are transmitting. The involvement of the cellular network in the control plane is the key difference between our system model with that defined in Mobile Adhoc NETworks (MANET) [103]. Moreover, D2D communication is mainly used for single-hop communications [98], which does not inherit the multihop routing problem of MANET [104, 105].

1.6 Discussions on Interference Model

There are two popular interference models, namely, the physical model and the protocol model [106]. Under the physical model, a transmission is considered successful if and only if the signal to interference and noise ratio (SINR) exceeds a certain threshold, where the interference includes all other concurrent transmissions. Under the protocol model, a transmission is successful if and only if the receiving node is in the transmission range of the corresponding transmitting node and is out of the interference range of all other transmitting nodes.

The physical model is considered to be a better characterization of interference (but also more difficult to analyze) than the protocol model. The main difficulties are two folds. First, SINR is a non-convex function of transmitting powers; an optimization problem in the physical model is usually non-convex and NP-hard in general [107]. Second, the aggregated interference at a receiver may vary sig-

nificantly with respect to time according to the transmission behaviors of all its neighbors, which makes the analysis difficult.

To circumvent the complexity issue associated with the physical model for large-sized networks, the protocol model has been widely used by researchers in wireless networking community as a way to simplify the mathematical characterization of the physical layer. Under the protocol model, the impact of interference from a transmitting node is binary and is solely determined by whether or not a receiver falls within the interference range of this transmitting node. Due to such simplification, the protocol model can be easily applied to analyse large-sized wireless ad-hoc and sensor networks [108–111]. However, since the protocol model has not accounted for aggregated interference from multiple interfering nodes, the accuracy of characterizing interference is compromised.

For both the protocol model and the physical model, power control is an effective physical layer technique to control the network topology so as to increase spatial reuse through controlling the effect of interference. With the power control capability, we could adjust the transmission power and thus reduce the interference range of some transmission so as to achieve scheduling feasibility for other transmissions. However, the enlarged design space also introduces much more complexity in the mathematical modelling, problem formulation and solution procedure.

The authors in [112] [113] have developed a formal mathematical model for link scheduling feasibility under the influence of power control. This model extends existing protocol interference model for wireless networks where power control (and thus transmission range and interference range) is now part of the optimization space. Based on this model, the joint power control, scheduling and flow routing problem is formulated as a mixed integer nonlinear programming (MINLP) problem. They develop a centralized solution procedure based on the branch-and-bound technique. The authors in [107] further consider the joint power control, scheduling and flow routing problem based on the physical interference model. The problem is also formulated as a MINLP and branch-and-bound technique is used as a centralized solution procedure. However, since the formulated MINLP is NP-hard in general, it cannot be directly applied in practice, but rather as a performance benchmark for other algorithms developed for practical implementation.

The authors in [114] [115] further consider the problem about how to correctly use the protocol interference model for wireless networks and try to bridge the gap between protocol and physical models. The physical model is widely considered as a reference model for physical layer behaviour but its application is limited by

its complexity. On the other hand, the protocol model is simple but the accuracy is compromised. The authors in [114] [115] propose a new concept called "reality check" and present a method of using a protocol model with reality check for wireless networks. Subsequently, they show that by appropriate setting of the interference range in the protocol model, it is possible to narrow the solution gap between the two models. The simulation results confirm that this gap is indeed small (or even negligible). Therefore, their proposed method of joint reality check and interference range setting retains the protocol model as a viable approach to analyse wireless networks.

Similarly, in the domain of dynamic spectrum management, the authors in [116] show that if the conflict graphs are optimized properly, they can produce spectrum allocations that closely match those derived from the physical interference model. The authors further propose Physical confLict grAph geNerator (PLAN), a systematic framework to produce conflict graphs based on physical interference characteristics. PLAN first applies an analytical framework to derive the criterion for identifying conflicting neighbors, capturing the cumulative effect of interference. PLAN then applies a local conflict adjustment algorithm to address heterogeneous interference conditions and improve spectrum allocation efficiency.

In this thesis, the interference relationship is characterized by the interference matrix, which corresponds to the conflict graph in the protocol model. The techniques in [114] [115] [116] can be used to generate an appropriate conflict graph which caters for the aggregated physical interference to some extent and bridges the gap between protocol and physical models.

1.7 Motivations and Contributions

This thesis studies the spectrum sharing problems among a group of spatially distributed Tx-Rx user pairs in a spectrum commons. The users are able to make intelligent decisions on spectrum usage and choose transmission parameters based on learned spectrum dynamics and their competitors' decisions. As a result of their autonomous and intelligent behaviors and interactions, stability issues arise concerning whether the whole network would converge to an equilibrium solution which also provides efficiency and fairness for the users. We therefore study how to manage the spectrum access problem for such autonomous and spatially distributed users with the objective to achieve efficient spectrum sharing with fairness and scalability. As discussed in Section 1.1.3, basic spectrum sharing rules are needed in a

spectrum commons, which should follow three general principles: efficiency, fairness, and incentive compatibility.

To design incentive compatible spectrum sharing rules, non-cooperative games can be used to analyze the self-interested behaviors of the users (i.e., game players). An important solution concept to non-cooperative games is NE, which is incentive compatible for all players since no one has the incentive to deviate from such an equilibrium point. Stability issues arise when the users act non-altruistically in maximizing their own benefits. First of all, we need to know whether a NE exists for the game. Secondly, to search for the NE(s) of the game, we need to carefully design the underlying dynamics so that the game converges to the NE(s), i.e., the strategic interactions among the intelligent and self-interested users would converge to a steady-state equilibrium point. More desirably, the NE should be "stable" so that the game converges back to the NE after being perturbed by small disturbances (e.g., introduced by parameter estimation errors). Finally, we need to consider the efficiency and fairness of the NE. It is desirable to design the spectrum sharing rules so that the network operating point is incentive compatible, being on or close to the Pareto front, while providing a certain degree of fairness among the users.

1.7.1 Generalized Aloha Games

As a starting point, we first investigate the spectrum commons model with distributed Tx-Rx user pairs competing for transmission in a single random access channel. CSMA-type random access could be used, in which the users sense the channel first and then transmit in the absence of other traffic [14]. Alternatively, if there is no sensing before each transmission, Aloha-type random access could be used [14]. We first focus on the slotted-Aloha-type random access scheme of the distributed user pairs.

Aloha games study the MAPs of a group of non-cooperative users which share a channel to transmit via the slotted Aloha protocol. Chapter 3 extends the Aloha games to spatial reuse scenarios, and studies the system equilibrium and performance. Specifically, fixed point theory and order theory are used to prove the existence of a least fixed point as the unique NE of the game and the optimal choice of all players. The Krasovskii's method is used to construct a Lyapunov function and obtain the conditions to examine the stability of the NE. Simulations show that the theories derived are applicable to large-scale distributed systems of complicated network topologies. An empirical relationship between the network connectivity

and the achievable total throughput is finally obtained through simulations.

1.7.2 Heuristic Algorithm to Approach Pareto Front

In Chapter 4, we go beyond the generalized Aloha game, and study how future autonomous radios can make use of the developed theory to improve the overall system performance [117]. The most challenging issue is that, the Pareto-front [19] target rate is determined by the network as a whole, while in a distributed network each user usually has only limited local information and hence does not know how to achieve the Pareto-front throughput. As a result, if some or all the users are over-demanding, the resulting network can be unstable due to congestions. However, if the users set low target rates, the network is stable but the channel is not fully exploited. The challenge lies in how users can determine their equilibrium MAPs as a result of competing among themselves and yet still maintaining network stability.

In the generalized Aloha game, we derive the stability condition of the NE, which can be used to test whether a certain target rate is within the feasible throughput region. However, this testing condition requires complete knowledge on the network topology, which is neither practical nor scalable for an individual player to implement. Therefore, we need to design a self-adaptive algorithm for the players to self-adjust their target rates based on a set of pre-installed rules so that the network always approaches Pareto optimal bandwidth utilization automatically. In Chapter 4, we implement such an algorithm in a fully distributed manner, which requires no information exchange among the players. Each player repeatedly measures its current throughput and uses the measured value to make myopic best response to the current channel idle rate. Our simulations show that the system indeed achieves close to Pareto optimal performance while guaranteeing a certain degree of fairness. The algorithm is robust and can handle various practical issues such as the dynamic arrival/departure of players, parameter estimation errors, etc.

1.7.3 Clustering-based Control Theoretic Approach

In the algorithm proposed in Chapter 4, the distributed users heuristically search for Pareto-front target rates, and the system indeed settles down with a target rate that is close to the Pareto front. However, the users using such a heuristic approach have to monitor the channel activities continuously, and will experience several fluctuations before settling down since the network has to be driven into the unstable region to detect the crossing of the Pareto front. As the network

size increases, the system will experience more fluctuations and take longer time to converge. Hence it is worth to look into how to design a fast self-adaptive network rigorously.

The objective of Chapter 5 is to develop an intelligent algorithm to be embedded into the transceivers so that all users know how to self-tune their MAPs to achieve overall Pareto optimality in terms of network throughput under spatial reuse while maintaining network stability. While the optimal solution requires each user to have complete information about the network, our proposed scheme in Chapter 5 only requires users to have local information.

The fundamental of our proposed scheme is that the users will first self-organize into a number of non-overlapping neighborhoods, and the user with the maximum node degree in each neighborhood is elected as the local leader. Each local leader then adjusts its MAP according to a parameter R which indicates the radio intensity level in its neighboring region, whereas the remaining users in the neighborhood simply follow the same MAP value. We show that by ensuring $R \leq 2$ at the local leaders, the stability of the entire network can be assured even when each user only has partial network information. For practical implementation, we propose each local leader to use $R = 2$ as the constant reference signal to its built-in proportional and integral (PI) controller. The settings of the control parameters are discussed and we validate through simulations that the proposed method is able to achieve close-to-Pareto-front throughput.

1.7.4 Joint MAP Tuning and Channel Selection Games in Multi-Channel Spatial Aloha

To further improve the network performance, multiple collision channels can be considered in Aloha networks with spatial reuse. However, as discussed in Section 1.3.2, the problem of joint MAP tuning and channel selection has not been addressed, which motivates our design in Chapter 5.

Chapter 5 uses the multi-channel spatial Aloha model to describe a distributed autonomous wireless network where a group of Tx-Rx user pairs share multiple collision channels via slotted-Aloha-type random access. The design objective is to enable each autonomous user i to select a channel c_i and decide a MAP q_i to improve its throughput, while providing a certain degree of fairness among the users. Game theoretic approaches are applied, where each user i is a player who chooses the strategy (c_i, q_i) to improve its own throughput. To search for a NE, a multi-leader

Stackelberg game is formulated to iteratively obtain a solution on each dimension of the (c_i, q_i) strategy. Initially, multiple Stackelberg leaders are elected to manage the MAPs of all players. Then under the resulting MAP profile, each player iteratively chooses its channel to improve its throughput. An oscillation resolving mechanism is further proposed to stabilize the design in some special cases where the operating points of some players in a local region would oscillate between the two dimensions of the myopic search.

Compared to existing methods of pre-allocating MAPs, the proposed game further improves the overall network throughput by iteratively tuning the MAPs toward max-min throughput in each subnet. Simulation results show that the proposed game gradually improves the total throughput until reaching a NE, which also provides good throughput fairness for the players.

1.7.5 A Stackelberg Game Model for Spatial CSMA Networks

Slotted-Aloha-type random access has been used in the above works. In Chapter 7, we investigate another type of random access scheme, i.e., CSMA, under spatial reuse.

Chapter 7 studies the performance of overlay D2D communication links via CSMA-type random access. We assume that the D2D links have heterogeneous rate requirements and different willingness to pay, and each of them acts non-altruistically to achieve its target rate while maximizing its own payoff. Spatial reuse is allowed if the links are not interfering with each other. A non-cooperative game model is used to address the resource allocation among the D2D links, at the same time leveraging on the ICN model to address the physical channel access issue. We propose a Stackelberg game in which the base station in the cellular network acts as a Stackelberg leader to regulate the individual payoff by modifying the unit service price so that the total D2D throughput is maximized. The problem is shown to be quasi-convex and can be solved by a sequence of equivalent convex optimization problems. The pricing strategies are designed so that the network always operates within the feasible throughput region. The results are verified by simulations.

1.8 Organization of the Thesis

The rest of the thesis is organized as follows. In Chapter 2 we introduce the spatial Aloha model in single channel and multi-channel scenarios, which lays the basis for the studies in Chapter 3 to Chapter 6. Then we introduce the ICN model which will be used in Chapter 7.

Chapter 3 to Chapter 7 are dedicated to each of the contributions in Section 1.7.1 to Section 1.7.5, respectively. Then we summarize the thesis in Chapter 8 and point out possible future research directions.

Chapter 2

System Models and Problem Statements

In this chapter we first introduce the spatial reuse model in distributed wireless networks. Then we introduce the spatial Aloha model in single channel and multi-channel scenarios, and state the problems to be solved. Finally we introduce the ICN model which is the basis for our study in Chapter 7.

2.1 Spatial Reuse Model

Consider a distributed wireless network with N transmitters, where each transmitter has its unique designated receiver. Each Tx-Rx user pair shares a common collision channel with other users, via slotted-Aloha or CSMA type of random access. Spatial reuse is considered, i.e., if the users are located sufficiently far apart, then they can transmit in the same frequency band simultaneously without causing any performance degradation to each other. Such a spatial reuse model can be characterized by an "interference graph" as in [70], or similarly by an "contention graph" as in [86]. The interference estimation methods in [118] can be applied to obtain the interference graph.

As an example, three Tx-Rx pairs and their equivalent interference graph are shown in Fig. 2.1, where users 1 and 3 can transmit concurrently without collisions but neither of them can transmit together with user 2. Such interference relations can be characterized by an *interference matrix* $\mathbf{A}$. For the topology given in Fig. 2.1,

$$\mathbf{A} = \begin{bmatrix} 0 & 1 & 0 \\ 1 & 0 & 1 \\ 0 & 1 & 0 \end{bmatrix}$$

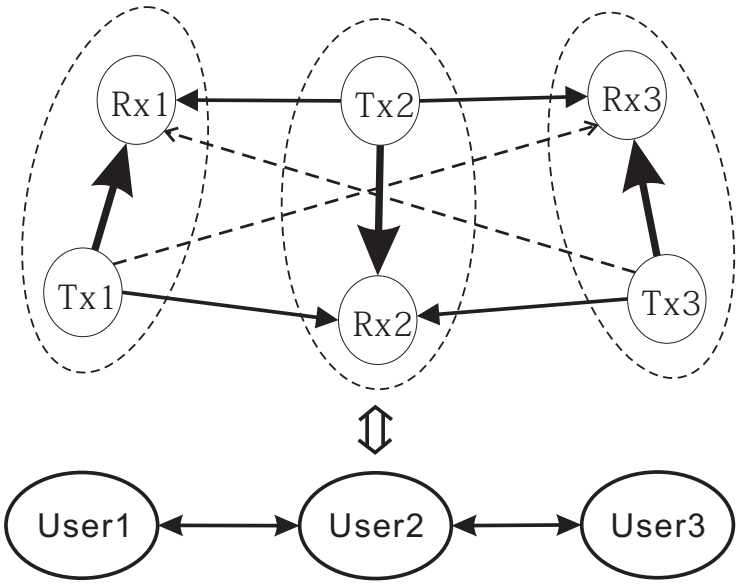

Figure 2.1: 3 Transmit-Receive Pairs and the corresponding Interference (Contention) Graph [2]. In the upper part of the figure, the solid-thick arrow represents the transmission from a transmitter to its designated receiver; the solid-thin (dash-thin) arrow represents the non-negligible (negligible) interference from a transmitter to other unintended receivers.

in which $a_{12} = 1$ means user 2 is a *neighbor* of user 1, $a_{13} = 0$ means user 3 is not a neighbor of user 1, etc. By default, $a_{ii} = 0, \forall i$.

The interference matrix characterizes the spatial distribution and frequency reuse capability of the users. Each user has different neighboring users who directly affect its transmission. For a successful transmission for user i, $i \in \mathcal{N} = \{1, 2, \cdots, N\}$, all of user i's neighbors (user j with $a_{ij} = 1$), should not transmit. We assume that every user's transmission queue is continuously backlogged, i.e., the transmitter of every user always has a packet to transmit to its designated receiver.

2.2 Single-Channel Spatial Aloha

We first consider a distributed wireless network in which a group of Tx-Rx pairs share a common collision channel via slotted-Aloha-type random access. These Tx-Rx user pairs are allowed to reuse the channel if they receive negligible interference from others. With the defined interference matrix in Section 2.1, if we assume that each user i chooses a MAP q_i in slotted Aloha, then the throughput θ_i can be obtained as:

$$\theta_i = q_i \prod_{a_{ij}=1} (1 - q_j), \forall i \in \mathcal{N}. \tag{2.1}$$

The equation indicates that for a successful transmission for user i, all those users which will interfere with its transmission (user j where $a_{ij} = 1$), should not transmit. It can be seen that the equations obtained here do not have a symmetric structure since the MAPs of some of the users are missing in some of the equations, depending on the network interference topology. This is unlike the relationship obtained from a fully connected network [49], where $a_{ij} = 1, \forall i \neq j$; in this situation, the equations exhibit symmetric structures.

As a starting point, we first investigate the spectrum commons model with distributed Tx-Rx user pairs competing for transmission in a single collision channel using slotted Aloha. Under such a scenario, an autonomous user would naturally want to transmit more and obtain higher bandwidth utilization. This results in competition among the users on the common collision channel. If everyone wants to transmit more, the contention level will be high and all pairs will suffer, whilst if everyone transmits at a lower probability, the bandwidth is not fully exploited. Our objective is to develop tailored algorithms so that each user has self-autonomous capability to enable the network to operate at one stable equilibrium solution that is close to the Pareto-front [19] throughput.

Challenges arise in the above problem. First of all, how to model the interactions and behaviors of the users if each of them is interested in maximizing its own benefit? If a non-cooperative game model is adopted, how to formulate the game under spatial reuse? In the formulated game, does there exist a NE? Is it the unique NE? Furthermore, if a NE exists, how to design the underlying dynamics so that the game would converge to the NE? More desirably, is the NE "stable" in the sense that the game would converge back to the NE after being perturbed by small disturbances (e.g., introduced by parameter estimation errors)? These questions will be addressed in Chapter 3.

Secondly, we need to consider the efficiency and fairness of the NE. In particular, how to approach the Pareto-front throughput solution using only limited local information, while providing a certain degree of fairness for the users? This is a challenging problem. Since the users are inter-connected either directly or indirectly, the network stability condition, and hence the achievable throughput region and Pareto front, would most likely involve having complete information of the network (including the complete topology information and the MAPs of all users). However, in reality, the spatially distributed users only possess local views, i.e., no user has a full global view of the network, or the network is too complex for a user to gather all information and make practical use of such knowledge. Moreover, even

if the Pareto front is known, we also need to design the spectrum sharing rules so that the final operating point not only is close to the Pareto front, but also provides a certain degree of fairness for the users.

The above challenges motivate our design of a heuristic algorithm to be presented in Chapter 4 and a control theoretic method to be presented in Chapter 5. We will also show that our solutions achieve close-to-Pareto-front throughputs while at the same time taking into account the fairness issues among the users.

2.3 Multi-Channel Spatial Aloha

In some situations, multiple channels could be available for transmission. The autonomous radios are allowed to decide not only the MAP but also the channel it can transmit on. Consider a distributed wireless network with N transmitters, where each transmitter has its unique designated receiver. Each Tx-Rx user pair selects one of the K orthogonal channels for transmission, and shares channel access with other users via slotted-Aloha. We make the following assumptions:

• In each time slot each user is allowed to access a single channel.

• Every user's transmission queue is continuously backlogged, i.e., the transmitter of every user always has a packet to transmit to its designated receiver.

• Each user perfectly estimates the load on all channels [73] (i.e., monitors the channel utilization for a sufficient time, or by enabling local information exchange about MAP).

• For simplicity, we assume that the channel conditions of all the channels at all the users remain stable for a relatively long period of time.

If the users are located sufficiently far apart, then they can transmit in the same frequency band simultaneously without causing any performance degradation to each other. For the example in Fig. 2.1, users 1 and 3 can transmit concurrently without collisions but neither of them can transmit together with user 2, given that these users are sharing the same channel. Such interference relations can be characterized by an interference matrix $\mathbf{A}$, as introduced in Section 2.1. With the interference matrix, assuming that each user i chooses a MAP q_i, then the throughput θ_i in the single channel case can be obtained as in (2.1).

Then we generalize to the case with K orthogonal channels. Hereafter, we assume the network starts with all users transmitting in one of the channels, where the interference matrix $\mathbf{A}$ is applied. Only those neighboring users transmitting on the same channel can interfere with each other. The design objective is to distribute

(a) K=1, G=1 [70] (b) K=2, G=3

Figure 2.2: 4 Users Topology

these users among all channels. We shall adopt the following notations. Denote $\mathcal{K} = \{1, 2, \cdots, K\}$ as the available channel set, and $c_i \in \mathcal{K}$ as the channel selected by user $i, \forall i \in \mathcal{N}$. Since we assume that all users experience the same channel conditions on all channels, the neighboring relationship remains. After the channel allocation, all users are partitioned into G groups, where each group $\mathcal{M}_g (g \in \mathcal{G} = \{1, \cdots, G\})$ corresponds to a connected sub-network, and $\cup_{g=1}^{G} \mathcal{M}_g = \mathcal{N}$. These subnets are disconnected from others, i.e., $\mathcal{M}_{g_1} \cap \mathcal{M}_{g_2} = \emptyset, \forall g_1, g_2 \in \mathcal{G}, g_1 \neq g_2$, either because they operate on different channels, or they are on the same channel but spatially disconnected. Then the throughput for user i is

$$\theta_i = q_i \prod_{j:a_{ij}=1, c_j=c_i} (1 - q_j), \forall i \in \mathcal{N}. \tag{2.2}$$

For example, consider the interference graph in Fig. 2.2a, with the corresponding interference matrix $\mathbf{A} = \begin{bmatrix} 0 & 1 & 0 & 0 \\ 1 & 0 & 1 & 1 \\ 0 & 1 & 0 & 1 \\ 0 & 1 & 1 & 0 \end{bmatrix}$. Now assume that two channels are available and the channel allocation is $\underline{c} = (1, 2, 1, 1)$ as indicated in Fig. 2.2b. Then there are 3 subnets, i.e., $\mathcal{M}_1 = \{1\}$, $\mathcal{M}_2 = \{2\}$ and $\mathcal{M}_3 = \{3, 4\}$. The throughput for each user, according to (2.2), is $\theta_1 = q_1$, $\theta_2 = q_2$, $\theta_3 = q_3(1 - q_4)$, $\theta_4 = q_4(1 - q_3)$, respectively.

We further observe that, under a certain channel allocation profile, we can improve the users' throughputs and provide a certain degree of fairness by properly managing the MAPs of the users. For the example in Fig. 2.2b, we can tune up the MAPs as $\underline{q} = (1, 1, 1/2, 1/2)$ so that max-min throughput is achieved in each subnet, i.e., $\underline{\theta} = (1, 1, 1/4, 1/4)$.

Problems arise in the above settings. Specifically, how to enable the autonomous users to properly choose their channels and tune their MAPs so that the network

throughput is improved while providing a certain degree of fairness for the users? In the above distributed wireless network model where users make autonomous decisions based on local information, how to model and analyze such strategic interactions? These questions will be addressed in Chapter 5, in which we propose to use a game-theoretic approach to handle the joint MAP tuning and channel selection problem.

2.4 Spatial CSMA

Slotted-Aloha-type random access has been used in the above models. In this section, we introduce another type of random access scheme, i.e., CSMA, under spatial reuse.

2.4.1 Spatial Reuse and Contention Graph

Consider the situation where there are N D2D links (i.e., Tx-Rx pairs) in the network sharing a dedicated inband overlay channel via CSMA-type random access. These D2D links can transmit in the same frequency band simultaneously if they do not cause any performance degradation to each other. We assume that the CSMA network is hidden-node-free, which can be achieved by properly setting the carrier-sensing power threshold as in [119] [120]. Such a spatial reuse model can be characterized by a "contention graph" as in [86]. For simplicity, only a connected network is considered, and if the network is not connected, then it can be divided into several independent connected sub-networks and dealt with separately. We assume that the contention graph is un-directed and the transmission queue of each D2D link is continuously backlogged, i.e., the transmitter of every D2D link always has a packet to transmit to its designated receiver. An example for three D2D links is shown in Fig. 2.1, where D2D links 1 and 3 can transmit concurrently without collisions but neither of them can transmit together with link 2. In such cases, link 2 is a neighbor of link 1, but link 3 is not.

2.4.2 Ideal CSMA Network Model

In the CSMA random access method, a link senses the channel before transmitting. Based on such a carrier-sensing relationship, a link will refrain from transmitting if any of its neighbors is transmitting. In the ICN model, each link maintains a countdown timer, whose value t_{cd} is modelled as a continuous random variable with

an arbitrary distribution [86]. The timer value t_{cd} counts down if the channel is sensed as idle, and is frozen if the channel is sensed as busy. When the channel becomes idle again, the countdown of t_{cd} resumes until $t_{cd} = 0$, upon which the link transmits a packet. The transmission time t_{tr} is a random variable with an arbitrary distribution. For simplicity, we have adopted uniform distributions for both t_{cd} and t_{tr} in our simulations.

At any time, a link is either transmitting or idle. Denote the state of link i as $s_i \in \{0, 1\}$, where $s_i = 1$ if link i is transmitting and $s_i = 0$ otherwise. When $s_i = 0$, link i is either actively counting down or frozen, depending on whether a neighboring link j is transmitting or not. We shall denote the system state of a N-link ICN by a N-tuple binary vector $\underline{s} = [s_1, s_2, \cdots, s_N]$ or simply by a string $s_1 s_2 \cdots s_N$. Notice that $s_i = s_j = 1$ is not allowed if links i and j are neighbors, for the reasons that they can sense each other and the probability of them counting down to zero simultaneously is negligibly small under ICN due to the adopted continuous random variables [86]. Therefore, each feasible state corresponds to an independent set [86] of the contention graph.

As an example, for the contention graph in Fig. 2.1, the five independent sets are $\emptyset$, $\{1\}, \{2\}, \{3\}, \{1, 3\}$. By default, we also include $\emptyset$, which corresponds to $\underline{s} = \underline{0}$, as an independent set. The collection of these feasible system states are denoted by the set

$$\mathcal{S} = \{[0, 0, 0], [1, 0, 0], [0, 1, 0], [0, 0, 1], [1, 0, 1]\}. \tag{2.3}$$

If we denote the state $\underline{s}$ with $s_j = 0, \forall j \in \mathcal{N} = \{1, 2, \cdots, N\}$ as $\underline{e}_0$, and the state $\underline{s}$ with $s_i = 1, s_j = 0, \forall j \neq i$ as $\underline{e}_i$, then $\mathcal{S}$ can be denoted as

$$\mathcal{S} = \{\underline{e}_0, \underline{e}_1, \underline{e}_2, \underline{e}_3, \underline{e}_1 + \underline{e}_3\}. \tag{2.4}$$

2.4.3 Stationary Distribution

Here we summarize the stationary distribution of the system states based on the results in [86]. If the transmission time and countdown time are exponentially distributed, then the system state $\underline{s}(t)$ is a time-reversible Markov process. The state transition diagram of the example in Fig. 2.1 is shown in Fig. 2.3, where there are 5 feasible system states. Each transition from a state in the left to a state in the right represents the beginning of a link transmission, while the reverse transition represents the ending of the same link transmission. For example, the

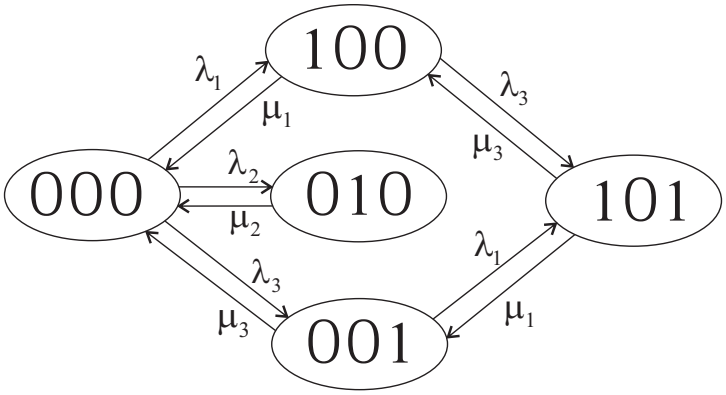

Figure 2.3: State Transition Diagram for Fig. 2.1

transition from 001 to 101 represents the beginning of link 1's transmission while link 3 is transmitting. Similarly, the transition from 101 to 001 represents the ending of link 1's transmission while link 3 continues its transmission.

The transition rate of a link from idle state to transmission state is $\lambda = 1/E[t_{cd}]$, while the transition rate from transmission state to idle state is $\mu = 1/E[t_{tr}]$. Therefore, a higher rate λ and a lower rate μ would suggest a higher intensity of the link to access the channel. The *access intensity* (AI) [86] of a link is then defined as the ratio of its mean transmission time to its mean countdown time: $\rho = E[t_{tr}]/E[t_{cd}] = \lambda/\mu$. Note that a higher value of AI suggests a higher intensity to access the channel. We further introduce the *transmission aggressiveness* (TA) [92], which is defined as the natural logarithm of AI ρ, i.e., $r = \log_e \rho$. Since natural logarithm is a monotonically increasing function, a higher value of AI would correspond to a higher value of TA, which suggests the link is more aggressive to transmit.

Given a profile of AIs $\underline{\rho} = [\rho_1, \rho_2, \cdots, \rho_N]$, the stationary probability of the state $\underline{s} \in \mathcal{S}$ is shown in [86] to be given by

$$p_{\underline{s}} = 1/Z \cdot \textstyle\prod_{i:s_i=1} \rho_i, \forall \underline{s} \in \mathcal{S}, \tag{2.5}$$

where

$$Z = \textstyle\sum_{\underline{s} \in \mathcal{S}} \prod_{i:s_i=1} \rho_i. \tag{2.6}$$

and by default, $p_{\underline{e}_0} = 1/Z$. In (2.6), when evaluating $p_{\underline{s}}$, the notation $\prod_{i:s_i=1} \rho_i$ means that for each state $\underline{s}$, only those transmitting links are involved in the multiplication. Collectively, we can write the state probability distribution as a vector $\underline{p} = [p_{\underline{s}_1}, p_{\underline{s}_2}, \cdots, p_{\underline{s}_{|\mathcal{S}|}}]$, where $|\mathcal{S}|$ is the cardinality of the set $\mathcal{S}$, i.e., the number of

feasible states.

Similarly, if we replace AIs by TAs and define a profile of TAs $\underline{r} = [r_1, r_2, \cdots, r_N] = \log_e \underline{\rho}$ for all links, the stationary state probabilities are given by

$$p_{\underline{s}} = 1/Z \cdot \exp(\textstyle\sum_{i=1}^{N} s_i r_i), \forall \underline{s} \in \mathcal{S}, \tag{2.7}$$

where

$$Z = \textstyle\sum_{\underline{s} \in \mathcal{S}} \exp(\sum_{i=1}^{N} s_i r_i). \tag{2.8}$$

As an illustration, consider the state transition diagram in Fig. 2.3. Since the system state is a time-reversible Markov process, the stationary probability distribution should satisfy

$$\begin{cases} p_{100} = \rho_1 \cdot p_{000}, \\ p_{010} = \rho_2 \cdot p_{000}, \\ p_{001} = \rho_3 \cdot p_{000}, \\ p_{101} = \rho_1 \cdot p_{001} = \rho_3 \cdot p_{100} = \rho_1 \cdot \rho_3 \cdot p_{000}, \\ p_{000} + p_{100} + p_{010} + p_{001} + p_{101} = 1. \end{cases} \tag{2.9}$$

Solving the equations in (2.9) yields

$$p_{000} = 1/(1 + \rho_1 + \rho_2 + \rho_3 + \rho_1\rho_3) = 1/Z, \tag{2.10}$$

where Z is given in (2.6). Once Z is evaluated, other state probabilities can be easily computed.

Despite the idealized assumption about instantaneous sensing and continuous backoff time, the ICN model does capture the essence of CSMA under spatial reuse. It is shown in [86] that the stationary probability distribution in (2.5) holds even if both the transmission time and countdown time are not exponentially distributed, given that the ratio of their mean $\rho_i = E[t_{tr,i}]/E[t_{cd,i}]$ for each link $i \in \mathcal{N}$ remains unchanged. On the other hand, in the discrete time model, the stationary probability distribution will deviate from (2.5) due to collisions. Fortunately, when RTS/CTS handshaking is used and under the same TAs, the stationary distribution will approach that given in (2.5) since the collision period will be comparatively small for a sufficiently large holding time [95].

Finally, it then follows from (2.7) and (2.8) that the throughput or mean service

rate of link i is given by

$$\theta_i = \sum_{\underline{s}\in\mathcal{S}} s_i p_{\underline{s}} = \frac{\sum_{\underline{s}\in\mathcal{S}} s_i \exp(\sum_{i=1}^{N} s_i r_i)}{\sum_{\underline{s}\in\mathcal{S}} \exp(\sum_{i=1}^{N} s_i r_i)}, \forall i \in \mathcal{N}, \tag{2.11}$$

which is the sum of the stationary state probabilities defined in (2.7) in which link i is actively transmitting (i.e., $s_i = 1$). In vector form, if we define the vector $\underline{\theta} = [\theta_1, \theta_2, \cdots, \theta_N]$, then the N equations in (2.11) can be collectively written as

$$\underline{\theta} = \sum_{\underline{s}\in\mathcal{S}} p_{\underline{s}} \underline{s}. \tag{2.12}$$

where $\underline{s}$ is the N-dimensional vector used to represent a system state.

2.4.4 Problem Statement

Based on the above ICN model, the discussion in this subsection is on how to efficiently model the resulting D2D network if the CSMA channel access mechanism is adopted by all D2D links. If the objective of the network is to maximize the sum-rate of all transmitting links, and the BS gives no control on the admission and transmission of links, then [92] has successfully solved this problem. The solution is computed in a completely distributed manner. However, as pointed out earlier in Section 1.4, such a fully cooperative model is too idealistic and there is no consideration on the utility heterogeneity and selfish behaviors of the links. In fact, Cagalj *et al.* have shown that even the presence of a few selfish users may lead the CSMA network to collapse [96], while proper pricing or penalty mechanisms lead to overall improvement [97]. Therefore, it may be better to build a pricing framework so that each link tries to maximize its payoff function when competing for resources, rather than someone tries to take advantage when the network is in operation and drive the network to unstable states. Furthermore, maximizing the sum-rate may not distribute the resources according to demand because links with low demand may be assigned to transmit at higher rate due to its spatial location.

To address the above concerns, in Chapter 7 we incorporate a game theoretic framework into the ICN model to harness the selfish behaviors of a group of non-cooperative spatially distributed CSMA users (D2D links) with heterogeneous rate requirements.

Chapter 3

Aloha Games with Spatial Reuse

3.1 Introduction

A detailed review on Aloha games has been made in Section 1.3.1. In this chapter, the Aloha game model in [49] is generalized to include the spatial reuse capability, named as a *generalized Aloha game*. Unlike the model in [49], the use of spatial reuse here distorts the symmetric structure in the expressions to evaluate the NE solution. As a result, a new Lyapunov function needs to be constructed to prove the convergence of a generalized Aloha game.

Also notice that our generalized Aloha game is different from the multi-packet reception (MPR) Aloha game model in [42], although they both allow multiple packets to be successfully received simultaneously. In [42], the users are assumed to be indistinguishable; every user knows the current number of backlogged users in the system; the MPR model is possible by enabling multiple captures in a single channel, or single capture via the use of multiple parallel channels; the stability conditions and stability region of the equilibrium strategy are based on the drift analysis of a Markov chain and the selfish behavior of users when the number of backlogged users goes to infinity. On the other hand, the generalized Aloha game in this chapter assumes that users are heterogeneous in their bandwidth requirements and their neighboring user environment; users have information about the MAPs of others; the MPR capability comes from the spatial reuse of a conventional Aloha collision channel; the stability issues are based on the Lyapunov stability analysis of a nonlinear system.

We introduce the model for the generalized Aloha game in Section 3.2, followed by some mathematical fundamentals on fixed point theory and order theory in Section 3.3. We next discuss the existence of a NE in Section 3.4. In particular,

we use fixed point theory and order theory to prove the existence of a least fixed point in the generalized Aloha game, which is the unique NE of the game and the most energy-efficient operating point for all players. In Section 3.5, we propose a method to prove the stability of the NE. The Krasovskii's method is used to construct the Lyapunov function and obtain the conditions to examine the stability of the NE. After obtaining the conditions to test for system stability, we summarize how to dynamically converge to the least fixed point in game iterations. Section 3.6 shows through simulations that the generalized Aloha game is applicable to large-scale distributed systems with complicated network topologies. An empirical relationship between the achievable total throughput and the network connectivity is finally obtained through our simulations. We conclude the chapter in Section 3.7.

3.2 Model for Aloha Games with Spatial Reuse

With the interference matrix defined in Section 2.1, we can now study the behavior of a generalized Aloha game. The objective of the game is for player i to select a suitable MAP q_i so that player i achieves its target rate y_i, $\forall i \in \mathcal{N} = \{1, 2, \cdots, N\}$, with the lowest possible transmission energy, i.e., each player uses the smallest MAP as it could to attain its target rate. The target rate combination $\underline{y} = [y_1, \cdots, y_N]$ is controlled by certain pricing strategies [60] or some commonly agreed adjusting rules that try to achieve Pareto efficiency [19]. When the target rate y_i is achieved, we have

$$y_i = q_i \prod_{a_{ij}=1} (1 - q_j), \qquad \forall i \in \mathcal{N}. \tag{3.1}$$

The equation indicates that for a successful transmission for player i, all those players which will interfere with its transmission (player j where $a_{ij} = 1$), should not transmit. It can be seen that the equations obtained here do not have a symmetric structure since the MAPs of some of the players are missing in some of the equations, depending on the network interference topology. This is unlike the relationship obtained from a fully connected network [49], where $a_{ij} = 1, \forall i \neq j$; in this situation, the equations exhibit symmetric structures. We now formally state the generalized Aloha game as follows:

Players: Distributed Tx-Rx pairs, $i \in \mathcal{N}$, who compete for a single collision channel to transmit via slotted-Aloha-type random access scheme.

Actions: Each player i chooses a MAP $q_i \in [0, 1]$, $\forall i \in \mathcal{N}$.

Objectives: Each player i ($i \in \mathcal{N}$) aims to minimize the transmission energy

consumption in attaining its target rate y_i, i.e.,

$$\begin{aligned} \min \quad & q_i \\ \text{s.t.} \quad & y_i = q_i \prod_{a_{ij}=1}(1-q_j). \end{aligned} \tag{3.2}$$

The solution of a generalized Aloha game is NE, which is defined as an action profile (in our case, $\underline{q}^* = [q_1^*, \cdots, q_N^*]$) in which each action is a best response to the actions of all the other players [34]. To be qualified as a NE of the generalized Aloha game, the constraints of all players have to be satisfied first, or in other words, we can directly examine the solutions to the set of equations in (3.1). Interesting questions arise related to the problem. By definition, since all the MAPs are real-valued and cannot exceed 1, some of the solutions to (3.1) that do not satisfy these constraints should be discarded. Among the remaining solutions, is there an optimal one existing for all players, or multiple solutions each favoring different subgroups of players? In case if there are multiple solutions to (3.1), how to make the players reach the consensus to choose the same solution? If the consensus can be made, how to dynamically reach that solution in game iterations?

Suppose the iterative approach in [49] is applied to (3.1) to find out the solutions, i.e., the MAP of player i at the $(m+1)$th iteration of the game is given by

$$q_i^{(m+1)} = \min\{\frac{y_i}{\prod_{a_{ij}=1}(1-q_j^{(m)})}, 1\}, \quad \forall i \in \mathcal{N}. \tag{3.3}$$

If a solution $\underline{q}_s = [q_{s,1}, q_{s,2}, \cdots, q_{s,N}]$ exists, it should satisfy

$$q_{s,i} = \min\{\frac{y_i}{\prod_{a_{ij}=1}(1-q_{s,j})}, 1\}, \quad \forall i \in \mathcal{N}. \tag{3.4}$$

Besides satisfying the equality constraints in (3.1), if there exist multiple feasible solutions, we will prove in Section 3.4 that there exists an optimal solution which enable each player to operate with the minimal MAP. This optimal solution $\underline{q}^*$ is then the unique NE of the generalized Aloha game defined in (3.2). Mathematically, if we introduce a binary relation "$\preceq$" between two real-valued vectors $\underline{a}, \underline{b}$, which is defined as component-wise less than or equal to, i.e., $\underline{a} \preceq \underline{b} \Leftrightarrow a_i \leq b_i, \forall i \in \mathcal{N}$, then the NE $\underline{q}^*$, as compared to other solutions $\underline{q}_s$, would satisfy $\underline{q}^* \preceq \underline{q}_s$.

3.3 Mathematical Foundation

In this section, we introduce the Brouwer's fixed-point theorem (in order to prove the existence of solutions to (3.4)), the Kleene fixed-point theorem (in order to prove the existence of a least fixed point, which is later shown to be the unique NE of the game), and some related definitions. These proofs involve an N-dimensional vector function $\underline{F} = (f_1, f_2, \cdots, f_N)^T$, whose component $f_i(\underline{q})(i \in \mathcal{N})$ is a real-valued function of $\underline{q} \in \Gamma$, where $\Gamma \subset \mathbb{R}^N$.

Theorem 3.1 (Brouwer's fixed-point theorem [121])**.** *Every continuous vector function $\underline{F}$ from a convex compact set Γ (where $\Gamma \subset \mathbb{R}^N$) to Γ itself has a fixed point, i.e., there is a point $\underline{q} \in \Gamma$ such that $\underline{F}(\underline{q}) = \underline{q}$.*

Definition 3.1. *A **binary relation** over a set $\Gamma \subset \mathbb{R}^N$ is a collection of ordered pairs in Γ.*

Definition 3.2. *A binary relation "$\preceq$" over a set $\Gamma \subset \mathbb{R}^N$ is a **partial order** if it is reflexive, antisymmetric, and transitive, i.e., $\forall \underline{a}, \underline{b}, \underline{c} \in \Gamma$,*

(a) reflexivity: $\underline{a} \preceq \underline{a}$;

(b) antisymmetry: if $\underline{a} \preceq \underline{b}$ and $\underline{b} \preceq \underline{a}$, then $\underline{a} = \underline{b}$;

(c) transitivity: if $\underline{a} \preceq \underline{b}$ and $\underline{b} \preceq \underline{c}$, then $\underline{a} \preceq \underline{c}$.

Definition 3.3. *A subset S of a partially ordered set $(\Gamma, \preceq)$ is called **directed** if, for any $\underline{a}, \underline{b} \in S$, there is $\underline{c} \in S$ such that $\underline{a} \preceq \underline{c}$ and $\underline{b} \preceq \underline{c}$.*

Definition 3.4. *A partially ordered set $(\Gamma, \preceq)$ is said to be **complete**, and hence a **complete partial order**, if there is a least element of Γ (denoted by $\perp$) and every directed subset $S \subset \Gamma$ has a least upper bound $\sup S \in \Gamma$.*

Definition 3.5. *Let $(\Gamma, \preceq)$ be a partially ordered set. A vector function $\underline{F} : \Gamma \to \Gamma$ is **monotonic** or **order-preserving** if whenever $\underline{a} \preceq \underline{b}$, we have $\underline{F}(\underline{a}) \preceq \underline{F}(\underline{b})$.*

Definition 3.6. *Given a partially ordered set $(\Gamma, \preceq)$, a vector function $\underline{F} : \Gamma \to \Gamma$ is **Scott-continuous** if, for every directed subset S of Γ, $\sup \underline{F}(S) = \underline{F}(\sup S) \in \Gamma$.*

Theorem 3.2 (Kleene fixed-point theorem [122] [123])**.** *Let $(\Gamma, \preceq)$ be a complete partial order, and let $\underline{F} : \Gamma \to \Gamma$ be a Scott-continuous vector function. Then $\underline{F}$ has a least fixed point, which is the supremum of the ascending Kleene chain of $\underline{F}$.*

The ascending Kleene chain of $\underline{F}$ is the chain

$$\perp \preceq \underline{F}(\perp) \preceq \underline{F}(\underline{F}(\perp)) \preceq \cdots \preceq \underline{F}^n(\perp) \preceq \cdots$$

obtained by iterating $\underline{F}$ on the least element $\perp$ of Γ.

Expressed in a formula, the theorem states that

$$\mathbf{LFP}(\underline{F}) = \sup_{n\to\infty} \underline{F}^n(\perp) \tag{3.5}$$

where **LFP** denotes the least fixed point, which is less than or equal to all other fixed points by some partial order.

3.4 Equilibrium of the Generalized Aloha Game

In this section, we prove the existence of solutions to (3.4), and the existence of a least fixed point which would later be shown to be the unique NE in the generalized Aloha game. We specify the aforementioned N-dimensional vector function $\underline{F} = (f_1, f_2, \cdots, f_N)^T$, whose component f_i is defined as a real function given by

$$f_i(\underline{q}) = \min\{\frac{y_i}{\prod_{a_{ij}=1}(1-q_j)}, 1\}, \quad \forall i \in \mathcal{N}. \tag{3.6}$$

The function f_i maps $\underline{q} = [q_1, \cdots, q_N] \in [0,1]^N$ into the ith component of the vector function $\underline{F}$. The reason to define (3.6) will become clearer shortly.

3.4.1 Existence of Solutions

The equations defined in (3.6) and Brouwer's fixed-point theorem are used to examine the existence of solutions to (3.4). From definition, the fixed point of the vector function $\underline{F}$, $\underline{q}_s = (q_{s,1}, q_{s,2}, \cdots, q_{s,N})$, is given by solving $\underline{F}(\underline{q}_s) = \underline{q}_s$, or $f_i(\underline{q}_s) = q_{s,i}, \forall i \in \mathcal{N}$. By substituting such a relationship into (3.6), it results in the solution having the same form as that obtained in (3.4). This means that the solution to (3.4) can be understood as a fixed point to the defined vector function $\underline{F}$. Since the continuous vector function $\underline{F}$ maps a point $\underline{q}$ from the convex compact set $\Gamma \equiv [0,1]^N$ to Γ itself, according to Brouwer's fixed-point theorem, there exists a point $\underline{q}_s$ such that $\underline{q}_s = \underline{F}(\underline{q}_s)$, i.e., (3.4) follows.

It is now clear why (3.6) is defined, as the fixed point behavior of (3.6) is equivalent to the original equality constraints defined in (3.1) except that we explicitly include the bound $q_i = 1$ in (3.6) to ensure that $\underline{F}$ maps into a compact set. One issue to take note is that by using (3.6) to replace (3.1), an extraneous solution $\underline{q}_s = \underline{1}$ is introduced to the original equality constraints defined in (3.1). This solution is not desirable since all players continuously transmit and all transmissions

will result in contention. Fortunately, this undesirable solution to (3.1) can be easily identified and discarded.

Since the fixed points are proper only if they exist in $(0,1)^N$, we focus on such solutions in the following discussion. We will show that if multiple fixed points exist in $(0,1)^N$, there should exist a most energy-efficient one.

3.4.2 Existence of a Least Fixed Point

In the discussion for the generalized Aloha game, the following properties about "$\preceq$" over the set Γ hold:

(a) By Definitions 3.1 & 3.2, the binary relation "$\preceq$" over the set $\Gamma = [0,1]^N$ is a partial order, since it is reflexive, antisymmetric, and transitive.

(b) By Definitions 3.3 & 3.4, the partially ordered set (Γ, $\preceq$) is a complete partial order. The least element of Γ is given by $\underline{0}$. For every directed subset $S \subset \Gamma$, the least upper bound of S is the largest element in S, thus $\sup S \in \Gamma$. Therefore, (Γ, $\preceq$) is a complete partial order.

We are now ready to prove the following propositions.

Proposition 3.1. *The vector function $\underline{F}$ in (3.6) is an order-preserving function over the complete partial order (Γ, $\preceq$).*

For any two vectors $\underline{q}, \underline{p} \in \Gamma$, where $\underline{q} \preceq \underline{p}$, we have

$$\min\{\frac{y_i}{\prod_{a_{ij}=1}(1-q_j)}, 1\} \leq \min\{\frac{y_i}{\prod_{a_{ij}=1}(1-p_j)}, 1\},$$

for $i \in \mathcal{N}$. According to Definition 3.5, the proposition holds.

Proposition 3.2. *For the vector function $\underline{F}$ defined by (3.6), if there exist multiple fixed points in $(0,1)^N$, then a least fixed point exists, which is less than or equal to all other fixed points, according to the partial order "$\preceq$" over the set Γ.*

According to Definition 3.6, the vector function $\underline{F}$ defined by (3.6) is Scott-continuous, because for every directed subset S of Γ, $\sup \underline{F}(S) = \underline{F}(\sup S) \in \Gamma$, which follows from the order-preserving properties of $\underline{F}$.

In summary, by Kleene fixed-point theorem, the vector function $\underline{F}$ defined by (3.6) has a least fixed point, which is less than or equal to all other fixed points, in the partial order "$\preceq$". Moreover, the least fixed point can be obtained by iterating $\underline{F}$ on the least element of Γ, i.e.,

$$\mathbf{LFP}(\underline{F}) = \sup_{n\to\infty} \underline{F}^n(\underline{0}). \tag{3.7}$$

3.4.3 Initialization

Eq.(3.7) suggests that the players can choose initial MAPs $\underline{q}^{(0)} = \underline{0}$ to reach the least fixed point by game iteration. Actually we are able to prove that the initial MAPs $\underline{q}^{(0)}$ can be set as any point in the set $I \equiv [0, y_1] \times [0, y_2] \times \cdots [0, y_N]$, i.e., $\underline{q}^{(0)} \preceq \underline{y}$. This can be done using Kleene fixed-point theorem. By replacing $\Gamma \equiv [0, 1]^N$ with $\Gamma' \equiv [q_1^{(0)}, 1] \times [q_2^{(0)}, 1] \times \cdots [q_N^{(0)}, 1]$, one can easily use the earlier approach to show that Γ' is convex and compact, and can verify that $(\Gamma', \preceq)$ is a complete partial order. Moreover, from the structure of the continuous vector function $\underline{F}$ defined by (3.6), one easily sees that $\underline{F}(\underline{q}) \succeq \underline{y} \succeq \underline{q}^{(0)}$, therefore $\underline{F}$ maps a point $\underline{q}$ from Γ' to Γ' itself. Finally, one can also verify that $\underline{F} : \Gamma' \to \Gamma'$ is a Scott-continuous vector function. Therefore, by Kleene fixed-point theorem, the least fixed point can be obtained by iterating $\underline{F}$ on the least element of Γ', i.e.,

$$\mathbf{LFP}(\underline{F}) = \sup_{n \to \infty} \underline{F}^n(\underline{q}^{(0)}), \underline{q}^{(0)} \in I. \tag{3.8}$$

Notice that the actual feasible region for initial MAPs is larger than I. Later in Section 3.6.1 we will numerically show that, for a stable NE, there exists a neighborhood Ψ of this NE such that the system starting from any point in Ψ will converge to this NE. However, while the value of the least fixed point is not known at the point of evaluating, it might be sufficient to look for initial probabilities just from the region I.

3.4.4 Discussion

The existence of a least fixed point is of great significance. If there exist multiple fixed points (i.e., multiple solutions to (3.1)) in Γ, every selfish player will choose the fixed point which is best for itself. If the least fixed point exists, then the MAP for every player will be the least at this point, thus this fixed point is also the most energy-efficient for every player. As a result, every player will choose this fixed point as the operating point. Therefore, the least fixed point is the unique NE of the generalized Aloha game. Finally, we have proved that the players can choose any initial MAPs $\underline{q}^{(0)} \in I$ to reach the least fixed point by game iteration. These results have not been pointed out in the existing work published in [49] [60], where the Aloha game model is first brought up.

On the other hand, (3.8) does not guarantee that such an iteration process is stable, i.e., the solution may still diverge due to small disturbance at this fixed

point. In the next section, we will discuss the method to prove the stability of the NE.

3.5 Stability of the Equilibrium Point

This section investigates the stability of a generalized Aloha game defined by the iteration process in (3.3). Stability is a desired property of the NE. A stable NE can absorb small disturbances within a certain neighborhood Ψ, e.g., due to the inaccuracy in estimating other players' MAPs. On the other hand, if a NE is not stable, then the game iteration process will diverge to some undesirable states such as $\underline{q} = \underline{1}$, which unfortunately leads to network congestion and results in zero throughputs for everyone. Another motivation is that by understanding the conditions to maintain network stability, we hope to acquire good knowledge to design the intelligence inside future self-autonomous radios. We will discuss this in section 3.6 using an example.

To prove the stability of the resulting NE, we follow the pattern from [49] and approximate the generalized Aloha game by the Jacobi update scheme:

$$\underline{q}^{(m+1)} = \underline{q}^{(m)} + \epsilon(\underline{F}(\underline{q}^{(m)}) - \underline{q}^{(m)}) \tag{3.9}$$

where ϵ is a fixed small positive number and $\underline{F}$ is defined by (3.6). For sufficiently small ϵ, (3.9) can be approximated by a continuous-time game:

$$\dot{\underline{q}}(t) = \underline{g}(\underline{q}(t)) = \underline{F}(\underline{q}(t)) - \underline{q}(t) \tag{3.10}$$

In the presence of spatial reuse, functions defined in (3.6) do not have a symmetric structure since the MAPs of some of the players are missing in some of the equations, depending on the network interference topology. As a result, the Lyapunov function $\Lambda(\underline{q})$ in [49] is no longer applicable to the scenarios with spatial reuse. Therefore, it is necessary to develop a more general Lyapunov function to examine the stability of the solutions.

3.5.1 Krasovskii's Method

We use a new method to construct a Lyapunov function to prove system stability, namely the Krasovskii's method [44].

Theorem 3.3 (Krasovskii's Method)**.** *Consider the non-linear system defined by* $\dot{\underline{x}} = \underline{g}(\underline{x})$*, with the equilibrium point of interest being the origin. Let* $\boldsymbol{J}(\underline{x})$ *denote the Jacobian matrix of the system, i.e.,* $\boldsymbol{J}(\underline{x}) = \partial \underline{g}/\partial \underline{x}$*. If the matrix* $\boldsymbol{B}(\underline{x}) = \boldsymbol{J}(\underline{x}) + \boldsymbol{J}^T(\underline{x})$ *is negative definite in a neighborhood* Ψ*, then the equilibrium at the origin is asymptotically stable. A Lyapunov function for this system is given by* $\Lambda(\underline{x}) = \underline{g}^T(\underline{x})\underline{g}(\underline{x})$*.*

Define $\mathbf{C}(\underline{q}) = -\mathbf{B}(\underline{q}) = -[\mathbf{J}(\underline{q}) + \mathbf{J}^T(\underline{q})]$, where $\mathbf{J}(\underline{q})$ is the Jacobian matrix of the system in (3.10). For those fixed points in $(0,1)^N$, the entries of $\mathbf{J}(\underline{q})$ can be calculated as follows:

$$[\mathbf{J}(\underline{q})]_{ij} = [\partial \underline{g}/\partial \underline{q}]_{ij} = \frac{\partial g_i}{\partial q_j} = \begin{cases} -1 & i = j \\ 0 & i \neq j, a_{ij} = 0 \\ \frac{f_i(\underline{q})}{1-q_j} & i \neq j, a_{ij} = 1 \end{cases} = \begin{cases} -1 & i = j \\ \frac{a_{ij} f_i(\underline{q})}{1-q_j} & i \neq j \end{cases} \tag{3.11}$$

Notice that at a fixed point in $(0,1)^N$, $\dot{\underline{q}}(t) = \underline{g}(\underline{q}(t)) = \underline{F}(\underline{q}(t)) - \underline{q}(t) = 0$, i.e.,

$$q_{s,i} = f_i(\underline{q}_s) = \frac{y_i}{\prod_{a_{ij}=1}(1 - q_{s,j})}. \tag{3.12}$$

Therefore, the entries of $\mathbf{C}(\underline{q}_s)$ at the fixed point can be obtained from (3.11) and (3.12):

$$\begin{aligned} [\mathbf{C}(\underline{q}_s)]_{ij} &= -[\mathbf{J}(\underline{q}_s) + \mathbf{J}^T(\underline{q}_s)]_{ij} \\ &= \begin{cases} 2 & i = j \\ -\frac{a_{ij} q_{s,i}}{1-q_{s,j}} - \frac{a_{ji} q_{s,j}}{1-q_{s,i}} & i \neq j \end{cases} \end{aligned} \tag{3.13}$$

An equivalent condition for the positive definiteness of $\mathbf{C}(\underline{q}_s)$ is stated in Lemma 3.1 [124].

Lemma 3.1. *The real-valued square matrix* $\boldsymbol{C}_{N\times N}$ *is positive definite if and only if* $\det \boldsymbol{C}_i > 0$ *for* $i = 1, 2, \cdots, N$*, where* $\boldsymbol{C}_i$ *is the leading principal sub-matrix of* $\boldsymbol{C}$ *determined by the first* i *rows and columns.*

Alternatively, a sufficient condition for the positive definiteness of $\mathbf{C}(\underline{q}_s)$ is that $\mathbf{C}(\underline{q}_s)$ be diagonally dominant [124], i.e.,

$$\sum_{j=1}^{N} \left(\frac{a_{ij} q_{s,i}}{1 - q_{s,j}} + \frac{a_{ji} q_{s,j}}{1 - q_{s,i}}\right) < 2, \quad \forall i \in \mathcal{N}. \tag{3.14}$$

If $\mathbf{C}(\underline{q}_s)$ is positive definite, according to the Krasovskii's method, the follow-

ing proposition holds with the corresponding Lyapunov function being $\Lambda(\underline{q}) = \underline{g}^T(\underline{q})\underline{g}(\underline{q})$.

Proposition 3.3. *If there is a fixed point $\underline{q}_s \in [0,1]^N$ with $\boldsymbol{C}(\underline{q}_s)$ being positive definite, then there is a neighborhood $\Psi \subset [0,1]^N$ of $\underline{q}_s$ such that: for any initial MAPs $\underline{q}(0) \in \Psi$, the function $\underline{q}(t)$ obeying the dynamics (3.10) will converge to $\underline{q}_s \in \Psi$ as $t \to \infty$.*

For sufficiently small ϵ, Proposition 3.3 can be adjusted to make a statement about the convergence of (3.9) at a fixed point $\underline{q}_s$. Following the postulation in [49], we also postulate that the fixed points that are stable for (3.10) are also stable when $\epsilon = 1$, i.e., for the original iteration (3.3).

In summary, we can verify the positive definiteness of $\mathbf{C}(\underline{q}^*)$ in order to judge the stability of the NE $\underline{q}^*$ in a generalized Aloha game. Certain necessary and sufficient conditions could be used, e.g., Lemma 3.1. Alternatively, the sufficient condition given in (3.14) can also be used, which is easier to implement and gives almost the same bound.

3.5.2 Stability Comparison between Multiple Fixed Points

Stability is a desired property of the NE. The price of instability is that the whole network would be congested and nobody can transmit successfully. This subsection compares the stability of the fixed points. Specifically, the following proposition suggests that the least fixed point is more likely to be stable than other fixed points. Therefore, the least fixed point not only is optimal in terms of energy efficiency, but also carries less risk of instability.

Proposition 3.4. *If the least fixed point is not stable in Aloha games, nor are other fixed points.*

Proof: Let's investigate the entries of $\mathbf{C}(\underline{q}_s)$ from (3.13) first.

$$c_{ij} = [\mathbf{C}(\underline{q}_s)]_{ij} = \begin{cases} 2 & i = j \\ -\frac{a_{ij}q_{s,i}}{1-q_{s,j}} - \frac{a_{ji}q_{s,j}}{1-q_{s,i}} & i \neq j \end{cases} \tag{3.15}$$

When $i \neq j$, c_{ij} is a non-increasing function of $\underline{q}_s$ in the partial order "$\preceq$", i.e., if two fixed points satisfy $\underline{q}_s \preceq \underline{p}_s$, then $c_{ij}(\underline{q}_s) \geq c_{ij}(\underline{p}_s), \forall i \neq j$.

Define a function $h(\underline{x}, \underline{q}_s)$ as follows:

$$h(\underline{x}, \underline{q}_s) = \underline{x}^T \mathbf{C}(\underline{q}_s)\underline{x} = \sum 2x_i^2 + \sum_{i \neq j} c_{ij}(\underline{q}_s)x_i x_j, \tag{3.16}$$

where $\underline{x} \in \mathbb{R}^N$ is the variable, and $\underline{q}_s$ is a parameter.

Now suppose the least fixed point $\underline{q}^*$ is not stable, i.e., $\mathbf{C}(\underline{q}^*)$ is not positive definite. According to the definition of positive definiteness [124], $\exists \underline{x} \neq \underline{0}, \underline{x} \in \mathbb{R}^N$, such that $h(\underline{x}, \underline{q}^*) \leq 0$.

Since $c_{ij} \leq 0, \forall i \neq j$, we can always find an $\underline{x}$ with $x_i x_j \geq 0, \forall i \neq j$, such that $h(\underline{x}, \underline{q}^*) \leq 0$. For such a given $\underline{x}$ and any other fixed point $\underline{p}_s \succeq \underline{q}^*$, we have

$$h(\underline{x}, \underline{q}^*) - h(\underline{x}, \underline{p}_s) = \sum_{i \neq j} x_i x_j (c_{ij}(\underline{q}^*) - c_{ij}(\underline{p}_s)) \geq 0. \tag{3.17}$$

Consequently, $h(\underline{x}, \underline{p}_s) \leq h(\underline{x}, \underline{q}^*) \leq 0$, i.e., $\mathbf{C}(\underline{p}_s)$ is not positive definite. Therefore, if the least fixed point is not stable, nor are other fixed points.■

In summary, we only need to focus on the stability of the least fixed point. If it is not stable, then no stable equilibrium point exists; if it is stable, then it will be the choice of all players, and the behavior of the remaining fixed points may not be of our concern since they are not energy efficient even if the solution is stable. The reason behind this can be easily interpreted as follows. If each player transmits more often but achieves the same throughput, it is just an indication that it is likely there are more collisions in the network and hence more likely that the network will become congested.

3.5.3 How to Dynamically Converge to the Least Fixed Point

We summarize our results. First, we construct an interference matrix $\mathbf{A}$ based on a given distribution of players. Second, for a given target rate combination $\underline{y} = [y_1, \cdots, y_N]$, we iteratively calculate the least fixed point $\underline{q}^*$ of the vector function $\underline{F}$ defined in (3.6) by choosing the initial point $\underline{q}^{(0)} \in I$. Third, we judge the stability of $\underline{q}^*$ by verifying the positive definiteness of the matrix $\mathbf{C}(\underline{q}^*)$ given in (3.13), based on Proposition 3.3. Finally, if the least fixed point $\underline{q}^*$ is stable, then all players can arrive at this equilibrium point through iterations, by choosing any initial point from the set I.

In short, for a combination of target rates satisfying the stability conditions

given by Proposition 3.3, all players can reach the least fixed point (i.e., the unique NE of the game) as a stable operating point, by choosing any initial MAPs $\underline{q}^{(0)} \in I$, among which $\underline{0}$ and $\underline{y}$ are two convenient choices.

3.6 Simulation Studies

In Section 3.6.1, we first demonstrate the existence of the least fixed point and the use of the Krasovskii's method to check its stability by using the three-player chain-like topology. The actual iteration process is simulated so as to test the stability of the fixed points predicted by the Krasovskii's method. The Region of Attraction (RoA) of the least fixed point is estimated by using the Lyapunov function. Then we study the behavior of the fixed points with one varying parameter y_i. Moreover, the combinations of maximum achievable target rates for the players are plotted. Finally, we go beyond the defined game and give simple illustrations on how future autonomous players can make use of the developed theory to improve the overall system sum-rate. In Section 3.6.2, our theory is applied to more complicated network topologies to examine the maximum achievable target rates, with the objective to understand the relationship between the spatial reuse capability and the network connectivity.

3.6.1 Three-player Chain-like Topology

Least Fixed Point

We use the three-player chain-like topology in Fig. 2.1 as an illustration. Assume $y_1 = y_2 = y_3 = 0.15$, then the fixed points can be obtained by solving (3.1), which yields 3 solutions: $[q_{s,1}, q_{s,2}, q_{s,3}] = [0.1952, 0.2316, 0.1952]$, $[0.5451, 0.7248, 0.5451]$, $[1.4097, 0.8936, 1.4097]$. Obviously the third solution is not feasible because two of the MAPs are greater than 1. The first two solutions are in $[0, 1]^3$ and are the feasible solutions to (3.1). Denote the first solution as $\underline{q}^*$ and second solution as $\underline{p}_s$. It is obvious that $\underline{q}^* \preceq \underline{p}_s$. Therefore, $\underline{q}^*$ is the least fixed point.

Krasovskii's Method

The system dynamics is given by:

$$\begin{cases} \dot{q_1} = g_1(\underline{q}) = \min\{y_1/(1-q_2), 1\} - q_1 \\ \dot{q_2} = g_2(\underline{q}) = \min\{y_2/(1-q_1)(1-q_3), 1\} - q_2 \\ \dot{q_3} = g_3(\underline{q}) = \min\{y_3/(1-q_2), 1\} - q_3 \end{cases} \tag{3.18}$$

The entries of $\mathbf{C}(\underline{q}_s)$ evaluated at a fixed point $\underline{q}_s$ can be obtained from (3.11) and (3.12):

$$\mathbf{C}(\underline{q}_s) = -[\mathbf{J}(\underline{q}_s) + \mathbf{J}^T(\underline{q}_s)] = \begin{bmatrix} 2 & -\frac{q_{s,1}}{1-q_{s,2}} - \frac{q_{s,2}}{1-q_{s,1}} & 0 \\ -\frac{q_{s,1}}{1-q_{s,2}} - \frac{q_{s,2}}{1-q_{s,1}} & 2 & -\frac{q_{s,2}}{1-q_{s,3}} - \frac{q_{s,3}}{1-q_{s,2}} \\ 0 & -\frac{q_{s,2}}{1-q_{s,3}} - \frac{q_{s,3}}{1-q_{s,2}} & 2 \end{bmatrix} \tag{3.19}$$

We now verify the stability of $\underline{q}^*$ and $\underline{p}_s$ using the Krasovskii's method by examining whether $\mathbf{C}(\underline{q}_s)$ given by (3.19) is positive definite. It can be claimed that $\underline{q}^*$ is stable while $\underline{p}_s$ is not.

Game Iteration Process

The iteration process of the generalized Aloha Game is given by (3.3). To verify the above claim about the stability of $\underline{q}^*$ and $\underline{p}_s$ using the Krasovskii's method, set $y_1 = y_2 = y_3 = 0.15$, set the initial MAPs $[q_1^{(0)}, q_2^{(0)}, q_3^{(0)}]$ equal to $[y_1, y_2, y_3]$ (P0), $\underline{q}^*$ and $\underline{p}_s$ separately, and run the process to see its actual performance.

We see from Fig. 3.1 that the iteration starting at P0 converges to $\underline{q}^*$ within 10 iterations. On the other hand, we also see that the iteration starting at $\underline{p}_s$ ends up oscillating between two points, [0.1952, 1, 0.1952] and [1, 0.2316, 1]. Therefore, $\underline{q}^*$ is stable while $\underline{p}_s$ is not. This is consistent with the previous claim using the Krasovskii's method.

Region of Attraction of the Least Fixed Point

The *Region of Attraction (RoA)* is defined as the set of all initial points from which the system will converge to the equilibrium point as time goes to infinity [43]. As was commented in [43], finding the exact RoA analytically might be difficult or even impossible. However, the Lyapunov function can be used to estimate the RoA. From Theorem 3.3 and Proposition 3.3, if the least fixed point is verified to be stable,

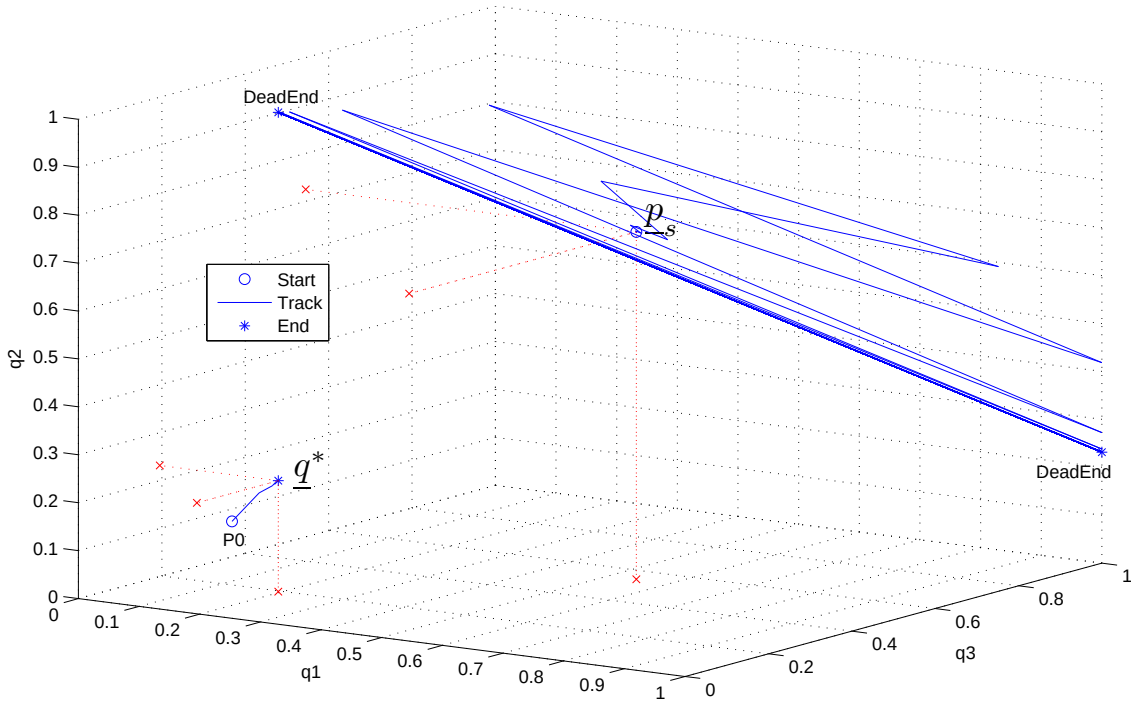

Figure 3.1: The Iteration Process. P0 converges to $\underline{q}^*$; $\underline{p}_s$ is unstable.

then the neighborhood Ψ specified using the Krasovskii's method is within the RoA. Therefore, for the three-player chain-like topology with $y_1 = y_2 = y_3 = 0.15$, we estimate the RoA for the least fixed point (i.e., the NE $\underline{q}^*$), by verifying the positive definiteness of $\mathbf{C}(\underline{q})$.

In Fig. 3.2, the region under the mesh surface provides an estimate of the RoA of the NE $\underline{q}^*$. Clearly the region I (the cuboid near the origin) defined in Section 3.4.3 is within the RoA and can be obtained much easier. However, such an estimation is still quite conservative. For the described game iteration process, we actually observe that the set of points satisfying $\underline{q} \prec \underline{p}_s$ are all within the RoA of the NE $\underline{q}^*$.

Bifurcation of the Fixed Points

For the three-player chain-like topology, we study here the behavior of the fixed points with y_2 varying, while keeping $y_1 = y_3 = 0.15$. For different values of y_2, we solve (3.1), and plot the solutions accordingly in Fig. 3.3 (denote the least fixed point as $\underline{q}^*$, the second fixed point as $\underline{p}_s$; the third solution is outside $[0,1]^3$).

From Fig. 3.3 we observe that, as y_2 increases from 0 to 0.246, there exist two real-valued fixed points $\underline{q}^*, \underline{p}_s$ with $\underline{q}^* \preceq \underline{p}_s$. We verify using the Krasovskii's method that $\underline{q}^*$ is stable while $\underline{p}_s$ is not. When $y_2 = 0.246$, $\underline{q}^*$ and $\underline{p}_s$ coincide and obtain a critical equilibrium $\underline{q}_c^* = [0.3138, 0.5223, 0.3138]$, which corresponds to a

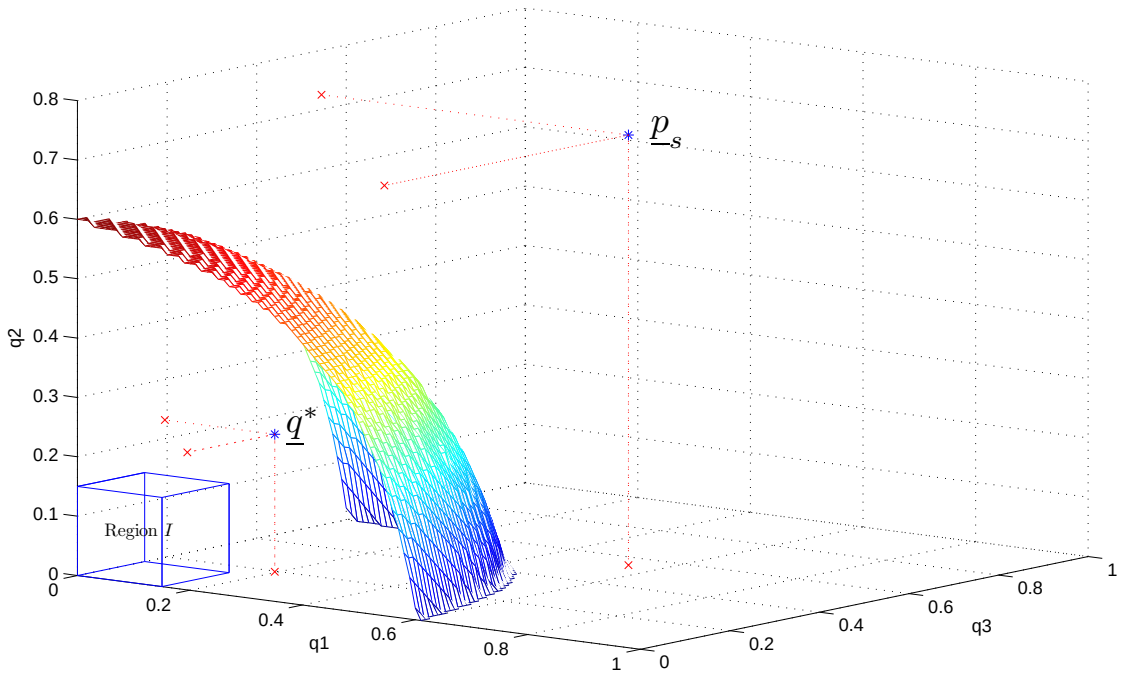

Figure 3.2: Estimation of the Region of Attraction for the NE $\underline{q}^*$

zero eigenvalue of the Jacobian matrix $\mathbf{J}(\underline{q}_c^*)$. If y_2 further increases, the fixed points disappear, i.e., there is no real-valued fixed point in $[0,1]^3$ (except the extraneous one $\underline{q}_s = \underline{1}$ introduced by including the bound $q_i = 1$ in (3.6)). This phenomenon is mathematically named as *Fold Bifurcation* [125]. This bifurcation is characterized by a single bifurcation condition that the Jacobian matrix $\mathbf{J}(\underline{q}_c^*)$ has a codimension-one zero eigenvalue at the critical equilibrium point [125].

Similar simulations with y_1 or y_3 being the varying parameter have been carried out, and we observe similar fold bifurcation of the fixed points. Therefore, for the three-player chain-like topology, we postulate that at most one stable fixed point exists and it is the least fixed point.

We also extend the simulations to cases with more players and different topologies. Due to computational complexity of calculating all the solutions of (3.1), we only examine cases with no more than 8 players. We observe three interesting phenomena: (1) there are at most two real-valued fixed points in $(0,1)^N$; (2) these two fixed points exhibit fold bifurcation with any of the target rate y_i being selected as the varying parameter and the remaining fixed; (3) among these two fixed points, the least fixed point is stable while the other is not, before they coincide and disappear. However, a rigorous mathematical proof of such bifurcation behavior of the fixed points is still difficult, and might require further investigation.

In the next two subsections, we demonstrate how to extend the results obtained

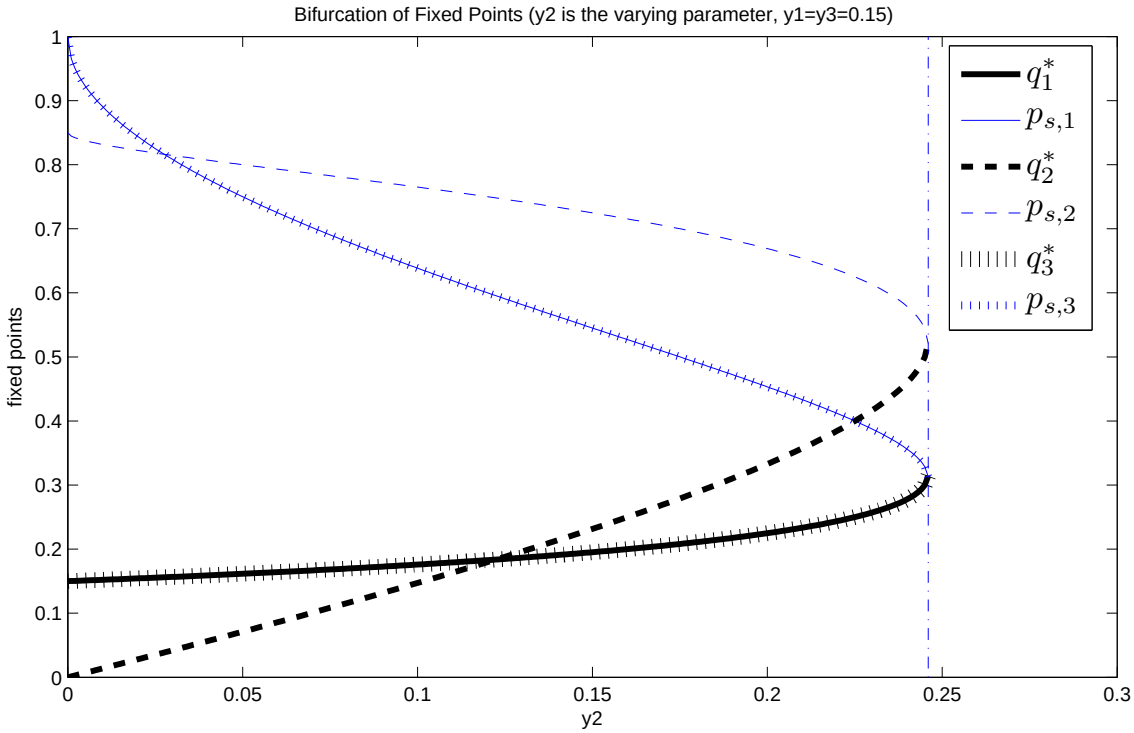

Figure 3.3: Bifurcation of the Fixed Points (y_2 is the varying parameter, $y_1 = y_3 = 0.15$)

from the stability study and apply beyond the described game.

Feasible Region of Target Rates

We compare the maximum achievable target rates between a three-player chain-like topology and a fully connected topology (conventional Aloha games). We vary the combinations of the players' target rates $[y_1, y_2, y_3]$ and use the iterative approach to evaluate the least fixed point until the stability of this point cannot be achieved. We then plot the contour of y_2 for some given $[y_1, y_3]$.

From Fig. 3.4, it can be seen that the maximum achievable target rates in three-player chain-like topology are larger than those of the fully connected topology. For example, notice that $[y_1, y_3] = [0.15, 0.15]$ is below the target rate contour $y_2 = 0.15$ of the chain-like topology, thus the combination $[y_1, y_2, y_3] = [0.15, 0.15, 0.15]$ is achievable and a stable NE can be found. However, the same combination is not achievable for the fully connected topology.

An alternative way of illustrating the feasible target rate region (the region under the mesh surface) for the three-player chain-like topology is shown in Fig. 3.5. The upper boundary of this feasible region is the Pareto front [19], i.e., each point on the mesh surface is a target rate combination that achieves the Pareto optimal bandwidth utilization.

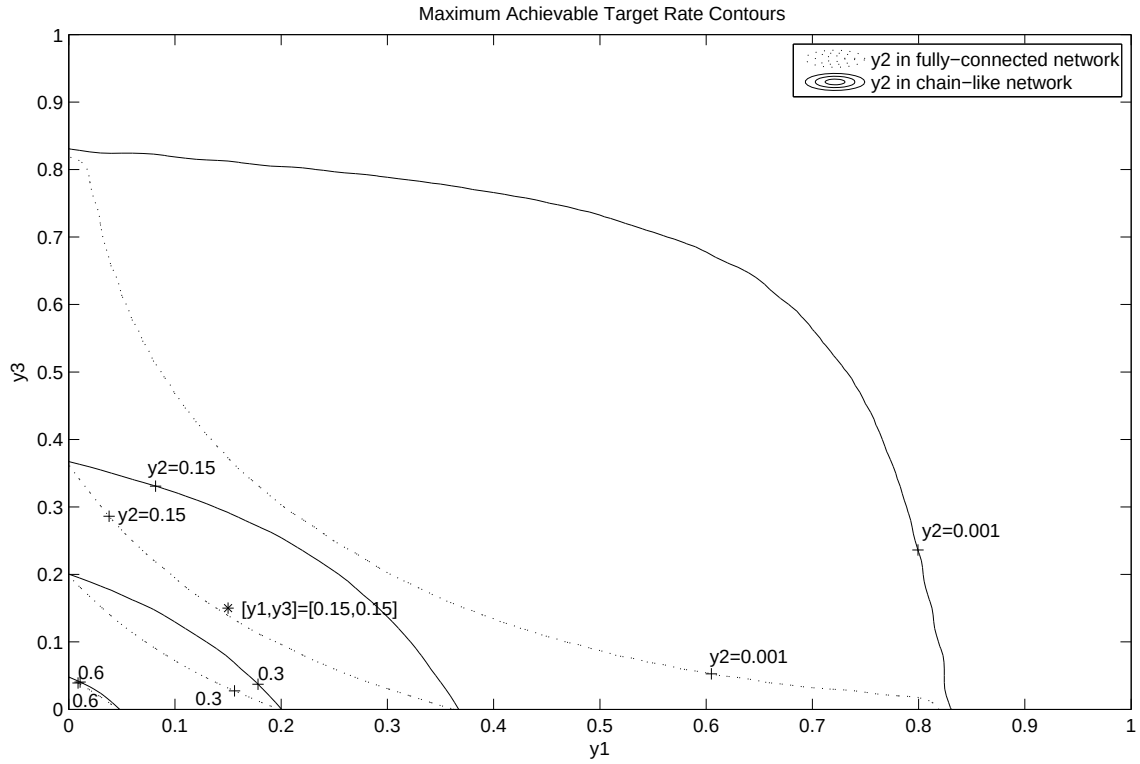

Figure 3.4: Contour Plot of the Maximum Achievable Target Rate

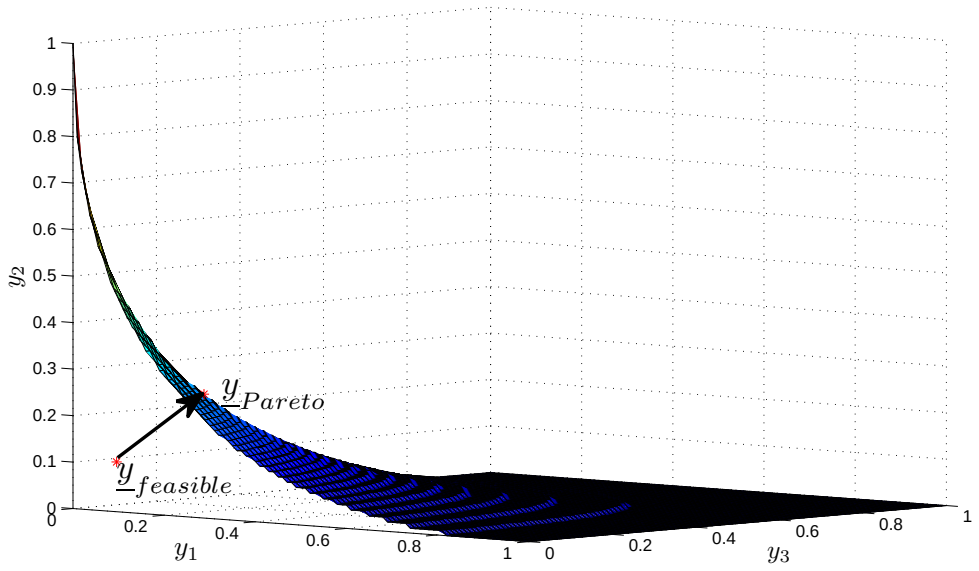

Figure 3.5: Feasible Target Rate Region for the 3-Player Chain-like Topology

Improving System Sum-Rate

Now suppose the three players have chosen $[y_1, y_2, y_3] = [0.15, 0.15, 0.15]$ as their target rates. According to the previous results, they will arrive at a stable operating point $\underline{q}^*$=[0.1952, 0.2316, 0.1952]. At this operating point which is the NE,

	k_{max} or b_{max}	$\underline{y}$	$\underline{q}^*$	Σy_i
original demand	1	[0.15,0.15,0.15]	[0.1952,0.2316,0.1952]	0.45
$\underline{y} \rightarrow k\underline{y}$	1.27	[0.1905,0.1905,0.1905]	[0.3336,0.4290,0.3336]	0.5715
$\underline{q}^* \rightarrow b\underline{q}^*$	1.94	[0.2086,0.1734,0.2086]	[0.3787,0.4493,0.3787]	0.5905

Table 3.1: Improving Sum-Rate by Proper Pricing Strategies

since the network is not fully loaded, intelligent players have the opportunity to further increase their throughputs until the network becomes critically stable, so as to achieve a better spectrum utilization efficiency. In the process of adjusting, all players should also ensure that the process is still governed by the underlying stability conditions defined by the generalized Aloha game.

There are many ways to achieve this and we will get different sum rates and fairness for all players. Two direct ways are: (a) each player proportionally increases its demand from y_i to ky_i, where $k \geq 1$. (b) each player proportionally increases its MAP from q_i^* to bq_i^*, where $b \geq 1$. The results are summarized in Table 3.1.

This example shows that we can increase the sum rate of all players by proper pricing strategies or some commonly agreed target-rate adjusting rules which guarantee certain criteria of fairness and maintain network stability. Conversely, the pricing strategies or target-rate adjusting rules can also be used to bring the target rates of the players back to the feasible region, if the players are over demanding and the resulting network is congested. The rationale behind this study is as follows. For future autonomous radios which compete to transmit like in the ISM band, we would like each device to equip with intelligence so that while competing to transmit, each transmission pair is also governed by the underlying rules so that maximum throughput can be achieved without affecting the network stability. This will result in a win-win situation for all transmission pairs. More vigorous design approach can be found in Chapter 4 and Chapter 5.

3.6.2 Spatial Reuse Gain versus Connectivity

Consider a distributed network with N players, which are randomly placed in a square region of a given area. One half of the players will have transmission range of 5 unit length, while the other half of players have transmission range of 3 unit length. For simplicity, we assume that all the distances between any transmitter and its designated receiver are much smaller than the distances between any two transmitters, so that a Tx-Rx user pair can be represented by a single node in the

topology. We further assume that those players who are in each other's transmission range will have significant interference on each other, and the two nodes are said to be connected. The interference matrix can then be constructed based on the generated network topology.

Performance as Player Density Increases

Player density is defined as the number of players per unit area. We first set $N = 20$, and the player density is increased by decreasing the spatial area under consideration. For each given player density, we run the simulation 100 times. Each time a random topology is generated, and for simplicity, we assume that all players have the same target rate. We increase this common target rate in steps of 0.001, and run the Krasovskii's method until the least fixed point is no longer stable. Consequently, this NE corresponds to the MAPs for the players to achieve the maximum target rate.

Fig. 3.6 shows that both the average throughput and the average MAP decrease as the player density increases. The average throughput curve gradually approaches the lower limit in which all players are fully connected (which is equivalent to the conventional Aloha games).

Performance as Number of Players Increases

In this subsection we fix the player density at 0.1, and increase the number of players by increasing the spatial area.

Fig. 3.7a shows that the average throughput and MAP for the players decrease as the number of players increases, for both fully connected network and the generalized Aloha game. It can be seen that the average throughput in the generalized Aloha game is significantly higher than that in a fully connected network. The achievable average throughput of the fully connected network drops below 0.01 when there are more than 40 players. This is comparatively low when compared to the generalized Aloha game, whose average throughput stays above 0.04 even when there are 100 players. We skip the simulation for the fully connected network when the number of players is more than 50.

Fig. 3.7b shows that the total throughput for the generalized Aloha game increases almost linearly as the number of players increases. On the other hand, the total throughput for the fully connected network remains at a low level around 0.37.

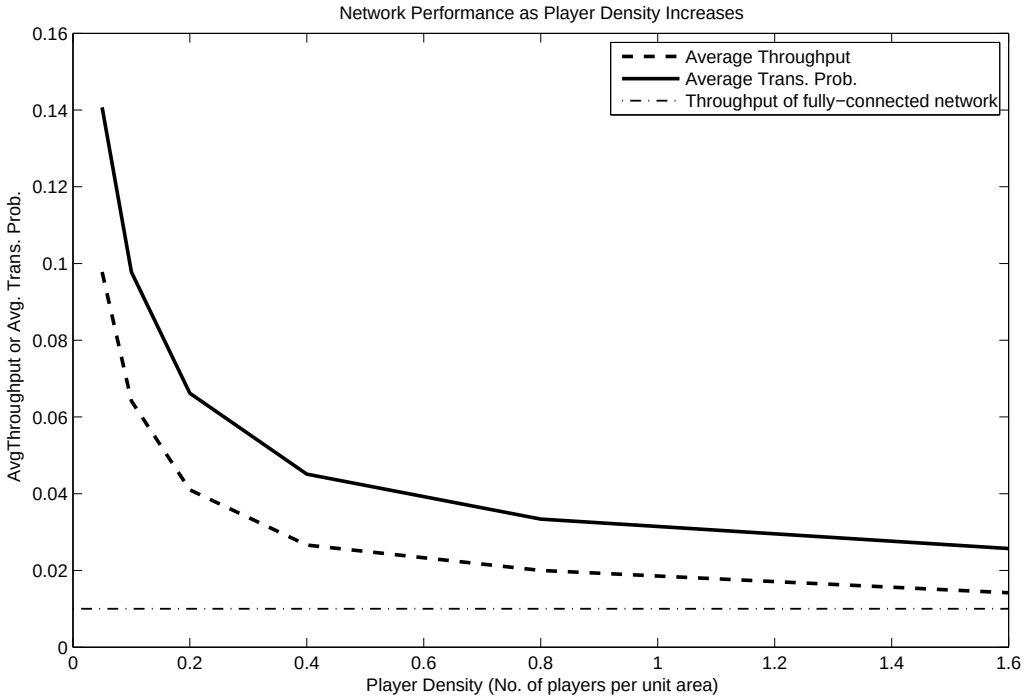

Figure 3.6: Effect of the Player Density on the Average Throughput (20 players in decreasing spatial area)

Relationship between Total Throughput and Connectivity

Define *connectivity* as the total number of links in the current network versus the total number of links in the fully connected case. In particular, connectivity equals to 1 in the conventional Aloha games. Connectivity therefore serves as an indication of spatial reuse capability. From the above observations, it can be seen that if the network is nearly fully connected, i.e., most of the players are within the interference range of each other, its throughput resembles to that of a conventional Aloha game. As the network connectivity drops, either due to decreased player density or due to a larger spatial area compared to the transmission range, the total achievable throughput increases, indicating an increased spatial reuse capability. We therefore postulate that there could exist a relationship between the reuse capability versus the network connectivity. We will use the data from the above two subsections, and present the relationship between total throughput and connectivity.

Fig. 3.8 shows that the total throughput decreases as the connectivity increases, regardless of the number of players involved. The relationship between total throughput (Y) and connectivity (X) can be approximated by an empirical

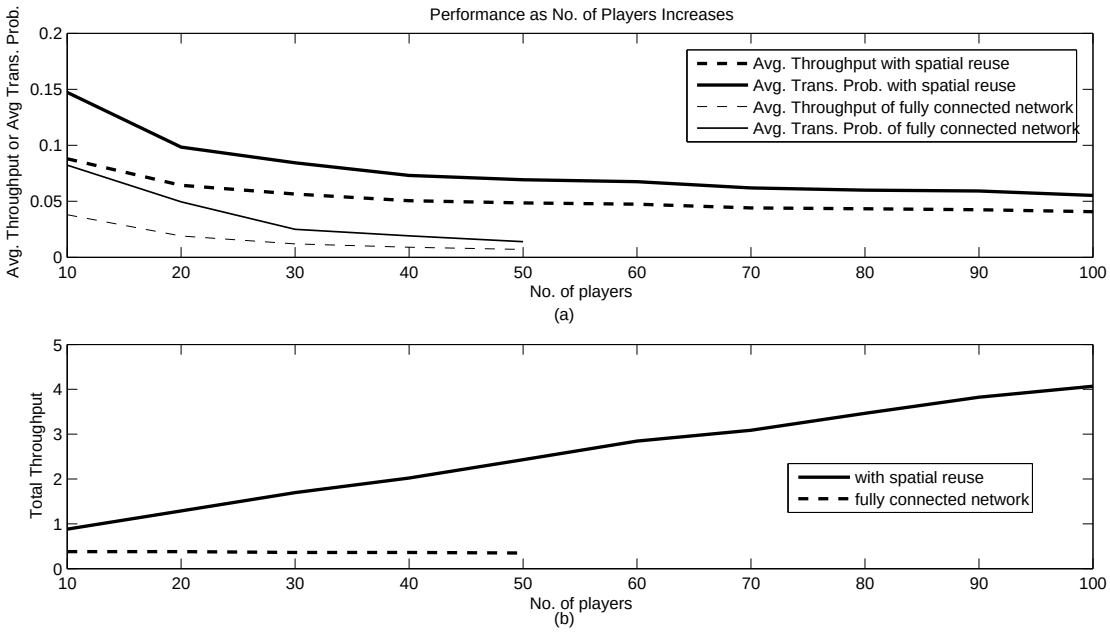

Figure 3.7: Effect of the Number of Players on the Average Throughput (Player density = 0.1, increase spatial area)

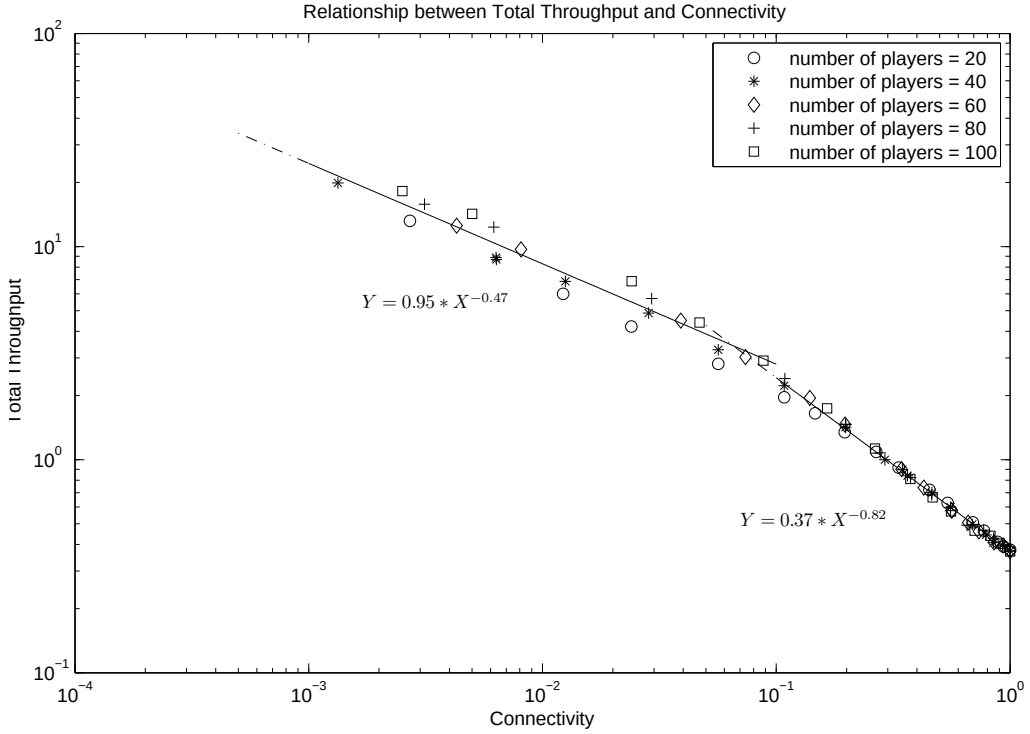

Figure 3.8: Relationship between Total Throughput and Connectivity

formula:

$$Y = \begin{cases} 0.95 * X^{-0.47} & 0.001 \leq X < 0.1 \\ 0.37 * X^{-0.82} & 0.1 \leq X \leq 1 \end{cases} \tag{3.20}$$

Notice that when connectivity is sufficiently low (below 0.001), the network actually degenerates into several independent connected sub-networks, whose connectivity is higher than the original network. In that case, we can apply the above formula separately to each connected sub-network.

3.7 Conclusions

In this chapter, we extend the slotted Aloha games to spatial reuse scenarios, namely, generalized Aloha games. We use fixed point theory and order theory to prove the existence of a unique NE in the generalized Aloha game. In particular, we use the Kleene fixed-point theorem to prove the existence of a least fixed point, which is the unique NE of the game and the most energy-efficient operating point for all players. We then propose to use the Krasovskii's method to prove the stability of the NE. After obtaining the conditions for system stability, we further prove that if the least fixed point is not stable, nor are other fixed points. These findings ensure the ease in finding the NE of a generalized Aloha game as we only need to focus on the least fixed point. If this point is stable, then all players can arrive at this NE through game iteration, by conveniently choosing $\underline{0}$ or $\underline{y}$ as the initial point.

We then show through simulation that the theory derived can be applied to large-scale distributed systems with complicated network topologies to study the maximum achievable throughput. An empirical relationship between the network connectivity and the achievable total throughput is finally obtained through simulations.

Pricing strategies or some target-rate adjusting rules are required to bring the target rates within the feasible region. This chapter has not yet addressed such issues for the generalized Aloha game, despite the simple illustration via the example of the three-player chain-like topology. Extension to this work could be the design of pricing strategies or target-rate adjusting rules for the players in a distributed manner to bring the target rates within the feasible region, or more desirably, toward an optimal combination of target rates which maximizes the total throughput of all players given certain fairness criteria. This motivates our works in Chapter 4 and Chapter 5.

Chapter 4

A Heuristic Algorithm to Approach Pareto Front in Spatial Aloha Networks

4.1 Introduction

In this chapter, we go beyond the generalized Aloha game in Chapter 3, and study how future autonomous radios can make use of the developed theory in decision making to improve the overall system performance. For example, consider the scenarios where autonomous Tx-Rx user pairs (i.e., players) are competing among themselves to transmit over the channel. If some or all the players are over-demanding (total target rate beyond the network capacity), the resulting network is unstable and all pairs will suffer from network congestions. On the other hand, if the players set a low target rate, the network is stable but the bandwidth is not fully exploited. We therefore call for a set of target-rate adjusting rules which are commonly agreed by the players, and enable the players to improve their throughputs without affecting the network stability. This will result in a win-win situation for all transmission pairs. In order to accomplish such goals, we therefore develop an autonomous Pareto optimality achieving algorithm beyond the generalized Aloha game.

Our main contributions in this chapter are as follows. First of all, we implement the algorithm in a fully distributed manner, which requires no information exchange among the players. As is commented in [50], the cost of information gathering needs to be considered when designing games in communication networks. In our algorithm, each player measures its current throughput and uses it to make myopic

best response to the current channel idle rate. Therefore, there is no communication overheads in performing information exchange among the players. Moreover, channel sensing is necessary and needs to be performed only once for a player to set its initial target rates when it joins the network. Secondly, we design a set of target-rate adjusting rules to control the players' behaviors in a distributed manner. Each player uses its measured throughput to dynamically adjust its target rate so that all players have their throughputs adaptively approaching the Pareto optimal bandwidth utilization. The predefined rules can be set to guarantee certain criteria of fairness. Finally, the algorithm is robust and can handle various practical issues such as dynamic arrival/departure of players, parameter estimation errors, etc.

We present the details of our algorithm in Section 4.2, then we describe how the measured throughput can be obtained from practical channel collision scenarios in Section 4.3. We test our algorithm through simulations in Section 4.4 and conclude the chapter in Section 4.5.

4.2 Fully Distributed Algorithm

From the analytical results in Chapter 3, we know that there exists a feasible region of the target rate combination $\underline{y}$. The upper boundary of this feasible region is the Pareto front [19]. We illustrate the feasible target rate region (the region under the mesh surface) for the 3-player chain-like topology in Fig. 4.1. Each point on the surface is a target rate combination that achieves the Pareto optimal bandwidth utilization.

The overall design objective is to achieve Pareto optimal bandwidth utilization for all players. While all the players self-adjust their target rates to approach the Pareto front, it is necessary to guarantee system stability with a predefined way of maintaining certain fairness among the players. The general ideas behind such target rate adjustment are as follows:

1) Suppose the initial target rate combination $\underline{y}_{init}$ is within the feasible region (as illustrated in Fig. 4.1). After the system is stabilized and $\underline{y}_{init}$ is achieved, the players find that there is room to increase their transmission rates, thus repeatedly increasing the target rates in some predefined manner until reaching a point $\underline{y}_{div}$ beyond the Pareto front.

2) Since $\underline{y}_{div}$ is outside the feasible region, the system will diverge to $\underline{q} = \underline{1}$, and $\underline{\theta} = \underline{0}$. We can then reduce $\underline{y}_{div}$ in some predefined manner to bring it back to the feasible region. We can refine the steps of decrement so that the target rate

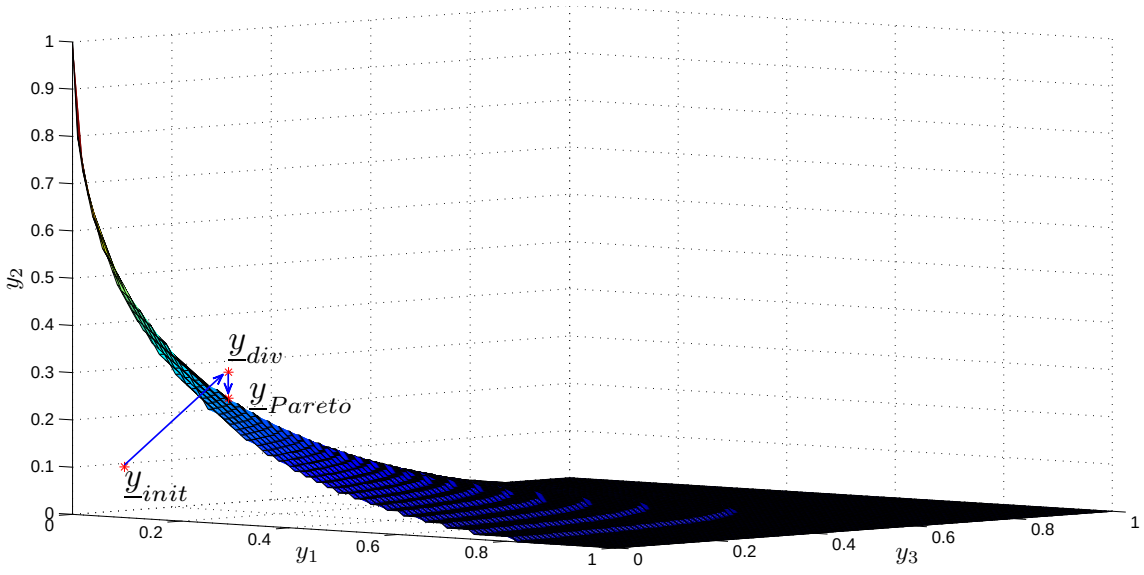

Figure 4.1: Feasible Target Rate Region, 3-Player Chain-like Topology

combination will come to a point $\underline{y}_{Pareto}$ on the Pareto front.

3) We should guarantee certain criteria of fairness among the players. For example, a player with a larger target rate should increase less when the target rate combination goes from $\underline{y}_{init}$ to $\underline{y}_{div}$, and decrease more when it goes from $\underline{y}_{div}$ to $\underline{y}_{Pareto}$.

The above target rate adjusting mechanism is designed to provide best effort transmissions for users with elastic traffic. This is different from [60] which is designed for users with inelastic bandwidth requirements, though they both try to adjust the target rates to maintain system stability and achieve better bandwidth utilization. Another difference is that the target rate adjustment in [60] is centrally controlled by network pricing strategies. As a result, our model can find its applications when distributed Tx-Rx pairs are competing among themselves to transmit over the channel. If everyone wants to transmit more, the interference level will be high and all pairs will suffer, whilst if everyone transmits at a low probability, the bandwidth is not fully exploited. Therefore, we would like each device to equip with intelligence so that while competing to transmit, each transmission pair is also governed by the underlying rules so that maximum throughput can be achieved without affecting the network stability.

4.2.1 System Diagram

In the channel collision model, each player i transmits with a certain probability q_i. Simultaneously transmitted packets are either successful or in collision according to the relationship specified by the interference matrix. Then each player i can monitor its successful rate (throughput) θ_i, and use it to 1) make myopic best response to the current channel idle rate; 2) dynamically adjust its target rate from $y_{i,init}$ according some pre-installed target-rate adjusting rules. For the example of 3-player chain-like topology, the general implementation scheme is shown in Fig. 4.2.

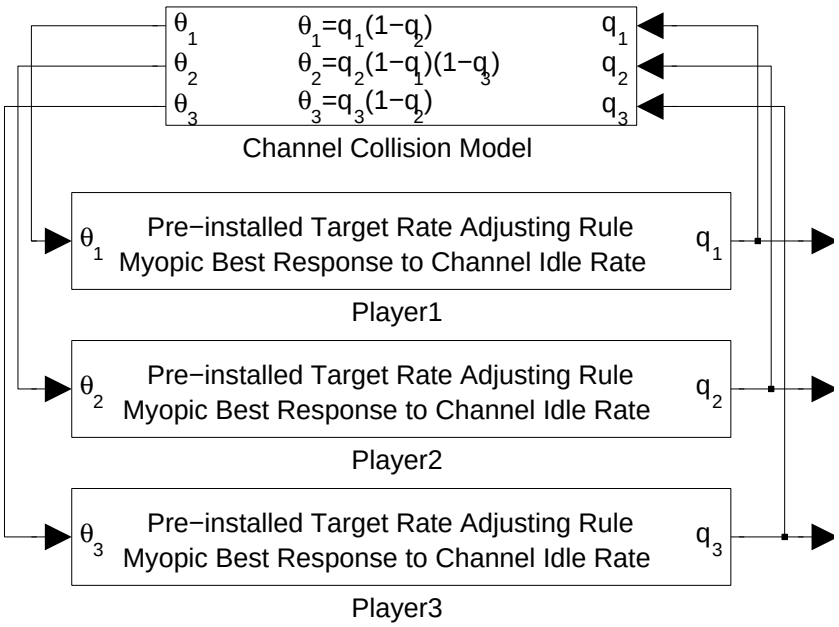

Figure 4.2: System Diagram for 3-Player Chain-like Topology

4.2.2 Myopic Best Response to Channel Idle Rate

The channel idle rate of player i's neighborhood is defined as the probability that none of player i's neighbors are transmitting in a slot, i.e., $x_i := \prod_{a_{ij}=1}(1-q_j)$. Given a target rate y_i, player i's myopic best response to the channel idle rate in the $(m+1)$th iteration is given in (3.3). Since a fully distributed algorithm requires no information exchange among the players, x_i should be estimated by player i itself.

For the initial channel idle rate $x_i^{(0)}$, a one-time channel sensing is needed, i.e., player i listens to the channel for some time and counts the number of idle slots to obtain $x_i^{(0)}$. Afterwards, player i starts transmitting, and $x_i^{(m)}, (m \geq 1)$

can be obtained from the measured throughput $\theta_i^{(m)}$, which requires no channel sensing. Specifically, since the measured throughput in the mth iteration is $\theta_i^{(m)} = q_i^{(m)} \prod_{a_{ij}=1}(1 - q_j^{(m)}) = q_i^{(m)} x_i^{(m)}$, we then have $x_i^{(m)} = \theta_i^{(m)}/q_i^{(m)}$.

4.2.3 Pre-Installed Target-Rate Adjusting Rules

Initializing Target Rates

When player i powers on, it first synchronizes to its neighbors. Then player i sets its initial target rate $y_{i,init}$ based on $x_i^{(0)}$. During the one-time sensing process, player i also finds the number of active neighbors, i.e., $N_i = \sum_j a_{ij}$. Then player i uses x_i^{1/N_i} to calculate the geometric mean of $1 - q_j, \forall j$ with $a_{ij} = 1$. Player i then assumes the MAP of every of its neighbors to be $\bar{q}_{-i} := 1 - x_i^{1/N_i}$.

In terms of fairness, we set player i's initial target rate in approximation to the average target rate of its neighbors. Since the achieved throughput of a player is no larger than its MAP due to collisions, therefore, under the current $\bar{q}_{-i}$, we guess the average target rate of player i's neighbors $\bar{y}_{-i} \leq \bar{q}_{-i}$. Therefore, we design $y_{i,init} = \bar{q}_{-i}^{\gamma}$, in which the exponent parameter $\gamma \geq 1$ so that $y_{i,init} \leq \bar{q}_{-i}$.

We also apply a minimum and a maximum initial target rate m_{init} and M_{init} ($0 < m_{init} < M_{init} \leq 1$). m_{init} is needed in the case that none of player i's neighbors are active when player i powers on, and hence player i attempts to transmit with a small initial target rate. M_{init} is used to proportionally control the size of the increment. Therefore, the Target Rate Initializing Curve is designed as:

$$y_{i,init} = \max\{m_{init}, M_{init} \cdot \bar{q}_{-i}^{\gamma}\}, \gamma \geq 1. \tag{4.1}$$

Increase Target Rates from Inside to Outside the Feasible Region

After the system stabilizes and $\underline{y}_{init}$ is achieved, we can increase the target rates by a step size, and wait for the system to stabilize again. Then we increase the target rates again until the system diverges (with target rate combination $\underline{y}_{div}$).

Based on fairness criteria, the player who currently has a larger target rate should increase less in the above process. Conversely, the player who has a smaller target rate deserves a larger step size. The Target Rate Increment Curve is given in (4.2). M_{inc} is used to proportionally control the increment size, while $(1 - y_i)^{\alpha}$ is used so that the increment steps are refined and gradually decrease as the target

rate increases.

$$\Delta_{i,inc} = M_{inc} \cdot (1 - y_i)^{\alpha}, \alpha \geq 1, 0 < M_{inc} \leq 1. \tag{4.2}$$

Reduce Target Rates from Outside the Feasible Region to the Pareto Front

Since the system diverges under $\underline{y}_{div}$, we reduce the target rates by a step size and wait for the system to stabilize. If the system still diverges, we reduce the target rates again until the system becomes stable (with target rate combination $\underline{y}_{Pareto}$).

Based on fairness criteria, the player who currently has a larger target rate should decrease more. The Target Rate Decrement Curve is given in (4.3). M_{dec} is used to proportionally control the size of decrement, while y_i^{β} is used so that the decrement steps are refined and gradually decrease as the target rate decreases.

$$\Delta_{i,dec} = M_{dec} \cdot y_i^{\beta}, \beta \geq 1, 0 < M_{dec} \leq 1. \tag{4.3}$$

When player i detects divergence and reduces its target rate from y_i to y_i', it will lock the MAP $q_i = y_i'$ for some time, so that the previously high contention it caused to other players will be removed.

Increase Target Rates again when Channel Idle Rate Significantly Rises

The system finally settles down and achieves maximum bandwidth utilization $\underline{y}_{Pareto}$. Later when some of player i's neighbors leave the collision channel, player i might detect significant rise of the channel idle rate. In such cases, it will attempt to increase its target rate again. The curve in (4.2) can be used again to increase the target rates. An alternative way is to predict the amount of increment currently available for player i, and set the increment accordingly.

The amount of increment available for player i is upper bounded by $(\frac{x_i}{x_{i,inf}} - 1)y_i$. $x_{i,inf}$ is the lowest value of x_i recorded whenever the system is stable. In other words, $x_{i,inf}$ stands for the highest level of contention under which the system is still stable. ($x_{i,inf}$ should be reset to 1 and recorded again when divergence happens.) If we observe that $x_i = b \cdot x_{i,inf}, (b \geq M_{rise} > 1)$, i.e., there is a significant rise of the channel idle rate, and we keep q_i unchanged, then ideally we can achieve a higher throughput $\theta_i' = q_i \cdot x_i = q_i \cdot b \cdot x_{i,inf} = b \cdot \theta_i$. Therefore, the amount of increment available for player i is upper bounded by $(\frac{x_i}{x_{i,inf}} - 1)y_i$.

Another design principle is based on fairness criteria. The player who has a

larger target rate should increase less aggressively, although it might have a larger amount of increment available. Therefore, we apply a factor of $(1-y_i)^\rho, \rho \geq 0$ to the target rate increment. Finally, the Target Rate Increment Curve (Channel Idle Rate Rises) is given in (4.4).

$$\Delta_{i,inc2} = (x_i/x_{i,inf} - 1)y_i \cdot (1-y_i)^\rho, \rho \geq 0 \tag{4.4}$$

4.2.4 Measured Throughput Characteristics

The measured signal is the throughput θ_i that player i achieves during one iteration time. We need to characterize it to judge the convergence or divergence of the system.

When the system is converging, the absolute gap between the target rate and the measured throughput will diminish with time, and finally go to 0 when the system becomes stable. The dynamic characteristics is $|y_i - \theta_i^{(m)}| \leq |y_i - \theta_i^{(m-1)}|$. The steady-state characteristics is $|y_i - \theta_i| \leq m_{gap}$, where m_{gap} is a small positive threshold value.

When the system is diverging, the measured throughput θ_i is less than the target rate y_i, and θ_i keeps decreasing until it becomes 0. During the diverging process, the dynamic characteristics is $y_i - \theta_i^{(m)} > y_i - \theta_i^{(m-1)} > 0$. If θ_i drops below a certain threshold, i.e., $y_i - \theta_i \geq M_{gap} > 0$, player i will judge the system as diverging. Another scenario for player i to judge system divergence is that player i has reached the dead-end situation, i.e., $q_i = 1, \theta_i = 0$.

4.3 Modelling Practical Packet Collisions

4.3.1 Estimating Throughput

So far we have been using the mathematical model in (2.1) to model the channel collisions. We now describe how player i's throughput can be estimated from practical packet collision scenarios. Suppose each iteration consists of L_I slots. In the mth iteration, player i generates $\lfloor q_i^{(m)} \cdot L_I \rfloor$ packets, and randomly scatter these packets in the L_I slots. We then use the interference matrix to judge the status of each player's packets, i.e., successful or in collision. Then player i counts the number of successful packets $N_{suc,i}^{(m)}$ in the mth iteration. Its throughput is then estimated by $\hat{\theta}_i^{(m)} = N_{suc,i}^{(m)}/L_I$. This $\hat{\theta}_i$ is used as the measured throughput in our algorithm.

4.3.2 Measures Taken to Handle Estimation Error

1) The estimation error of $\hat{\theta}_i$ compared to its genuine value θ_i is mainly affected by the iteration length L_I. The larger L_I is, the smaller the estimation error. However, a larger L_I also means that it takes longer time (even with the same number of iterations) for the system to converge.

2) We apply a L_q-taps mean-value filter to player i's MAP q_i, so as to smooth out the trembling effect introduced by the estimation error of $\hat{\theta}_i$.

3) We compose every L_B iterations as a block, and assume the players to be block synchronized. Player i makes a judgement about system convergence or divergence at the end of each block. The measured throughput is averaged over each block to reduce the effects of the estimation error. In this way, the judgements made will result in smaller errors.

4.4 Simulation Studies

We implement our scheme for $N = 11$ players with an interference topology given in Fig. 4.3. The parameters for the target rate adjusting curves are: γ=1.5, m_{init}=0.01, M_{init}=0.8; α=25, M_{inc}=0.02; β=1.2, M_{dec}=0.2; ρ=0.35, M_{rise}=1.1. The threshold parameters for the measured throughput characteristics are: m_{gap}=0.005, M_{gap}=0.025. The parameters for the practical packet collision model are: L_I=2000, L_q=10, L_B=4. Suppose the channel bit rate is 20Mbps and the packet length is 100 bits, then the slot time is $5\mu s$. In this case, L_I=2000 means that iterations take place every 10 ms.

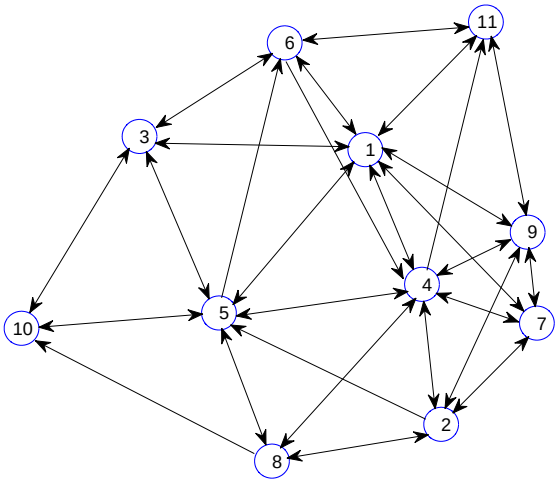

Figure 4.3: Interference Topology for 11 Players

The simulation consists of 3 phases. *Phase 1*: Player 1 $\sim$ 10 power on sequentially at iterations $= 1, 10, 20, 30, \cdots, 90$, while player 11 remains at power-off. *Phase 2*: Player 11 powers on at iterations $= 2000$. *Phase 3*: Player 1 powers off at iterations $= 4000$. The results are plotted in Fig. 4.4.

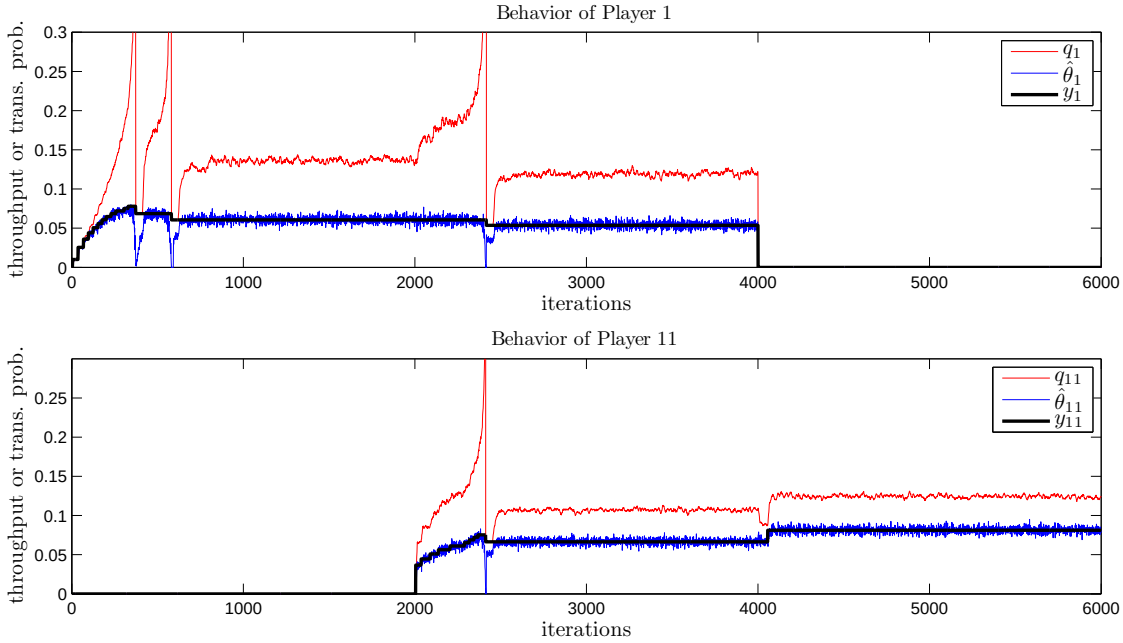

Figure 4.4: Behaviors of Player 1 and Player 11

Phase 1: Player 1 $\sim$ 10 power on sequentially, and the system settles down within 1000 iterations. Upon starting up, player 1 attempts transmitting with a small initial target rate. Then it gradually increases the target rate in diminishing steps until the system diverges. When divergence is detected, player 1 reduces its target rate in diminishing steps. The procedure repeats until the system becomes stable and achieves $\underline{\hat{y}}_{Pareto}$ close to the Pareto front. Notice that there exists a trade-off between the convergence time and the distance to the Pareto front. If we decrease the target rate in very small steps, then $\underline{\hat{y}}_{Pareto}$ will be very close to the Pareto front. However, the system will experience a longer period of divergence before it settles down.

We can use the analytical method in Chapter 3 to find the "distance" between $\underline{\hat{y}}_{Pareto}$ and the Pareto front, i.e., we proportionally increase $\underline{\hat{y}}_{Pareto}$ until it is not achievable according to the analytical method. The increased ratio $k(k \geq 1)$ then indicates such distance. For phase 1, $k = 1.05$. In addition, the mean value and standard deviation of $\underline{\hat{y}}_{Pareto}$ is 0.0689 and 0.0093 respectively. The standard deviation is small compared to the mean value, thus suggesting a certain degree of fairness among the players. Finally, the estimation error of $\hat{\theta}_i$ is well handled, and

the steady state error between the average $\hat{\theta}_i$ and y_i is close to 0.

Phase 2: Player 11 sets $y_{11,init}$ close to the current target rates of its neighbors. As player 11 gradually increases its target rate and raises the contention level of its neighbors, the system diverges some time later. Both players 1 and 11 detect divergence and reduce their target rates. The process repeats until the system stabilizes with $k = 1.08$. The mean value and standard deviation of $\underline{\hat{y}}_{Pareto}$ is 0.0653 and 0.0131 respectively.

Phase 3: Player 1 powers off and player 11 detects significant rise of the channel idle rate, thus increasing its target rate based on the prediction given in (4.4). The system finally stabilizes again with $k = 1.09$. The mean value and standard deviation of $\underline{\hat{y}}_{Pareto}$ is 0.0770 and 0.0100 respectively.

Brief summary: Phase 1 illustrates the target-rate adjusting rules envisioned at the beginning of Section 4.2. The target rate increment process and decrement process are illustrated. After the adjustment, the system stabilizes and achieves close to Pareto optimal bandwidth utilization (distance to Pareto front $k = 1.05$, close to 1). Phase 2 demonstrates the dynamics in the players' throughputs when a new player enters the system. The newly entered player chooses a proper initial target rate close to the average value of its neighbors. Moreover, after dynamic target rate adjustment, the system becomes stable again and achieves close to Pareto optimal performance ($k = 1.08$). Phase 3 demonstrates the case when an existing player leaves the system. The remaining players are able to detect the bandwidth opportunity left over by the leaving player, and adjust their target rates accordingly so that the system still operates at a point close to the Pareto front ($k = 1.09$). Finally, the standard deviation of $\underline{\hat{y}}_{Pareto}$ is small compared to its mean value in Phase $1 \sim 3$ respectively, suggesting a certain degree of fairness among the players.

4.5 Conclusions

This chapter goes beyond the Aloha games with spatial reuse in Chapter 3, and develops an autonomous Pareto optimality achieving algorithm that enables the players to maximize their throughputs without affecting the network stability. The algorithm is implemented in a fully distributed manner, which requires no information exchange among the players. Our simulations show that the system indeed achieves close to Pareto optimal performance while guaranteeing a certain degree of fairness. The algorithm is robust and can handle various practical issues such as the dynamic arrival/departure of players, parameter estimation errors, etc.

Chapter 5

Efficient and Scalable Distributed Autonomous Spatial Aloha Networks via Local Leader Election

5.1 Introduction

In this chapter, we consider a distributed wireless network in which a group of Tx-Rx user pairs share a common collision channel via slotted-Aloha-type random access. These users are allowed to reuse the channel if they receive negligible interference from others. Such a network model is studied using stochastic geometry by Baccelli *et al.* in [126], and named as *spatial Aloha*. In [126], the *Poisson bipolar network model* has been used, where the locations of the transmitters are modeled as a homogeneous Poisson point process. Based on the assumption of homogeneity, the network-wide performance of a large distributed network can be derived from the statistical average performance of a typical user. These approaches predict the achievable performance of the network but give no information about network stability during its operation. Indeed, it is mathematically challenging to obtain the stability conditions of the equilibrium solutions due to the *nonsymmetric* structure in the equations formulated for a partially connected network. How to enable the autonomous users to self-behave yet achieve high efficiency, good fairness and operation stability becomes the design objectives. This motivates our work in this chapter.

For better utilization of spatial reuse and network scalability, clustering is used in our design. Clustering algorithms in wireless networks typically appear in the context of ad hoc [127] [128] and sensor networks [129], where a flat network topology

is divided into a set of connected clusters that cover all nodes in the network. These algorithms are mainly designed to perform cluster-based routing and to achieve scalable network management, whereas our proposed clustering method tries to resolve the concurrent transmission issue among Tx-Rx pairs, and focuses on the attainable throughput and the stability of the spatial Aloha network. In [130], a cluster of sensor nodes operating in slotted Aloha is studied. The authors consider the issue of partitioning the nodes and available frequencies into groups so as to maximize the system throughput. However, the setting is different from ours since we focus on the single channel case and with spatial reuse. In [131], the authors study the effect of clustered topologies on the throughput of spatial Aloha using stochastic geometry. The results suggest that if the nodes have local information about their topological neighborhood, then the system performance can be improved if the nodes can locally adjust their transmission parameters, which also motivates this work.

Instead of viewing the distributed network from the statistical perspective, we zoom into the micro-level design of a deployed network with any given topology. We specifically develop tailored algorithms so that each user has self-autonomous capability to enable the network to operate at one stable equilibrium solution that is close to the Pareto-front [19] throughput predicted by the generalized Aloha games in Chapter 3. In the algorithm proposed in Chapter 4, the distributed users heuristically search for Pareto-front target rates, and the system indeed settles down with a target rate that is close to the Pareto front. However, the users using such a heuristic approach have to monitor the channel activities continuously, and will experience several fluctuations before settling down since the network has to be driven into the unstable region to detect the crossing of the Pareto front. As the network size increases, the system will experience more fluctuations and take longer time to converge. Hence it is worth to look into how to design a fast self-adaptive network rigorously.

To provide *faster convergence* to a stable operating point that is close to the Pareto-front throughput predicted by the generalized Aloha game, we apply the control theoretic approach to update the MAPs of spatial Aloha networks in this chapter. The control theoretic approach is used to provide reliable and optimal configuration of 802.11 WLANs [132], however, no spatial reuse is considered as only one common access point is used. Similar approaches have also been applied to implement the Distributed Opportunistic Scheduling (DOS) algorithm [133], where each node contends for the channel with a certain access probability and gives up the transmission opportunity if the channel quality is below a certain threshold. The

authors further propose a game-theoretic approach to design a decentralized penalty mechanism to control selfish users [134]. However, although the PHY layer channel quality is jointly considered with the MAC layer channel contention in DOS, spatial reuse has not been included in their study. PI controllers are adopted in the above works. Other applications of PI controllers include the design of feedback-based clock synchronization in wireless sensor networks [135].

The novelties of our proposed *Spatial Aloha via local Leader Election (SALE)* scheme [136] are listed as follows:

• Each user can self-regulate its transmission parameter to ensure that the network always operates in the stable region and yet achieves close-to-Pareto-front throughput, by using only local information about its neighbors.

• Rigorous theoretical reasoning for a condition to achieve the above objective. By using the stability conditions derived in the generalized Aloha game [2], we show that a local parameter *Radio Intensity Metric (RIM)*, denoted as R, can be used to indicate the cumulative radio intensity level of each user within its one-hop communication range — a RIM value of less than or equal to 2 for all users can guarantee network stability.

• The implementation aspects including the integration of PI controllers on local leaders are addressed. As commented by [132], one of the key issues in building the control system is to discover a *constant reference signal* which relates to the desired system performance (e.g., maximum throughputs). Specifically, a user which has the maximum node degree in a certain neighborhood is elected as the local leader, and the remaining users in this neighborhood follow the same value of MAP. Each local leader adjusts its MAP according to the value of RIM computed based on its local information, and uses R=2 as the constant reference signal in its built-in PI controller.

• Fast and smooth tuning of MAP. The PI parameters in the controller are designed to achieve a good trade-off between fast convergence and the transient behavior. On the contrary, the heuristic algorithm in Chapter 4 is an engineering approach with no guarantee in convergence rate, and the network operating point would experience several fluctuations before settling down.

• Fast convergence regardless of the number of users or user densities, which is guaranteed by the Ziegler-Nichols rules (see Section 5.3.3) that adapt the PI parameters to various user densities (associated with different node degree at the local leader).

• Low complexity, high scalability and low signalling overhead compared to the

heuristic algorithm. See Section 5.3.6.

• Extensive simulations are performed to verify that the proposed SALE scheme has much faster convergence rate, better scalability and better fairness than the heuristic algorithm, while achieving close-to-Pareto-front throughputs.

The rest of the chapter is organized as follows. We investigate the throughput optimality conditions in spatial Aloha Networks and introduce the design parameter RIM in Section 5.2. Based on RIM, we design the control system for the SALE scheme in Section 5.3. Then we evaluate the system performance through simulations in Section 5.4. We conclude the chapter in Section 5.5.

5.2 Throughput Optimality Conditions

In this section, we explain how a local parameter RIM can be defined and utilized by each user in the spatial Aloha network to judge for system optimality using only local information.

5.2.1 Optimal Conditions

For any MAP vector $\underline{q} = [q_1, q_2, \cdots, q_N] \in [0,1]^N$, the N equations in (2.1) define a vector function $\underline{\theta}(\underline{q}) = [\theta_1, \theta_2, \cdots, \theta_N]$, whose value space is an N-dimensional region. The upper boundary ($\theta_i > 0, \forall i \in \mathcal{N}$) of this region is formed by the critical values of $\underline{\theta}(\underline{q})$, with the critical points $\underline{q} \in (0,1)^N$. Mathematically, this corresponds to the Jacobian matrix $\mathbf{J} = \frac{\delta \underline{\theta}}{\delta \underline{q}}$ being singular [137], i.e., the determinant of $\mathbf{J}$ at the critical point is 0:

$$\begin{aligned} &\det(\mathbf{J}) = |\tfrac{\delta \underline{\theta}}{\delta \underline{q}}| = D(\underline{q}) \cdot \prod_{i=1}^{N} \tfrac{\prod_{a_{ij}=1}(1-q_j)}{1-q_i} = 0 \\ &\Rightarrow D(\underline{q}) = 0, \end{aligned} \tag{5.1}$$

where

$$D(\underline{q}) = \begin{vmatrix} 1-q_1 & -a_{12}q_1 & \cdots & -a_{1N}q_1 \\ -a_{21}q_2 & 1-q_2 & \cdots & -a_{2N}q_2 \\ \vdots & \vdots & \ddots & \vdots \\ -a_{N1}q_N & -a_{N2}q_N & \cdots & 1-q_N \end{vmatrix}. \tag{5.2}$$

Similar derivations for the maximum throughputs of the original Aloha system (centralized, no spatial reuse) can be found in Section III-B of [138] by Abramson. Notice that when the network is fully connected, i.e., $a_{ij} = 1, \forall i \neq j$, (5.1) is

equivalent to formula (26) (27) in [138]. In a very specific case, if all MAPs are equal to q in a fully connected network of N users, then the maximum throughput is achieved at $q = 1/N$.

Since $D(\underline{q})$ involves all the MAPs and the complete interference matrix $\mathbf{A}$, it is not possible for an individual user to test for this optimal condition. In practice, generally only local information about neighbors is readily available for each user. To acquire information beyond this will require large transmission overheads and the design will suffer from large delay. We therefore shall look for certain sub-optimal yet locally implementable testing conditions. The optimal condition in (5.1) gives the maximum throughput boundary and can be used to benchmark the optimality of any sub-optimal schemes.

5.2.2 Sub-optimal Conditions

From the analytical results in Chapter 3, a sufficient condition for a target rate $\underline{y}$ to be feasible is that we can find a corresponding operating point $\underline{q}$ so that the matrix $\mathbf{C}(\underline{q})$ is positive definite. We retrospect on the analysis in Section 3.5 and find a sufficient condition for $\mathbf{C}(\underline{q})$ to be positive definite, i.e., $\mathbf{C}(\underline{q})$ is strictly diagonally dominant [124]:

$$R_i = \sum_{j=1, j\neq i}^{N} \left(\frac{a_{ij}q_i}{1-q_j} + \frac{a_{ji}q_j}{1-q_i}\right) < 2, \quad \forall i \in \mathcal{N}. \tag{5.3}$$

Here we define R_i as the *Radio Intensity Metric (RIM)* for user i. In other words, if (5.3) is satisfied, the corresponding target rate $\underline{y}$ is achievable, i.e., at the operating point $\underline{q}$, the throughput θ_i equals to the target rate $y_i, \forall i \in \mathcal{N}$, or the target rate falls within the feasible region (but not necessarily on the maximum throughput boundary). The converse of this, on the other hand, is not necessarily true.

We now examine the physical meaning of RIM. Firstly, RIM is a local metric since R_i consists of q_i and the q_j terms with $a_{ij} = 1$, i.e., each user i only needs the information about its neighbors to calculate the parameter R_i. Secondly, from (5.3) we observe that R_i is related to the number of user i's neighbors, i.e., $N_i = \sum_{j\in\mathcal{N}} a_{ij}$. Also notice that R_i is monotonic with respect to q_i and $q_j (a_{ij} = 1)$. In other words, the more neighbors with the higher MAPs, the larger the value of R_i. Therefore, RIM can be used to indicate the cumulative radio intensity level in the neighborhood of user i.

After all the $R_i, \forall i \in \mathcal{N}$ are obtained, the condition (5.3) is sub-optimal to (5.1)

but is now locally implementable. The basic implementation idea is to tune the MAPs of all users so that the condition (5.3) is *critically* satisfied, hence achieving a sub-optimal network throughput. In other words, the MAPs of all users are tuned so that $R_l = 2, \forall l \in \Omega; R_j < 2, \forall j \notin \Omega$, where Ω is a certain subset of $\mathcal{N}$. Such an idea will be incorporated into our proposed scheme in Section 5.3.

5.3 The SALE Scheme

In this section we present the design principle for our proposed scalable and efficient scheme using (5.3), named as *Spatial Aloha via local Leader Election (SALE)*. In the SALE scheme, the users will first self-organize into a number of non-overlapped neighborhoods. There are many ways to approach the Pareto front surface defined in (5.1). One possible way is for the users in each neighborhood to adopt the same MAP to fulfill the fairness criterion, as it is also easier to analyze and implement.

5.3.1 Local Leader Election under Equal MAP

From the definition of RIM in (5.3), if we assume equal MAP in user i's neighboring region, then the value of R_i is related to the number of user i's neighbors given by $N_i = \sum_{j \in \mathcal{N}} a_{ij}$. In graph theory [139], N_i is also known as the *node degree* of user i. Therefore, if the MAPs of all users in a certain neighborhood are the same and gradually increase from zero, then the one with the highest node degree in this neighborhood will dissatisfy the condition (5.3) first (here we assume that the interference relationship among users is symmetric, i.e., $a_{ij} = a_{ji}, \forall i, j$). Therefore, unless the users have homogeneous node degrees (regular graph), their RIM values cannot reach 2 at the same time. We call the user with a locally highest RIM value as a *local leader*. The key principle behind the proposed scheme is to identify these local leaders, since they are most likely to cause network instability due to interference from more neighbors. Mathematically, this means that the RIM of the local leader is more likely to exceed 2 than any of the followers in the same neighborhood. If we keep the RIM for the local leader(s) at 2, all the followers will have a RIM not exceeding 2 and according to (5.3), the network will be operating in the stable region. We next introduce how to identify these local leaders, which consists of two steps: 1) Preliminary Local Leader Election; 2) Leadership Validation.

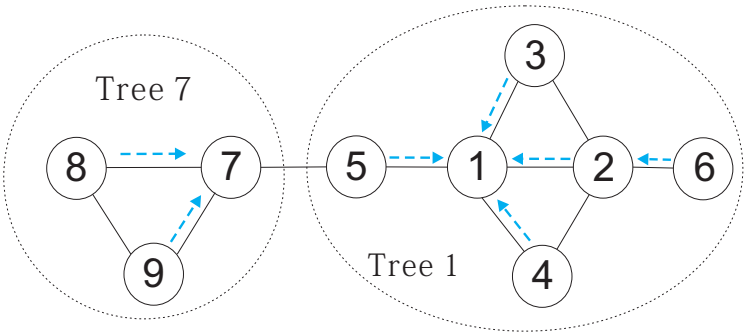

Figure 5.1: 9 Users Topology

Preliminary Local Leader Election

Only two rounds of information exchange among each user and its neighbors are needed to complete the preliminary local leader election process. In the first round, each user i broadcasts its identity number (ID) i to its neighbors. After the first round of broadcasting, each user i will be able to count its node degree N_i. In the second round, each user i broadcasts its ID i and its node degree N_i to its neighbors. Then user i will compare its node degree (and ID) with those of its neighbors. If N_i is the largest, then user i will be aware of its role as a local leader (for simplicity, when two or more candidates are connected, the one with lower ID wins). Otherwise, user i acts as a *follower* of one of its neighbors k who has the highest node degree (or neighbor which has the same node degree but lower ID). Such a user k is called the *parent* of user i, and user i is a *child* of user k. Note that a parent need not be the local leader. For the example in Fig. 5.1, user 2 is the parent of user 6, but is also a child of leader 1. As a result, the whole network is grouped into several disjoint *trees* [139] (previously we have been using the term "neighborhood"), with each local leader being the *root* of the tree, and the users with no children being the *leaves*. The tree containing leader l is thus called tree l, which behaves like an independent neighborhood. The *height* H_l of tree l is the length from the root to a leaf which is the farthest away. For the example in Fig. 5.1, there are two trees with leaders 1 and 7 being the roots respectively. The child-parent relationship is denoted by dashed blue arrows. Tree 7 has a height of 1, while tree 1 has a height of 2, with the longest path being $6 \to 2 \to 1$.

A remark to make here is that there is no requirement for each user to have the knowledge for neighbors beyond two hops. Although a neighborhood may have users at two or more hops away, there is no need for each node to know who is in the neighborhood. Once the child-parent relationship has been identified, all users

who can trace back to the same local leader define a neighborhood. The concept of a neighborhood or disjoint tree is just a virtual concept to explain the grouping of users who move as a group while adjusting their MAPs.

Leadership Validation

The essential property of a local leader l is that it has the locally highest RIM value R_l. Therefore, if $R_l \leq 2$, then all its neighbors would have a RIM value no greater than 2, hence the stability condition in (7) is satisfied. The preliminary local leader elected in the above process is the one with the highest node degree. When multiple candidates are connected, the one with the smallest ID is elected. However, choosing candidates based on smaller ID might not always guarantee the leader to have a locally highest RIM value, in cases when the tree under consideration is affected by other trees (more details will be discussed in Section 5.3.4). We therefore introduce a leadership validation mechanism to handle these exceptions.

During each iteration of update, all users monitor their own RIM values. If a user l_1 finds that $R_{l_1} > 2$, then it declares leadership and activates its PI controller to achieve $R_{l_1} = 2$. If there is a preliminary leader l_2 connected to user l_1 which hears the leadership declaration, the preliminary leader l_2 should shut down its PI controller and regard user l_1 as its parent, i.e., both users perform an exchange in the leadership. If there is no neigboring preliminary leader, user l_1 is a new leader with a separate neighborhood which consists of all its followers. In cases when two or more connected users declare leadership, the one with smaller ID wins.

An example will be given in Section 5.3.4 to illustrate the leadership validation process.

5.3.2 Control System Design

So far in the presented approach, although the theory predicts that the network can operate in the stable region, the MAP tuning process may still exhibit oscillatory behavior if improperly designed. An example is given by the heuristic algorithm in Chapter 4, in which a user is able to detect the Pareto front solution provided that it detects the sudden drop in its throughput when it gradually increases its MAP. By doing so, the network is already driven out of the stable region and the long monitoring process to collect the operating parameters will significantly affect the rate it converges to the steady state solution. To improve the tuning process, we adopt the control theoretic approach for the users to autonomously

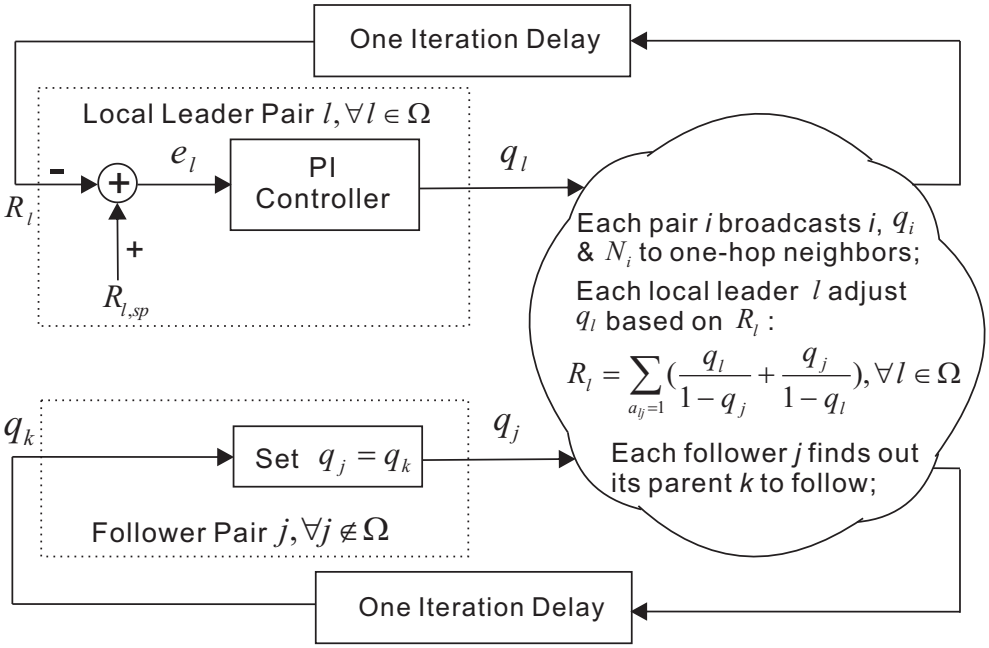

Figure 5.2: The SALE Scheme

adapt themselves toward the sub-optimal solution.

In each update iteration, each user i broadcasts its ID i, MAP q_i and node degree N_i to its neighbors. After the broadcasting, each user is able to compute its RIM value as in (5.3). Assume that the elected local leaders make up the set Ω. Each local leader $l \in \Omega$ sets its referenced RIM $R_{l,sp}$ to 2, and uses a PI controller [140, Ch.10] to adjust its MAP q_l in order to achieve $R_l = 2$. Each follower $j \notin \Omega$ follows its parent k, and sets $q_j(t+1) = q_k(t)$ (q_k ultimately follows the MAP q_l of its local leader l). Notice that when $R_l = 2$ is achieved, the RIM of the followers in tree l will not be greater than 2. If $R_l = 2, \forall l \in \Omega$, then the conditions in (5.3) will be critically satisfied, thus providing a sub-optimal network throughput. We will examine in Section 5.3.5 how close the design is to the Pareto front solution predicted by (5.1).

The control system shown in Fig. 5.2 is designed as follows. For each local leader l, the use of the PI controller is to eliminate the steady-state error [140, Ch. 10.1] while trying to achieve the desired reference signal $R_{l,sp} = 2$. The relationship between the input error signal $e_l(t) = R_{l,sp} - R_l(t)$ and the output $q_l(t)$ of the PI controller in discrete time (sampling time interval = 1) can be expressed as follows:

$$q_l(t) = K_{P,l} e_l(t) + K_{I,l} \sigma_l(t) = K_{P,l} e_l(t) + K_{I,l} \sum_{n=0}^{t} e_l(n), K_{P,l} > 0, K_{I,l} > 0, \quad (5.4)$$

where $\sigma_l(t) = \sum_{n=0}^{t} e_l(n)$ is the integral function, and $\{K_{P,l}, K_{I,l}\}$ are the proportional and integral parameters for the PI controller in leader l. Alternatively, we can use the recursive form below which requires no memory on the integral value σ_l:

$$q_l(t) = q_l(t-1) + K_{P,l}[e_l(t) - e_l(t-1)] + K_{I,l}e_l(t), K_{P,l} > 0, K_{I,l} > 0. \quad (5.5)$$

We can see from (5.4) that $q_l(t)$ stops changing after a certain time instant t_0, if and only if $e_l(t) = 2 - R_l(t) = 0, \forall t \geq t_0$ is achieved, i.e., $R_l = 2$ is achieved in the steady states. Taking z-transform on both sides of (5.4), the transfer function for the PI controller can be obtained as

$$C_{PI}(z) = Q_l(z)/E_l(z) = K_{P,l} + \frac{K_{I,l}}{1 - z^{-1}}. \quad (5.6)$$

The PI controller enables smooth adaptation of the MAP to achieve this desired RIM value. As commented by [141, p.174], when the goal is to asymptotically regulate the system output (RIM) to a "set point" ($R_{l,sp} = 2$), asymptotic regulation and disturbance rejection can be achieved by including "integral action" in the controller. Moreover, by properly tuning the PI parameters, the PI controller can achieve a good tradeoff between the response speed and stability while guaranteeing convergence, which is a major challenge when designing adaptive algorithms.

In the following two subsections, we perform the steady-state analysis, transient analysis, and PI parameter tuning for the above control system. In particular, we first consider a simple scenario with only one local leader, and then extend to more general cases with multiple local leaders.

5.3.3 Single Local Leader Case

Consider the simple case where there is only one local leader (thus only one tree) in the network. For such a network, the node degree is the highest at the local leader and decreases towards the leaves. For example, if tree 7 in Fig. 5.1 does not exist and the network only comprises of tree 1, the node degree decreases from the root (leader 1) towards the leaves (users 3, 4, 5, 6).

Steady-State Analysis

For the above scenario, the system will finally settle down with all MAPs being equal, and the RIM for the only local leader l at the steady state is given by:

$$R_l = \sum_{j=1, j\neq l}^{N} \left(\frac{a_{lj} q_l}{1-q_j} + \frac{a_{jl} q_j}{1-q_l}\right) = 2N_l \frac{q_l}{1-q_l} = R_{l,sp} = 2. \tag{5.7}$$

Therefore, when operating at the steady-state, every user has a MAP equal to

$$\tilde{q}_l = 1/(N_l + 1). \tag{5.8}$$

For the example of tree 1 in Fig. 5.1 (without tree 7), the steady-state MAPs of all users is equal to $\tilde{q}_1 = 1/(N_1 + 1) = 1/(4 + 1) = 0.2$.

In a very specific case, when the network is fully connected, the local leader l is directly connected to all the remaining users, hence $\tilde{q}_l = 1/(N_l + 1) = 1/N$, which coincides with the optimal condition in (5.1). Therefore, for any fully connected network, the SALE scheme is able to achieve a solution which falls on the Pareto front.

Throughput Sensitivity on RIM

The throughput at the local leader is

$$\theta_l = q_l (1 - q_l)^{N_l}. \tag{5.9}$$

Here we analyse the throughput sensitivity on the value of RIM around 2 at the local leader. When the RIM value is perturbed by a small value ϵ, i.e., $R_l = 2 + \epsilon$, according to (5.7), we have

$$q_l = (2 + \epsilon)/(2 + \epsilon + 2N_l). \tag{5.10}$$

Therefore, we can take the derivative of θ_l on the perturbation ϵ to observe the local sensitivity [142, p.251] of the throughput on the value of RIM at 2.

$$\frac{\partial \theta_l}{\partial \epsilon} = \frac{\partial \theta_l}{\partial q_l} \cdot \frac{\partial q_l}{\partial \epsilon} = [1 - (N_l + 1)q_l] \cdot (1 - q_l)^{N_l - 1} \cdot \frac{2N_l}{(2 + \epsilon + 2N_l)^2}. \tag{5.11}$$

From (5.11) we have

$$\frac{\partial\theta_l}{\partial\epsilon}|_{\epsilon=0} = \frac{\partial\theta_l}{\partial q_l}|_{q_l=\frac{1}{N_l+1}} \cdot \frac{\partial q_l}{\partial\epsilon}|_{\epsilon=0} = [1-(N_l+1)\frac{1}{N_l+1}]\cdot(1-\frac{1}{N_l+1})^{N_l-1}\cdot\frac{2N_l}{(2+2N_l)^2} = 0. \tag{5.12}$$

Therefore, the local sensitivity of the throughput θ_l on the value of RIM at 2 is 0, which means that the throughput θ_l is locally insensitive to small perturbations of the RIM value around 2.

Moreover, we can similarly obtain

$$\frac{\partial\theta_l}{\partial\epsilon}|_{\epsilon<0} = \frac{\partial\theta_l}{\partial q_l}|_{q_l<\frac{1}{N_l+1}} \cdot \frac{\partial q_l}{\partial\epsilon}|_{\epsilon<0} > 0, \tag{5.13}$$

$$\frac{\partial\theta_l}{\partial\epsilon}|_{\epsilon>0} = \frac{\partial\theta_l}{\partial q_l}|_{q_l>\frac{1}{N_l+1}} \cdot \frac{\partial q_l}{\partial\epsilon}|_{\epsilon>0} < 0. \tag{5.14}$$

The results from (5.12) to (5.14) suggest that the throughput θ_l is being maximized when $\epsilon = 0$, i.e., when the RIM value $R_l = 2$. Moreover, (5.13) suggests that when $\epsilon < 0$ or equivalently $R_l < 2$, there is a margin for the throughput θ_l to be improved since $\frac{\partial\theta_l}{\partial\epsilon} > 0$, i.e., the network around the location of user l is operating at a slightly underload situation. On the other hand, (5.14) suggests that when $\epsilon > 0$ or equivalently $R_l > 2$, the throughput θ_l decreases with R_l since $\frac{\partial\theta_l}{\partial\epsilon} < 0$, i.e., the network around the location of user l is operating at a slightly overload situation.

Now consider other users in the same neighborhood as user l. Firstly, if other users have the same node degree as user l (regular graph), then they are homogeneous in terms of MAP, RIM, and throughput. Therefore, their throughputs are also maximized when they have the same RIM value of 2. In such a homogeneous node degree case, the throughput under the RIM value of 2 would be on the Pareto front. On the other hand, if another user j has a smaller node degree N_j than that of user l, i.e., $N_j \leq N_l$, then the throughput of user j is

$$\theta_j = q_l(1-q_l)^{N_j}, \tag{5.15}$$

where $q_l = \tilde{q}_l = 1/(N_l+1)$ is the common MAP value in this neighborhood. Since

$$\frac{\partial\theta_j}{\partial q_l}|_{q_l=\tilde{q}_l} = [1-(N_j+1)\tilde{q}_l]\cdot(1-\tilde{q}_l)^{N_j-1} = [1-(N_j+1)\frac{1}{N_l+1}]\cdot(1-\frac{1}{N_l+1})^{N_j-1} \geq 0, \tag{5.16}$$

hence user j would be operating at the underload situation. As a result, since the

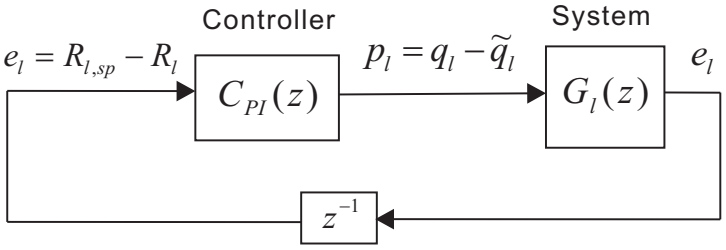

Figure 5.3: Block Diagram for the PI Controller at the Local Leader

followers normally do not fully exploit the transmission opportunities, the overall throughput solution is expected to be below the Pareto front. We will address this issue again in Section 5.3.5.

Transient Analysis

Before the system converges to the steady-state operating point, there exists a transient period in which $\underline{q}$ is varying. Here we use control theory to derive a sufficient condition to guarantee system stability. The block diagram for the PI controller at the local leader is shown in Fig. 5.3, where $C_{PI}(z)$ defined in (5.6) is the transfer function of the PI controller, $G_l(z)$ represents the transfer function of the spatial Aloha system to be controlled at the local leader l, and z^{-1} represents one sample time delay in the z-domain.

Define $p_l = q_l - \tilde{q}_l$ and $e_l = R_{l,sp} - R_l$ as the input and output of the system $G_l(z)$, respectively, where $\tilde{q}_l$ is the desired operating point given in (5.8), and p_l is a small perturbation around $\tilde{q}_l$. For simplicity of analysis, we simplify $G_l(z)$ by assuming no information propagation delay between the leader and its neighbors, i.e., $q_j(t) = q_l(t)$, $\forall j$ with $a_{l,j} = 1$. The transfer function $G_l(z)$ can then be obtained by linearising the non-linear function from (5.7):

$$R_l = (2N_l q_l)/(1 - q_l) \tag{5.17}$$

about the operating point $\tilde{q}_l$. Eq.(5.17) can be expressed using p_l and e_l as:

$$R_{l,sp} - e_l = (2N_l(p_l + \tilde{q}_l))/(1 - (p_l + \tilde{q}_l)). \tag{5.18}$$

Taking the derivative on both sides of (5.18), and evaluating at the operating point $p_l = q_l - \tilde{q}_l = 0$, we have:

$$\frac{de_l}{dt} = \frac{-2N_l}{[1 - (p_l + \tilde{q}_l)]^2}|_{p_l=0} \cdot \frac{dp_l}{dt} = \frac{-2N_l}{[1 - \tilde{q}_l]^2} \cdot \frac{dp_l}{dt} = K_l \cdot \frac{dp_l}{dt}, \tag{5.19}$$

where K_l is a constant related to N_l:

$$K_l = \frac{-2N_l}{[1-\tilde{q}_l]^2} = \frac{-2N_l}{[1-1/(N_l+1)]^2} = \frac{-2(N_l+1)^2}{N_l}. \tag{5.20}$$

Then we can discretize $e_l(t)$ and $p_l(t)$, and take the z-transform on both sides of (5.19):

$$(1-z^{-1})E_l(z) = (1-z^{-1})K_l P_l(z). \tag{5.21}$$

The transfer function $G_l(z)$ can then be obtained as:

$$G_l(z) = E_l(z)/P_l(z) = K_l. \tag{5.22}$$

In the following we study the linearized model and ensure its stability by appropriately choosing the PI parameters. Note that the stability of the linearized model guarantees that our system is locally stable, which means that small perturbations around the desired operating point $\tilde{q}_l$ can all be absorbed, i.e., the control system will eventually converge to the operating point $\tilde{q}_l$ after being perturbed.

According to the control theory [143, eq.(6.22)], we need to check that the following transfer function is stable:

$$H(z) = [1 - z^{-1}C_{PI}(z)G_l(z)]^{-1}C_{PI}(z), \tag{5.23}$$

i.e.,

$$\begin{aligned} H(z) &= [1 - z^{-1}\cdot(K_{P,l} + \frac{K_{I,l}}{1-z^{-1}})\cdot K_l]^{-1}\cdot(K_{P,l} + \frac{K_{I,l}}{1-z^{-1}}) \\ &= \frac{(K_{P,l}+K_{I,l})z^2 - K_{P,l}z}{z^2 - [1+K_l(K_{P,l}+K_{I,l})]z + K_l K_{P,l}}. \end{aligned} \tag{5.24}$$

According to the Schur-Cohn stability criterion [144, Sec. 3.2], a necessary and sufficient condition for a discrete-time system $H(z)$ to be stable is that its poles all lie within the unit circle, i.e., the roots of the characteristic equation:

$$C(z) = z^2 - [1 + K_l(K_{P,l} + K_{I,l})]z + K_l K_{P,l} = 0 \tag{5.25}$$

all lie within the unit circle in the complex z-domain. Furthermore, for a second order characteristic equation $A(z) = z^2 + a_1 z + a_2 = 0$, an equivalent stability

condition is given by the Jury's stability test [144, Theorem 3.3]:

$$a_2 < 1; \quad a_2 > -1 + a_1; \quad a_2 > -1 - a_1. \tag{5.26}$$

If we apply the Jury's stability test to (5.25), we have:

$$K_l K_{P,l} < 1 \tag{5.27}$$

$$K_l K_{P,l} > -1 - [1 + K_l(K_{P,l} + K_{I,l})] \tag{5.28}$$

$$K_l K_{P,l} > -1 + [1 + K_l(K_{P,l} + K_{I,l})] \tag{5.29}$$

Since $K_l < 0$, we only need $K_{P,l} > 0$ to satisfy (5.27). Eq. (5.29) can be equivalently reduced to $K_{I,l} > 0$. From (5.28), we have

$$-K_l(2K_{P,l} + K_{I,l}) < 2. \tag{5.30}$$

Hence a sufficient condition to guarantee stability is obtained:

$$\begin{cases} -K_l(2K_{P,l} + K_{I,l}) < 2, \\ K_{P,l} > 0, K_{I,l} > 0. \end{cases} \tag{5.31}$$

PI Parameter Tuning

In addition to guaranteeing stability, another consideration in selecting $\{K_{P,l}, K_{I,l}\}$ is to find a suitable trade-off between fast convergence and the transient oscillations. *Ziegler-Nichols* rules [140, Ch. 10.3] can be used for this purpose.

First, we compute the parameter K_U, which is defined as the $K_{P,l}$ value that leads to instability when $K_{I,l} = 0$; and the parameter T_I, which is defined as the oscillation period under these conditions. Then according to Ziegler-Nichols rules, $K_{P,l}$ and $K_{I,l}$ can be configured as follows:

$$K_{P,l} = 0.4K_U, \tag{5.32}$$

$$K_{I,l} = K_{P,l}/(0.85T_I). \tag{5.33}$$

To compute K_U, we first set $K_{I,l} = 0$ in (5.30), and we have

$$K_{P,l} < 1/(-K_l). \tag{5.34}$$

From (5.34), we take K_U as the value where the system may turn unstable:

$$K_U = 1/(-K_l). \tag{5.35}$$

Then set $K_{P,l}$ according to (5.32),

$$K_{P,l} = 0.4K_U = \frac{0.4}{-K_l} = \frac{0.4N_l}{2(N_l+1)^2} = \frac{0.2N_l}{(N_l+1)^2}. \tag{5.36}$$

With the $K_{P,l}$ value that renders the system unstable, a given set of input values may take great changes up to every time interval, yielding an oscillation period of two time intervals ($T_I = 2$). Then from (5.33),

$$K_{I,l} = \frac{K_{P,l}}{0.85T_I} = \frac{K_{P,l}}{1.7} = \frac{0.4}{1.7(-K_l)} = \frac{2N_l}{17(N_l+1)^2}. \tag{5.37}$$

In summary, using the $\{K_{P,l}, K_{I,l}\}$ values given in (5.36) (5.37), the SALE scheme is guaranteed to converge fast to a stable steady-state operating point given in (5.8).

5.3.4 Multiple Local Leaders Case

In order to study the scalability of the SALE scheme, we consider more general cases where there are multiple local leaders in the network. We use the simple example given in Fig. 5.1, with users 1 and 7 being the local leaders.

Steady-State Analysis

We have illustrated that after the local leader election process, the whole network is partitioned into several disjoint trees or neighborhoods. However, these trees are disjoint but their MAPs are not necessarily independent of each other. In our SALE scheme, the MAPs of all users in tree l are controlled by leader l, who adjusts its q_l based on R_l, which only involves the neighbors of leader l. Therefore, if leader l is not directly connected to a user in other trees, then the MAP in tree l will not be affected by other trees. For Fig. 5.1, the MAP in tree 1 is not affected by tree 7, however, the steady-state MAP of leader 7 is affected by user 5 which is a follower

in tree 1.

The steady state of the SALE scheme can then be determined as follows. For those independent trees, the analysis in Section 5.3.3 is readily applied to obtain the steady states. For leader l_1 who is affected by user m in tree l_2 (which happens normally when $N_{l_1} \leq N_{l_2}$), it should wait until the steady state of $\tilde{q}_m = \tilde{q}_{l_2}$ is calculated before calculating $\tilde{q}_{l_1}$ based on $R_{l_1} = 2$. To achieve the same RIM level $R_{l_1} = R_{l_2} = 2$ with a smaller node degree $N_{l_1} \leq N_{l_2}$, leader l_1 should have $\tilde{q}_{l_1} \geq 1/(N_{l_1}+1) \geq \tilde{q}_{l_2}$ in general. For Fig. 5.1, the steady state MAP in tree 1 can be obtained from (5.8) as $\tilde{q}_i = 1/(N_1+1) = 1/(4+1) = 0.2, \forall i \in \{1, \cdots, 6\}$. Then for leader 7,

$$R_7 = \sum_{j=5,8,9} \left(\frac{q_7}{1-q_j} + \frac{q_j}{1-q_7}\right) = 4 \cdot \frac{q_7}{1-q_7} + \frac{q_7}{1-\tilde{q}_5} + \frac{\tilde{q}_5}{1-q_7}. \tag{5.38}$$

By setting $R_7 = 2$ and substituting in $\tilde{q}_5 = 0.2$, we have $\tilde{q}_7 = 0.2598$. Thus the steady state MAP in tree 7 is $\tilde{q}_i = 0.2598, \forall i \in \{7, 8, 9\}$. It is easily verified that $\tilde{q}_7 > 1/(N_7+1) = 0.25 > \tilde{q}_1$. Notice that the steady state MAP in tree 7 is *not* trivially equal to $1/(N_7+1)$ as in the single leader case. Fortunately, our control system is able to converge to the steady state *automatically*.

Now consider adding another user 10 as a neighbor of user 8, as shown in Fig. 5.4. Here user 1 and user 7 are the preliminary local leaders. User 8 now has the same node degree as user 7, but user 7 is still elected as the preliminary local leader due to its smaller ID. As shown in the above analysis, the preliminary local leader 7 would push the MAP in the tree to be $\tilde{q}_i = 0.2598, \forall i \in \{7, 8, 9, 10\}$, which achieves $R_7 = 2$ but this would push the RIM of user 8 to $R_8 = 2.1$, which is higher than 2 and hence should be avoided. Somewhere in the process of following the MAP of user 7, user 8 should find itself a more suitable local leader than user 7. This example shows that the leadership should not be finalized simply based on smaller ID. In such a case, the leadership should be handed over to user 8. For the above example, in the midst of updating, when user 8 detects $R_8 > 2$, it declares leadership and activates its PI controller to achieve $R_8 = 2$. The preliminary leader 7 becomes a follower whose parent is the new leader 8. For simplicity, the child-parent relationship is only adjusted between the new and old leaders, while other followers stick to their original parent. For example, follower 9's parent is still user 7. The new child-parent relationship is shown in Fig. 5.4. Notice that after the leadership handover, the new leader 8 is not connected to any users in tree 1, hence the MAP in tree 8 becomes independent of tree 1. The equilibrium MAP in the

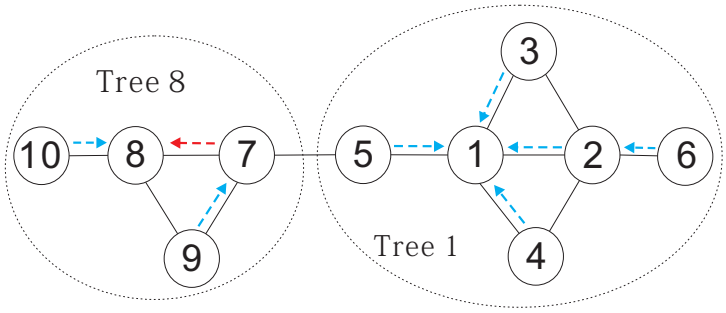

Figure 5.4: 10 Users Topology

tree led by leader 8 is 0.25, while $R_8 = 2$ and $R_7 = 1.91$.

Transient Analysis and PI Parameter Tuning

The stability is guaranteed through the following argument. When all trees are independent, the transient analysis and PI parameter tuning in each tree follow those in Section 5.3.3, hence stability is guaranteed. Each local leader l has its own PI controller, with the parameters $K_{P,l}, K_{I,l}$ given in (5.36) and (5.37), respectively. Again the PI parameter tuning only relies on the local information N_l, hence can be immediately performed after the local leader election. In particular, the system transfer function to be controlled at the local leader l_1 follows (5.22) after applying (5.20):

$$G_{l_1}(z) = K_{l_1} = -2(N_{l_1} + 1)^2/N_{l_1}. \tag{5.39}$$

If leader l_1 is affected by user m in tree l_2 (e.g., see Fig. 5.1), this happens normally when $N_{l_1} \leq N_{l_2}$. In this case, tree l_2 is independent of tree l_1, but tree l_1 depends on tree l_2 through user m. Tree l_2 reaches the steady state first, with $\tilde{q}_m = \tilde{q}_{l_2} \leq 1/(N_{l_1} + 1)$, which remains constant afterwards. For tree l_1, due to the impact of $\tilde{q}_m$, from (5.17) the RIM parameter for leader l_1 becomes:

$$R'_{l_1} = \sum_{j=1, j\neq l_1}^{N} \left(\frac{a_{l_1 j} q'_{l_1}}{1 - q_j} + \frac{a_{j l_1} q_j}{1 - q'_{l_1}}\right) = \frac{2(N_{l_1} - 1) q'_{l_1}}{1 - q'_{l_1}} + \frac{q'_{l_1}}{1 - \tilde{q}_m} + \frac{\tilde{q}_m}{1 - q'_{l_1}}, \tag{5.40}$$

where $\tilde{q}_m$ is now a constant, i.e., $d\tilde{q}_m/dt = 0$. In (5.40), we have used $'$ to denote the respective parameters to differentiate from the independent case. As a result of *fewer neighboring followers*, R'_{l_1} reacts more slowly to q'_{l_1} than in the independent case, hence we expect the absolute gain $|K_{l_1}|$ of the system $G_{l_1}(z)$ to decrease.

Specifically, if we apply the same linearisation procedure in Section 5.3.3 to

(5.40), then the system $G'_{l_1}(z)$ to be controlled at the local leader l_1 is:

$$G'_{l_1}(z) = K'_{l_1} = -\frac{2(N_{l_1}-1)}{(1-\tilde{q}'_{l_1})^2} - \frac{1}{1-\tilde{q}_m} - \frac{\tilde{q}_m}{(1-\tilde{q}'_{l_1})^2}, \tag{5.41}$$

where $\tilde{q}'_{l_1}$ is the operating point that achieves $R'_{l_1} = 2$ in (5.40). It can be verified using Mathematica [145] that $|K'_{l_1}| < |K_{l_1}|$ for all $N_{l_1} \geq 2$ and $0 \leq \tilde{q}_m \leq 1/(N_{l_1}+1)$. Similar results can be verified if leader l_1 is affected by more neighbors $m_1, m_2, \cdots$ that belong to other trees.

Then the PI parameters $\{K'_{P,l_1}, K'_{I,l_1}\}$ that guarantee system stability can be set from (5.36) and (5.37):

$$K'_{P,l_1} = \frac{0.4}{-K'_{l_1}} > \frac{0.4}{-K_{l_1}} = K_{P,l_1} = \frac{0.2N_{l_1}}{(N_{l_1}+1)^2}, \tag{5.42}$$

$$K'_{I,l_1} = \frac{0.4}{-1.7K'_{l_1}} > \frac{0.4}{-1.7K_{l_1}} = K_{I,l_1} = \frac{2N_{l_1}}{17(N_{l_1}+1)^2}. \tag{5.43}$$

Since $\{K_{P,l_1}, K_{I,l_1}\}$ are easy to obtain using N_{l_1} only, leader l_1 uses $\{K_{P,l_1}, K_{I,l_1}\}$ in practice. More importantly, since the current system $G'_{l_1}(z)$ has a smaller absolute gain $|K'_{l_1}|$ due to fewer neighboring followers, leader l_1 is using the less aggressive PI parameters $\{K_{P,l_1}, K_{I,l_1}\}$ (see Section 5.3.3) and hence system stability is guaranteed.

Throughput Sensitivity on RIM

Following the above settings, assume that the local leader l_1 is affected by user m in tree l_2, whose steady state MAP is $\tilde{q}_m$. The throughput at the local leader l_1 is

$$\theta'_{l_1} = q'_{l_1}(1-q'_{l_1})^{N_{l_1}-1}(1-\tilde{q}_m). \tag{5.44}$$

When the RIM value in (5.40) is perturbed by a small value ϵ around 2, i.e., $R'_{l_1} = 2+\epsilon$, by taking derivative on both sides of (5.40), we have

$$\frac{\partial q'_{l_1}}{\partial \epsilon} = -\frac{1}{K'_{l_1}} > 0. \tag{5.45}$$

Therefore, the derivative of θ'_{l_1} on the perturbation ϵ is

$$\frac{\partial \theta'_{l_1}}{\partial \epsilon} = \frac{\partial \theta'_{l_1}}{\partial q'_{l_1}} \cdot \frac{\partial q'_{l_1}}{\partial \epsilon} = (1-N_{l_1}q'_{l_1}) \cdot (1-q'_{l_1})^{N_{l_1}-2} \cdot (1-\tilde{q}_m) \cdot (-\frac{1}{K'_{l_1}}). \tag{5.46}$$

Notice that when $\epsilon = 0$, i.e., $R'_{l_1} = 2$, it can be verified from (5.40) that the operating point $\tilde{q}'_{l_1}$ should be no greater than $1/N_{l_1}$. Therefore, the local sensitivity of the throughput θ'_{l_1} on the RIM value R'_{l_1} around 2 is

$$\frac{\partial \theta'_{l_1}}{\partial \epsilon}|_{\epsilon=0} = \frac{\partial \theta'_{l_1}}{\partial q'_{l_1}}|_{q'_{l_1} \leq \frac{1}{N_{l_1}}} \cdot \frac{\partial q'_{l_1}}{\partial \epsilon}|_{\epsilon=0} \geq (1 - N_{l_1} \cdot \frac{1}{N_{l_1}}) \cdot (1 - \frac{1}{N_{l_1}})^{N_{l_1}-2} \cdot (1 - \tilde{q}_m) \cdot (-\frac{1}{K'_{l_1}}) = 0. \tag{5.47}$$

Therefore, in such cases there are still some margins for the throughput θ'_{l_1} to be improved, i.e., the network around the location of leader l_1 is operating at a slightly underload situation. Similar conclusions can be drawn when the leader l_1 is affected by more users in other trees. In the next subsection we discuss how close the throughput solution obtained by SALE is to the Pareto front.

5.3.5 "Distance" to Pareto Front

The Pareto front surface is obtained if we apply the sufficient and necessary testing criteria (5.1) to the network. Any point on this surface is the combination of throughputs which can be achieved by all users while keeping the network operating in a stable condition. The solution obtained in SALE generally stays below the Pareto front due to two reasons. First, the stability criteria (5.3) used in implementing the algorithm is only a sufficient condition. Second, some of the followers (especially those who are further away from the leader) may not have fully exploited the transmission opportunities. Hence, the feasible throughput region obtained by SALE is only a subset to that obtained by using (5.1).

Based on the sensitivity analysis in Section 5.3.3 and Section 5.3.4, in the homogeneous node degree case (regular graph), the users are homogeneous in terms of MAP, RIM, and throughput. Since the throughput solution for all users all have a RIM value of 2, the solution would stay on the Pareto front. However, in most practical cases where there are variations in the node degrees of users, the local leader election allows partitioning the network into several local neighborhoods. Each local leader, which has the highest node degree in its neighborhood, uses a PI controller to achieve a RIM value of 2. The remaining nodes in the same neighborhood have a smaller node degree than its local leader, and will have a RIM value no greater than 2. This suggests that normally the followers are operating at the underload condition, or at a distance below the Pareto front obtained by using (5.1).

We attempt to characterize such a throughput margin with the optimal one obtained in (5.1) by defining the "distance to Pareto" d_{pareto}. When we obtain

a solution $\underline{\theta} = [\theta_1, \theta_2, \cdots, \theta_N]$ in the SALE scheme, we continue to move in the direction $d \cdot \underline{\theta}$ ($d \geq 1$, i.e., proportionally increase the throughput of all users) until we find an operating point $\underline{q}$ that achieves $d_{pareto} \cdot \underline{\theta}$, and beyond this point there is no stable solution. In particular, when $d_{pareto} = 1$, the solution is on the Pareto front. As will be shown in the simulation results, the SALE scheme achieves a close-to-Pareto-front throughput, with d_{Pareto} below 1.05 for most of the topologies, i.e., we usually can obtain a solution which is less than 5% below the Pareto front.

5.3.6 Complexity, Scalability and Overhead of SALE

We summarize the SALE scheme in Algorithm 5.1. The proposed scheme shows the following advantages:

Low Implementation Complexity

a) It takes only two rounds of information exchange among each user and its neighbors to complete the preliminary local leader election. *b)* In each iteration, each user only needs to broadcast its ID, MAP, and node degree to its neighbors. *c)* Each user only uses information about its neighbors to update its MAP in each iteration. *d)* Each leader l implements a simple PI controller to adjust its MAP q_l so as to achieve $R_l = 2$, which corresponds to a throughput close to the Pareto front. *e)* The PI parameter tuning can be autonomously done by the local leader itself based on its node degree N_l, which guarantees stability and fast convergence. *f)* Each follower j only needs to find its parent k, and simply sets $q_j(t+1) = q_k(t)$ in each iteration. *g)* Only in some situations, there is a need to change the local leader. Therefore, the SALE scheme can be implemented autonomously with low complexity.

High Scalability

a) The SALE scheme is fully autonomous without any centralized controller. *b)* The whole network is grouped into several disjoint trees, within each tree there is a local leader controlling the MAPs in this tree. *c)* The Ziegler-Nichols rules adapt the PI parameters in (5.36) (5.37) to various user densities (associated with different node degree N_l at the local leader), thus guaranteeing fast convergence of MAPs at the local leaders. *d)* Given a certain user density, if the number of users increases, the number of local leaders also increases correspondingly, i.e., the whole network is grouped into more trees. As a result, the average number of users

Algorithm 5.1 The SALE Scheme

Preliminary Local Leader Election:
Each user i broadcasts its ID to its neighbors;
Each user i counts its number of neighbors (node degree) N_i;
Each user i broadcasts its ID and node degree N_i to its neighbors;
Each user i compares N_i with the node degrees of its neighbors. If N_i is the largest, then user i is elected as a local leader. Otherwise, user i is a follower, whose parent is the neighbor with the largest node degree. In cases when two or more candidates are connected, the one with smaller ID wins. Assume the local leaders make up a set $\Omega \subset \mathcal{N}$.

Control System:
$R_{l,sp} = 2$, $K_{P,l} = 0.2N_l/(N_l+1)^2, K_{I,l} = 2N_l/[17(N_l+1)^2], \forall l \in \Omega$;
$t = 0$, $\underline{q}(t) = \underline{0}$; $Declare_i = 0, \forall i \in \mathcal{N}$;
repeat:
    Each user i broadcasts its MAP $q_i(t)$ to its neighbors;
    Each user i computes $R_i(t) = \sum_{j=1,j\neq i}^{N}[a_{ij}q_i(t)/(1-q_j(t)) + a_{ji}q_j(t)/(1-q_i(t))]$;
    for each local leader $l \in \Omega$ **do**:
        $e_l(t+1) = R_{l,sp} - R_l(t)$;
        $q_l(t+1) = q_l(t) + K_{P,l}[e_l(t+1) - e_l(t)] + K_{I,l}e_l(t+1)$;
    end for
    for each follower $j \notin \Omega$ **do**:
        $q_j(t+1) = q_k(t)$, where user k is the parent of user j;
    end for

    Leadership Validation:
    for each user $i \in \mathcal{N}$ **do**:
        if $Declare_i = 1$ **then**:
            User i joins Ω and becomes a local leader. In cases when two or more connected users declare leadership, the one with smaller ID wins.
        else if user $i \in \Omega$ and its neighbor declares leadership **then**:
            the preliminary leader i quits from Ω, and follow the newly declared leader;
        end if
        if $R_i(t) > 2$ **then**:
            mark $Declare_i = 1$ and declare leadership in the next round of broadcast;
        else$Declare_i = 0$;
        end if
    end for

    $t = t + 1$;
until Convergence, i.e., $R_l(t) = R_{l,sp}, \forall l \in \Omega$.

in a tree, as well as the tree height, will not change significantly as the network size grows. Therefore, when a local leader l reaches the steady state ($R_l = 2$), the corresponding MAP q_l would not take too many hops to reach all the followers in tree l. *e)* As we will see in Section 5.4.4, the SALE scheme converges in around 30 iterations, regardless of the user density or the number of users in the network. Therefore, the SALE scheme provides fast convergence with high scalability.

Overhead of Information Exchange

The SALE scheme requires local information exchange for leader election and MAP adaptation. The local leader election requires two rounds of local information exchange about node ID and node degree. Thereafter, the MAP adaptation requires each user to broadcast its ID and MAP to its one-hop neighbors.

As mentioned in [146] to handle the case with information exchange, slotted Aloha usually has a framed structure consisting of a control phase for the information exchange and a normal phase for data transmission. In our case, we embed the message in the packet header. In a simplified model, assume that each packet originally (i.e. in the heuristic approach) has a header field and constant packet size, which at least contains the user ID or address. For the need of our algorithm, we add three subfields to the header, i.e., node degree subfield, MAP subfield and leadership declaration subfield, and each occupies 8 bits, 16 bits and 1 bit, respectively. We further assume each packet occupies a time slot and has a packet size of L_S bits, e.g., 250 bytes = 2000 bits, the newly added fractional overhead is then given by $25/L_S$=25/2000=0.0125.

The message exchange is realized in the following way. In each time slot, each user either sends a message to its neighbors according to its MAP, or listens to the channel to receive a message from its neighbors. Assume that each iteration in the SALE scheme corresponds to packet transmissions in L_F slots which is known as a frame, and all users are frame-synchronized. Since the transmission of a packet is subject to collision, some packets (and hence the added subfields) will not be received correctly by some users. However, for a sufficiently large L_F value, each user is likely to receive at least one packet from all its neighbors and hence gather enough information about all its neighbors through the subfields embedded in the received packets. By the end of each iteration, all users then update the MAP subfields for the next iteration according to the SALE scheme. Since the SALE scheme relies on an accurate estimation of node degree, we assume that each user counts and updates its node degree in every L_{ND} slots. L_{ND} can be chosen to be sufficiently

large to guarantee an accurate estimation of node degree. In our simulations, we choose $L_{ND} = 10L_F$ slots (i.e., 10 iterations) to guarantee an accurate estimation.

5.4 Performance Evaluation

In the simulations we assume the channel bit rate is r_b=20 Mbps, and each packet in slotted Aloha has L_S=2000 bits. Then the slot time is $L_S/r_b = 0.1$ ms. Each iteration in the SALE scheme corresponds to a frame of $L_F = 100$ slots (i.e., 10 ms), and the users are frame-synchronized. Each user counts and updates its node degree in every $L_{ND} = 10L_F = 1000$ slots (i.e., 10 iterations).

5.4.1 Parameter Tuning: Stability and Convergence Time

In Section 5.3 we claim that the PI parameters given in (5.36) (5.37) are able to guarantee system stability as well as fast convergence to the steady-state operating point. Here we illustrate this by using the example in Fig. 5.4. Three sets of PI parameters are used in the PI controllers respectively: $\{K_{P,l}/5, K_{I,l}/5\}$, $\{K_{P,l}, K_{I,l}\}$, and $\{5K_{P,l}, 5K_{I,l}\}$, where $\{K_{P,l}, K_{I,l}\}$ are obtained by (5.36) (5.37). The algorithm starts with small initial MAPs, e.g., $q_i = 0.05, \forall i$. The transient behaviors of R_1 are plotted in Fig. 5.5. Notice that each iteration in the SALE scheme corresponds to packet transmissions in $L_F = 100$ slots. The value of L_F is arbitrary and with the purpose to safe-guard the correct reception of neighbors' information in each iteration. This is similar to the use of L_{ND}. In fact, instances of message passing failure in a frame are rarely captured in our simulations. In the rare occasion if it happens, the transient variations caused by the delay of MAP feedback are well handled by the control system.

From Fig. 5.5 we can see that $\{K_{P,l}, K_{I,l}\}$ obtained by (5.36) (5.37) enable the system to converge to the steady state ($R_1 = 2$) within 30 iterations, i.e., 0.3s. In contrast, the conservative PI parameters $\{K_{P,l}/5, K_{I,l}/5\}$ take around 120 iterations (i.e., 1.2s) for the system to converge, while the aggressive PI parameters $\{5K_{P,l}, 5K_{I,l}\}$ render the system unstable. Similar results are observed for more complicated topologies, e.g., the 50 users case in Fig. 5.8 that will be introduced in Section 5.4.4. Therefore, the PI parameters given by (5.36) (5.37) indeed guarantee system stability with fast convergence.

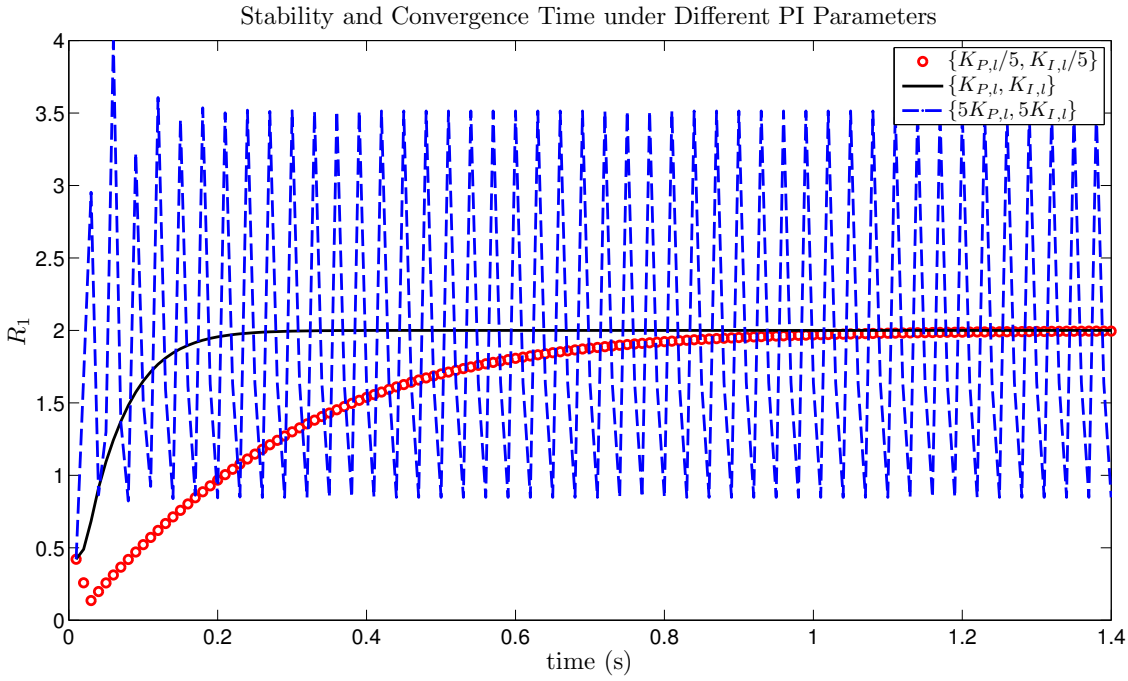

Figure 5.5: Stability and Convergence Time under Different PI Parameters

5.4.2 Steady State, Optimality and Fairness

For the same example given in Fig. 5.4, we demostrate more details about the steady state, throughput optimality and fairness among the users. The transient behaviors of RIM R_i, MAP q_i and throughput θ_i are plotted in Fig. 5.6 for users 1, 5, 7 and 8, respectively.

It takes around 40 iterations (i.e., 0.4s) for the system to converge. The preliminary local leader election can be completed in the first 10 iterations, in which each user counts its own node degree and exchanges information with its neighbors. Starting from the 11-th iteration, the PI controllers in leader 1 and leader 7 start working. At the 28-th iteration, user 8 (green line in Fig. 5.6) detects $R_8 > 2$ and takes over the leadership from the preliminary leader 7 (red diamond in Fig. 5.6). In the steady state, leader 1 and 8 have $R_1 = R_8 = 2$; the follower 5 has $R_5 = 1.08$ and has MAP $\tilde{q}_5 = \tilde{q}_1 = 0.2$; the follower 7 has $R_7 = 1.91$ and MAP $\tilde{q}_7 = \tilde{q}_8 = 0.25$. Regarding the throughput, generally the users with a higher node degree would have a lower throughput due to contentions from more neighbors. In this example, $\theta_1 < \theta_8 < \theta_7 < \theta_5$.

The distance to Pareto front d_{Pareto} is used to evaluate the throughput optimality. For our SALE scheme applied to Fig. 5.4, $d_{Pareto} = 1.02$, which suggests only 2% loss between the achieved throughput $\underline{\theta}$ and the Pareto front. Therefore,

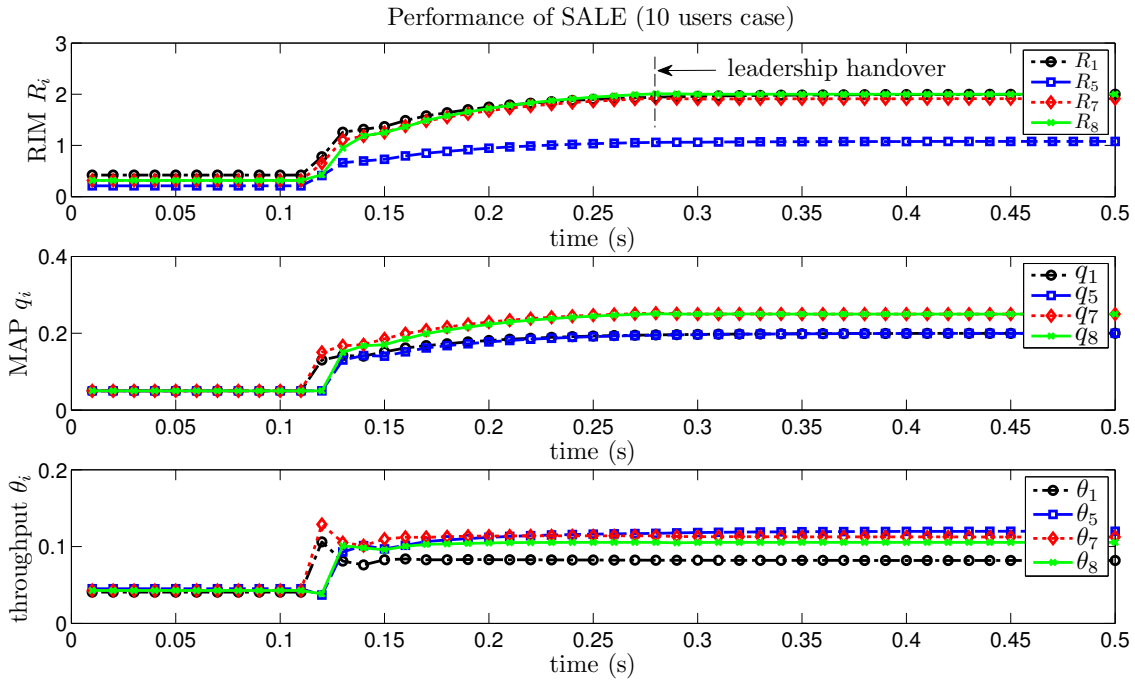

Figure 5.6: Performance of SALE, Topology in Fig. 5.4

although the sub-optimal condition (5.3) is used in our design, the result is very close to the actual optimal.

We also evaluate the throughput fairness among the users. When spatial reuse is considered, different users at different spatial locations usually have different connectivity. As a result, those users with a higher node degree usually receive more interference and consequently a lower throughput than those with a lower node degree. Therefore, it is difficult to give an exact measurement of fairness in such a heterogeneous network. We make an attempt to take this spatial characteristic into consideration, and weigh each user i's throughput by $N_i + 1$ (including user i and its neighbors), i.e., we define the *weighted throughput* for each user i as:

$$\tilde{\theta}_i = (N_i + 1) \cdot \theta_i, \forall i \in \mathcal{N}. \tag{5.48}$$

Then we compute the Jain's fairness index [147] for the weighted throughput $\underline{\tilde{\theta}}$:

$$Jain(\underline{\tilde{\theta}}) = \frac{(\sum_{i=1}^{N} \tilde{\theta}_i)^2}{N \cdot \sum_{i=1}^{N} \tilde{\theta}_i^{\,2}}. \tag{5.49}$$

Jain's index rates the fairness of an array of values $\underline{\tilde{\theta}} = [\tilde{\theta}_1, \tilde{\theta}_2, \cdots, \tilde{\theta}_N]$ where there are N users and $\tilde{\theta}_i$ is the weighted throughput for the ith user. The result ranges from $1/N$ (worst case) to 1 (best case), and it is maximum when all users receive

Table 5.1: Performance Comparison between the SALE Scheme and the Heuristic Algorithm

Topology	Scheme	$\overline{\theta_i}$	$\Sigma\theta_i$	$\overline{\theta}_{net,i}$	$Jain(\underline{\tilde{\theta}})$	d_{Pareto}	T_{conv}
Fig. 5.4	SALE	0.1246	1.2459	0.1230	0.9921	1.02	∼0.4s
	Heuristic	0.1158	1.1582	0.1158	0.9685	1.045	∼60s
Fig. 5.8	SALE	0.0578	2.8888	0.0571	0.9906	1.025	∼0.4s
	Heuristic	0.0535	2.6733	0.0535	0.9593	1.04	∼90s

the same allocation. For our SALE scheme applied to Fig. 5.4, $Jain(\underline{\tilde{\theta}}) = 0.9921$, which is close to 1 and suggests good fairness among the users.

5.4.3 Comparison with Heuristic Algorithm

Here we apply the heuristic algorithm in Chapter 4 to the same example in Fig. 5.4 and compare performance with the SALE scheme shown in Fig. 5.6. The algorithm in Chapter 4 assumes no information exchange among the users, and the users adapt their MAPs based on the measured throughput and channel idle rate, which require a relatively accurate estimation. In the simulations we choose each estimation period to consist of $L_I = 1000$ slots so that the adaptation in the heuristic algorithm works properly. Since the slot time is 0.1ms, each estimation period lasts 0.1s.

The transient states of the heuristic algorithm for user 1 are plotted in Fig. 5.7. As the users heuristically search for the Pareto front, the system experiences several fluctuations before settling down. The convergence time T_{conv} takes around 600 estimation periods, i.e., around 60s, which is much longer than that of the SALE scheme. Since other users experience similar transient states as user 1, their behaviors are not plotted for brevity. The steady-state performance is summarized in the upper part of Table 5.1 for the SALE scheme and the heuristic algorithm. Both schemes achieve a throughput $\underline{\theta}$ close to the Pareto front ($d_{Pareto} = 1.02, 1.045$ respectively), while the SALE scheme provides better fairness for the users (the heuristic algorithm has a lower Jain's index = 0.9685). Since the SALE scheme has an additional information exchange overhead of $25/L_S$=25/2000=0.0125, we also compare the average net throughput $\overline{\theta}_{net,i}$ in the table. Note that we assume both approaches use the same header except the three additional subfields in the SALE scheme, and the common parts of the header are included in computing the net throughputs.

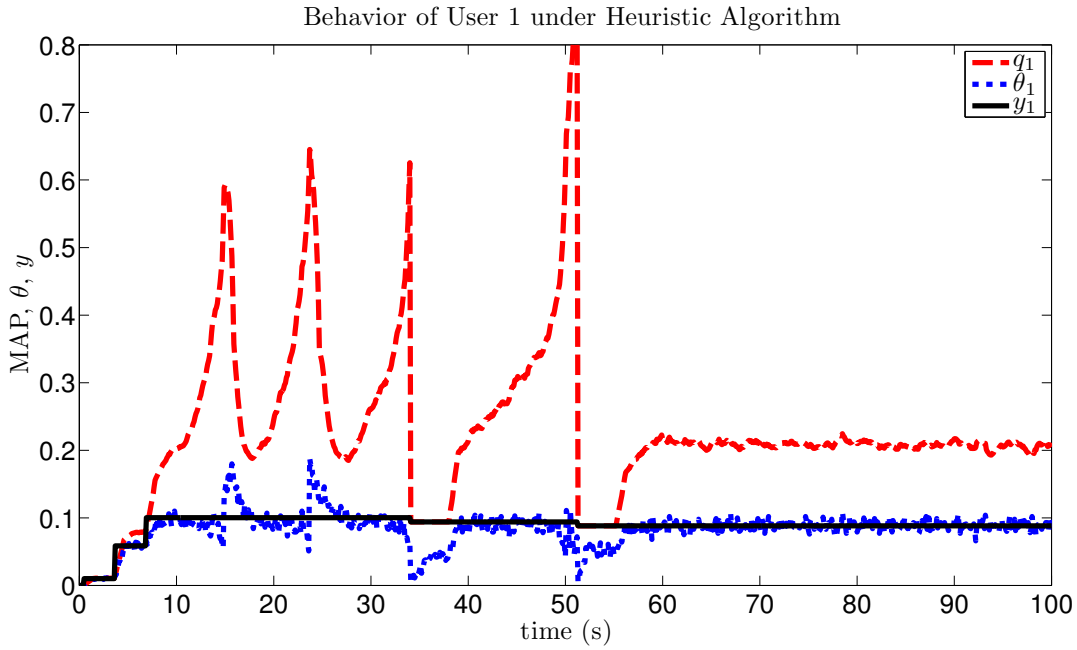

Figure 5.7: Performance of the Heuristic Algorithm, Topology in Fig. 5.4

5.4.4 Scalability of SALE

50 Users Case

Consider a distributed network with N users, which are randomly placed in a square region of a given area. For simplicity, we assume that all the distances between any transmitter and its designated receiver are much smaller than the distances between any two transmitters, so that a Tx-Rx pair (user) can be represented by a single node in the topology. We further assume that all users have transmission range of 5 unit length, and those users who are in each other's transmission range will have significant interference on each other, and the two users are said to be connected. Based on the above assumptions, we can generate a random connected topology with 50 users in a square region of area 500 (units), as plotted in Fig. 5.8.

We apply the SALE scheme to Fig. 5.8, and the whole network is shown to be grouped into 4 trees, governed by leaders $l \in \Omega = \{11, 17, 27, 42\}$ respectively. The users in different trees are marked by different shapes and colors, e.g., the largest tree is marked with red triangles, which is governed by leader 11 with the highest node degree $N_{11} = 10$. For clarity, the child-parent relationship is not shown in the figure. For comparison, we also apply the heuristic algorithm to the example in Fig. 5.8. The performances of the two schemes are summarized in the lower part of Table 5.1.

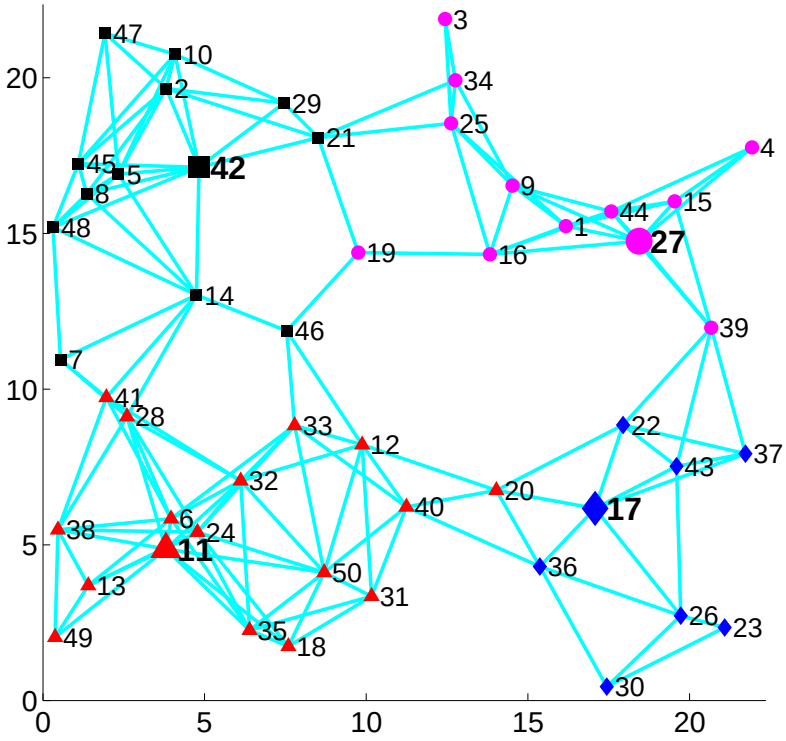

Figure 5.8: Randomly Generated Connected Topology with 50 Users

The heuristic algorithm converges in around 90s, longer than the 10 users case in Fig. 5.4. Therefore, the convergence time increases with the network size in the heuristic algorithm. In contrast, the SALE scheme still converges in around 0.4s, thus is more efficient as the network size increases. After the system converges, both schemes achieve throughputs $\underline{\theta}$ close to the Pareto front ($d_{Pareto} = 1.025, 1.04$ respectively), while the SALE scheme provides better fairness for the users, with a higher Jain's index $0.9906 > 0.9593$.

100 Users with Various User Density

We define the *user density* as the number of users per unit area. For the 50 users case above, the user density is 50/500=0.1. Now we generate a sequence of random connected topologies with various user density, by randomly scattering 100 users in a square region of various areas. In particular, when the square region has an area of 12.5, the network becomes fully connected (the diagonal line length is equal to the transmission range of 5). We apply the SALE scheme to these topologies and summarize the results in the upper part of Table 5.2.

As the user density increases from 0.1 to 8 (tend to a fully connected network), the network is grouped into fewer but bigger trees, and the maximum height of all

Table 5.2: Scalability of the SALE Scheme

Users	Area	Density	$\Sigma\theta_i$	$Jain(\underline{\tilde{\theta}})$	d_{Pareto}	T_{conv}	Leaders	Max. H_l
100	12.5	8	0.3697	1.0000	1	∼0.8s	1	1
	31.25	3.2	0.4075	0.9998	1.00	∼0.8s	1	2
	62.5	1.6	0.5240	0.9912	1.03	∼0.8s	1	2
	125	0.8	0.9246	0.9881	1.05	∼0.4s	1	2
	250	0.4	1.4922	0.9795	1.055	∼0.4s	1	4
	500	0.2	2.5146	0.9856	1.04	∼0.4s	2	4
	1000	0.1	5.1930	0.9823	1.02	∼0.4s	5	5
200	2000	0.1	9.9504	0.9800	1.01	∼0.4s	12	5
400	4000		18.8848	0.9692	1.01	∼0.4s	22	8
600	6000		27.2568	0.9757	1.02	∼0.4s	32	5
800	8000		37.2249	0.9771	1.015	∼0.4s	49	5
1000	10000		45.7275	0.9799	1.01	∼0.4s	54	5

trees gradually decreases to 1. As the user density increases, the total throughput decreases due to increased interference from more neighbors experienced by each user. However, regardless of the user density, the number of iterations for convergence is still around 40 iterations. Such fast convergence is guaranteed by the Ziegler-Nichols rules which adapt the PI parameters in (5.36) (5.37) to various user densities (associated with different node degree N_l at the local leader).

Note that as the user density increases above 1.6, the individual throughput drops significantly, and the probability of packet collision increases and affects the success rate of passing the subfield information. Hence we have to choose a larger frame of $L_F = 200$ slots in each iteration for the proposed SALE scheme. As a result, each iteration in these high-density topologies now takes 20ms and the convergence time is around 0.8s. Also note that similar problems exist for the heuristic algorithm in dense topologies, in which the individual user throughput is relatively small. To acquire a relatively accurate estimation for a small value of user throughput, a longer estimation period is required so as to suppress the relative error and keep the variance of the estimated throughput at a low level, in order for the MAP adaptation in the heuristic algorithm to work properly.

On the other hand, regardless of the user density, the network still achieves close-to-Pareto-front throughput, with d_{Pareto} around 1.05, i.e., only 5% below the Pareto front. In particular, d_{Pareto} is equal to 1 in the fully connected case, thus verifying the statement in Section 5.3.3 that our SALE scheme achieves a throughput on the Pareto front in a fully connected network. Finally, the SALE scheme provides good fairness for all users, with Jain's index around 0.98 (close to 1).

200∼1000 Users Cases

Here we keep the user density as 0.1, and increase the number of users by enlarging the area under consideration. Then we generate a sequence of random connected topologies with N=200, 400, 600, 800 and 1000, respectively. We apply the SALE scheme to these topologies and summarize the results in the lower part of Table 5.2.

From Table 5.2 we can see that, as the number of users increases, the number of local leaders also increases correspondingly, i.e., the whole network is grouped into more trees. As a result, the average number of users in a tree, as well as the tree height, will not change significantly as the network size grows. This is verified in Table 5.2 that the maximum tree height H_l remains around 6 regardless of the network size. Therefore, when a local leader l reaches the steady state ($R_l = 2$), the corresponding MAP q_l would only take around 6 hops to reach all the followers in tree l. From Table 5.2, the SALE scheme converges in around 40 iterations, i.e., 0.4s, regardless of the network size. Therefore, the SALE scheme provides fast convergence with high scalability.

In the steady state, the SALE scheme achieves a throughout $\underline{\theta}$ close to the Pareto front, with d_{Pareto} around 1.02 for all cases. Consequently, the total throughput $\Sigma\theta_i$ increases almost linearly with the number of users in the network. Meanwhile, the Jain's index is around 0.97 for all cases, suggesting good fairness among the users.

5.5 Conclusions

This chapter focuses on spatial Aloha networks, and attempts to approach global optimization of network throughput based on limited spread of local information and realize the model's quick convergence and stability. The SALE scheme is introduced, which can be autonomously implemented by users using only local information. Specifically, a user with maximum node degree in a certain neighborhood is elected as the local leader, and the remaining users in this neighborhood simply follow the same MAP. The SALE scheme makes use of a sufficient condition previously derived for the spatial Aloha network, which ensures the network to operate in the stable region if the RIM parameter R at the local leader(s) satisfies $R \leq 2$. In our design, the local leader adjusts its MAP by a build-in PI controller to achieve R=2. The resulting control system is sustained by mathematical foundations from control theory, which guarantees fast convergence and network stability. Most importantly, RIM is a local parameter based on only local information, which makes

the SALE scheme easy and systematic to implement with high scalability. Through simulations, we validate the fast convergence of the system to a steady-state operating point with close-to-Pareto-front throughputs and good fairness among the users, while comparing with our previous heuristic algorithm.

Chapter 6

Multi-Leader Stackelberg Games in Multi-Channel Spatial Aloha Networks

6.1 Introduction

In Chapters 3 to 5, we have been studying the single channel spatial Aloha model. To further improve the network performance, multiple collision channels can be considered. A detailed review on channel selection games in multi-channel Aloha networks with spatial reuse has been presented in Section 1.3.2.

The main contributions of this chapter are summarized as follows. We study the multi-channel Aloha networks with spatial reuse, with the objective to enable each autonomous user i to select a channel c_i and decide a MAP q_i to improve its throughput, while providing a certain degree of fairness among the users [148]. We apply the game theoretic approach to the problem, where each user i is a player who chooses the strategy (c_i, q_i) to improve its own throughput. To search for a NE, a *Multi-Leader Stackelberg Game (MLSG)* [74] is formulated to iteratively obtain a solution on each dimension of the (c_i, q_i) strategy.

First, multiple Stackelberg leaders are elected to manage the MAPs of all players. Then under the resulting MAP profile, each player iteratively chooses its channel to improve its throughput. Specifically, assume the current network consists of several sub-networks. These subnets are disconnected from others, either because they operate on different channels, or they are on the same channel but spatially disconnected. First of all, each subnet elects the player with the highest node degree to be the leader to manage this subnet. Within each subnet, the leader mandates the

MAPs of all players to be the same, and sets the MAP value to provide localized max-min throughput fairness for the players in this subnet. Such a myopic best response update performed by the leader requires only local information within its subnet. Secondly, under the resulting MAP profile, each player iteratively chooses its channel to improve its own throughput. The iteration dynamics follow the formulation in [70], whose convergence is guaranteed under the theory of potential games. An *Oscillation Resolving Mechanism (ORM)* is further proposed to stabilize the design in some special cases where the operating points of some players in a local region would oscillate between the two dimensions of the myopic search.

Compared to existing methods of pre-allocating MAPs as in [70], our iterative MAP management explicitly takes into account the localized fairness issue among the players, and is able to approximately achieve max-min throughput fairness in each subnet. Moreover, under the above fairness constraint, the MLSG game is able to further improve the overall network throughput iteratively compared to any pre-allocated MAPs. Simulation results show that, by playing the MLSG game, the overall network throughput is gradually improved until a NE is reached, and the resulting NE provides good throughput fairness for the players.

The rest of the chapter is organized as follows. We dedicate Section 6.2 to discuss the MLSG game in details. We evaluate the system performance through simulations in Section 6.3. We conclude the chapter in Section 6.4.

6.2 Multi-Leader Stackelberg Games

In this section we design a *Multi-Leader Stackelberg Game (MLSG)*, where each user i is a player who chooses the strategy (c_i, q_i) to improve its own throughput in the multi-channel spatial Aloha model introduced in Section 2.3. First, multiple Stackelberg leaders are elected to manage the MAPs of all players. Then under the resulting MAP profile, each player iteratively chooses its channel to improve its own throughput. The process will repeat until a stable solution is obtained.

6.2.1 MAP Management by Multiple Stackelberg Leaders

Assume the current network settles with G subnets, as described in Section 2.3. Each subnet $\mathcal{M}_g, g \in \mathcal{G}$ elects a player $l_g \in \mathcal{M}_g$ as the leader within this subnet. Further assume that each leader's management goal is to provide localized max-min throughput fairness for the players in its subnet, by mandating a proper common

MAP value for the players in this subnet to follow. Hence, the leader l_g solves the following optimization problem:

$$\begin{array}{ll} \max_{q_{l_g}} & \min_{i\in\mathcal{M}_g}\{\theta_i\} \\ \text{s.t.} & \begin{cases} \theta_i = q_i \prod_{j:a_{ij}=1,c_j=c_i}(1-q_j), \forall i \in \mathcal{M}_g, \\ q_i = q_{l_g}, \forall i \in \mathcal{M}_g, \\ 0 \le q_{l_g} \le 1. \end{cases} \end{array} \tag{6.1}$$

The optimization problem in (6.1) can be equivalently reduced to:

$$\begin{array}{ll} \max_{q_{l_g}} & \min_{i\in\mathcal{M}_g}\{\theta_i\} \\ \text{s.t.} & \begin{cases} \theta_i = q_{l_g}(1-q_{l_g})^{N_{i,g}}, \\ 0 \le q_{l_g} \le 1, \end{cases} \end{array} \tag{6.2}$$

where $N_{i,g}$ is the number of neighbors for user i (excluding user i itself) in subnet $\mathcal{M}_g$, which is also known in graph theory [139] as the *node degree* of user i in this subnet. Here we assume that the interference relationship among users is symmetric, i.e., $a_{ij} = a_{ji}, \forall i, j$. It is now obvious that the minimum throughput always happens at the player with the highest node degree in this subnet under the common MAP constraint. Since the leader l_g is responsible for solving the max-min problem in (6.2), it is natural to elect the player with the highest node degree as the leader l_g. For simplicity, in cases where there are multiple players in this subnet who have the same highest node degree, the one with the smallest ID is elected as the leader. The leader l_g then solves the max-min problem in (6.2) by actually maximizing its own throughput:

$$\begin{array}{ll} \max_{q_{l_g}} & \theta_{l_g} = q_{l_g}(1-q_{l_g})^{N_{l_g,g}} \\ \text{s.t.} & 0 \le q_{l_g} \le 1. \end{array} \tag{6.3}$$

which yields the optimal solution to (6.2) as:

$$q_{l_g} = 1/(N_{l_g,g}+1). \tag{6.4}$$

We thus formulate the problem of choosing the MAPs and subsequent spatial channel selection as a multi-leader Stackelberg game [74], where the player l_g with the highest node degree $N_{l_g,g}$ in each subnet $\mathcal{M}_g, g \in \mathcal{G}$ is elected to be the leader to manage the MAPs in this subnet. Within each subnet $\mathcal{M}_g$, the leader l_g mandates the MAPs of all players to be the same, and sets the MAP value as $1/(N_{l_g,g}+1)$ to provide max-min throughput fairness for the players in this subnet. Such a myopic

best response update by the leader requires only local information within its subnet. As a result, a MAP profile of all the players would be generated.

Note that the role of the Stackelberg leader in this chapter is slightly different from that of the local leader in Chapter 5, although they share some characteristics such as highest node degree, mandating equal MAP within its subnet, etc. The key difference lies in the information requirement. The local leader in Chapter 5 requires only one-hop information to make MAP adaptation, while the Stackelberg leader in this chapter requires local information within its subnet, i.e., it knows the highest value of node degree within its subnet. We allow the Stackelberg leader to have the above information so that (6.4) can be used to determine the MAP instead of using PI controller described in Chapter 5, and focus more on the joint issues with spatial channel selection. On the other hand, in the multiple-channel scenario, it is expected that the network can be divided into more non-overlapping subnets, each of which has fewer users and a lower user density than in the single-channel scenario. Therefore, the node degree information in a subnet would be relatively easy to acquire.

6.2.2 Spatial Channel Selection Process

Under the MAP profile resulting from the above MAP management process, each player then iteratively chooses its channel to improve its own throughput using the iteration dynamics formulated in [70]. Here we briefly rewrite the spatial channel selection subgame using our settings and notations:

Players: Distributed Tx-Rx pairs, $i \in \mathcal{N}$, who compete for K orthogonal channels to transmit via slotted-Aloha-type random access scheme.

Strategies: Each player i is allowed to choose a single channel $c_i \in \mathcal{K}$ to access. Its MAP $q_i \in [0,1]$ is assumed to be fixed and given, $\forall i \in \mathcal{N}$. We denote $\underline{c} = [c_1, c_2, \cdots, c_N]$ as the channel profile and $\underline{q} = [q_1, q_2, \cdots, q_N]$ as the MAP profile of all players.

Objectives: Each player i ($i \in \mathcal{N}$) aims to maximize its utility function $u_i(\underline{c}, \underline{q}, \mathbf{A})$, which is defined as the logarithm of its throughput θ_i in its transmitting channel:

$$u_i(\underline{c}, \underline{q}, \mathbf{A}) = \log \theta_i = \log[q_i \prod_{j:a_{ij}=1, c_j=c_i}(1-q_j)] \\ = \log q_i + \sum_{j:a_{ij}=1, c_j=c_i} \log(1-q_j), \forall i \in \mathcal{N}. \quad (6.5)$$

The solution of the spatial channel selection subgame is a NE of the subgame,

which is defined as a strategy profile (in our case, $\underline{c}^* = [c_1^*, \cdots, c_N^*]$) in which each player i's channel selection strategy c_i^* is a best response to the strategies of all the other players c_{-i}^* [34], i.e.,

$$c_i^* = \arg\max_{c_i \in \mathcal{K}} u_i(c_i, c_{-i}^*, \underline{q}, \mathbf{A}), \forall i \in \mathcal{N}. \tag{6.6}$$

Assume that asynchronous myopic best response is adopted, i.e., at any given time, only one player updates its channel selection, which aims to maximize its own utility defined in (6.5). To make a best response, each player needs to estimate the load on all channels and choose the one with the highest channel availability. If we assume that there exists one-hop information exchange about MAPs among the players, then on each channel $k \in \mathcal{K}$ player i observes:

$$v_i(k) := \prod_{j:a_{ij}=1, c_j=k} (1 - q_j), \tag{6.7}$$

which is the probability that the k-th channel is available. The myopic best response by player i is therefore given by

$$\tilde{c}_i = \arg\max_{c_i \in \mathcal{K}} u_i(c_i, c_{-i}, \underline{q}, \mathbf{A}) = \arg\max_{k \in \mathcal{K}} v_i(k), \forall i \in \mathcal{N}. \tag{6.8}$$

Under the above asynchronous myopic best response update, the convergence to a NE $\underline{c}^*$ of the subgame is guaranteed under the theory of potential games [70].

6.2.3 Iterative Play of the MLSG game

The MLSG game is then played iteratively based on the procedure given in the above two subsections until a NE is reached. Compared to existing methods of pre-allocating MAPs, the MLSG game further improves the overall network throughput by iteratively tuning the MAPs toward max-min throughput in each subnet. We summarize the iteration process of the MLSG game in Algorithm 6.1.

6.2.4 Oscillation Resolving Mechanism

Our simulation results show that convergence to a NE can always be achieved after a finite number of game plays, except in some cases the operating points of some players in a local region exhibit oscillation between the two dimensions of the myopic search. In order to resolve this problem, we introduce an *Oscillation Resolving Mechanism (ORM)* to stabilize the design.

Algorithm 6.1 Iteration Process of the MLSG Game

Initialize:
Player i stays on channel $c_i = 1$ (channel 1), for all $i \in \mathcal{N}$ (initially all players are in the same subnet);
Elect the player L with the highest node degree N_L as the leader;
Player i sets MAP $q_i = 1/(N_L + 1)$, for all $i \in \mathcal{N}$.

repeat:
    repeat:
        for $i = 1, \cdots, N$ players **do**:
            Estimate the channel availability $v_i(k)$ on each channel $k \in \mathcal{K}$;
            Choose the channel $c_i = \arg\max_{k \in \mathcal{K}} v_i(k)$;
        end for
    until No player changes its channel.

    for each connected subnet $\mathcal{M}_g, g \in \mathcal{G}$ **do**:
        Elect the player $l_g \in \mathcal{M}_g$ with the highest node degree N_{l_g} as the leader, which broadcasts $q_{l_g} = 1/(N_{l_g} + 1)$ to all other players in $\mathcal{M}_g$;
        Player i sets MAP $q_i = q_{l_g}$, for all $i \in \mathcal{M}_g$;
    end for
    (Oscillation Resolving Mechanism)
until No player changes its MAP.

Algorithm 6.2 Oscillation Resolving Mechanism

for $i = 1, \cdots, N$ players **do**:
    for $t = 2, 3, \cdots, T_{max}$ **do**:
        $C_i(t-1) = C_i(t)$;
        $Q_i(t-1) = Q_i(t)$;
    end for
    $C_i(t) = c_i$;
    $Q_i(t) = q_i$.

    for $T = 2, 3, \cdots, T_{max}/2$ **do**:
        for $h = 1, \cdots, T$ **do**:
            if $C_i(T_{max} - h + 1) = C_i(T_{max} - h + 1 - T)$
and $Q_i(T_{max} - h + 1) = Q_i(T_{max} - h + 1 - T)$
and $\exists t, s \in \{T_{max} - T + 1, \cdots, T_{max}\}$,s.t. $C_i(t) \neq C_i(s)$
and $\exists t, s \in \{T_{max} - T + 1, \cdots, T_{max}\}$,s.t. $Q_i(t) \neq Q_i(s)$ **then**
                Oscillation detected, with period $T_i = T$.
            end if
        end for
    end for

    if Oscillation detected **then**
        freeze operating point (c_i, q_i).
    end if
end for

The ORM mechanism is presented in Algorithm 6.2, which should be inserted in line 17 of Algorithm 6.1. Specifically, each player i keeps the history of its operating point (c_i, q_i) for the recent T_{max} rounds of the MLSG game play, denoted as $(C_i(t), Q_i(t)), t = 1, \cdots, T_{max}$. If the operating points oscillate with a certain period T_i, then player i would freeze its operating point at the first detected oscillation point (c_i, q_i). This simple mechanism stabilizes the whole network.

In the ORM mechanism, different number of comparisons ($T \leq T_{max}/2$) need to be performed when determining the oscillation period T_i of different player i. The procedure to detect the oscillation period T_i for each player i is presented from line 8 to line 17. To check for the oscillation period T, it requires at most $4T$ comparing operations (equal or different). Since we have to check for the value of T up to $T_{max}/2$, in the worst case, it takes $4 \cdot (2 + T_{max}/2) \cdot (T_{max}/2 - 1)/2 = (T_{max} + 4)(T_{max}/2 - 1)$ comparing operations, which is in the order of $O(T_{max}^2)$. The value of T_{max} required to capture the maximum possible oscillation period may depend on the number of users, user density, as well as the specific network topology, which needs future investigations to rigorously characterize. In the simulations we performed, we only capture oscillation periods of 2 or 3 happening at only one or two players.

6.3 Simulation Studies

6.3.1 Illustration of the MLSG Game: 10 Users Case

In this subsection we apply the MLSG game to the interference graph in Fig. 6.1a to illustrate the iteration process and the improvement over total network throughput. We first consider the case with $K = 2$ available channels, and the improvement steps of the MLSG game are plotted in Fig. 6.2a.

The game converges to a NE after $t_{move} = 10$ channel moves (for $t_{move} > 10$, no user is changing its channel and the total throughput remains unchanged thereafter). It can be seen from Fig. 6.2a that the MLSG game gradually improves the overall network throughput until reaching a NE. Specifically, there are two sudden rises in the total throughput, which are brought by two rounds of MAP management that occur at $t_{move} = 7 \sim 8$ and $t_{move} = 9 \sim 10$ respectively. When $t_{move} \leq 7$, the users are asynchronously updating their channels to improve their own throughputs, and the total throughput gradually improves as well. Then the channel selection subgame converges after $t_{move} = 7$, and the MAP management process improves

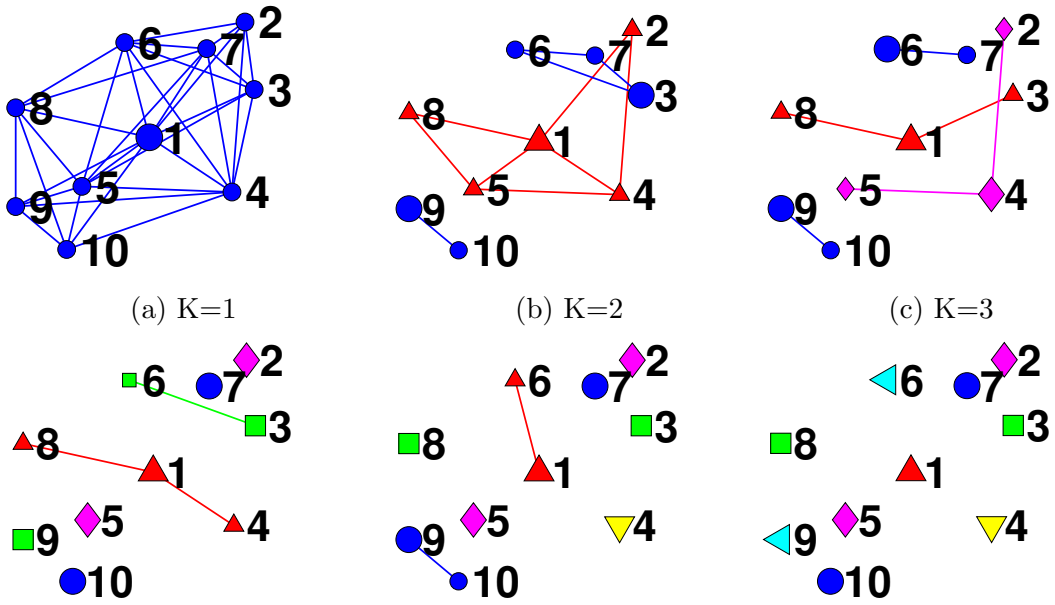

(a) K=1 (b) K=2 (c) K=3

(d) K=4 (e) K=5 (f) K=6

Figure 6.1: 10 Users Topology, with 1∼6 Channels

the total throughput by tuning the MAPs towards max-min throughput in each subnet. As a result, the total throughput is significantly improved under the fairness constraint. Similarly, there is another round of spatial channel selection subgame and MAP tuning between $t_{move} = 8 \sim 10$, and the total throughput is further improved until converging to a NE.

Notice that the game could actually start with any pre-allocated MAPs as in [70]. However, the pre-allocated MAPs might be unfair if some users are allocated much larger MAPs than other users in the same subnet. If the game starts with such unfairly pre-allocated MAPs, then it is possible that the total throughput would decrease at first, as a result of the MAP management which re-allocates the MAPs to approximately provide max-min throughput fairness for the users in each subnet. After that, our MAP management process is able to further improve the total network throughput iteratively under the fairness constraint.

We then apply the MLSG game to the same interference graph with more available channels. The improvement steps of total network throughput with $K = 2 \sim 6$ channels are plotted in Fig. 6.2b. Similar to the $K = 2$ case, the MLSG game gradually improves the total network throughput until reaching a NE. In particular, the sudden rise(s) of the total throughput in each case is a result brought by the MAP management process.

The final channel allocation results for $K = 1, \cdots, 6$ are plotted in Fig. 6.1, where we use different colors and shapes to denote different channels, and the leader

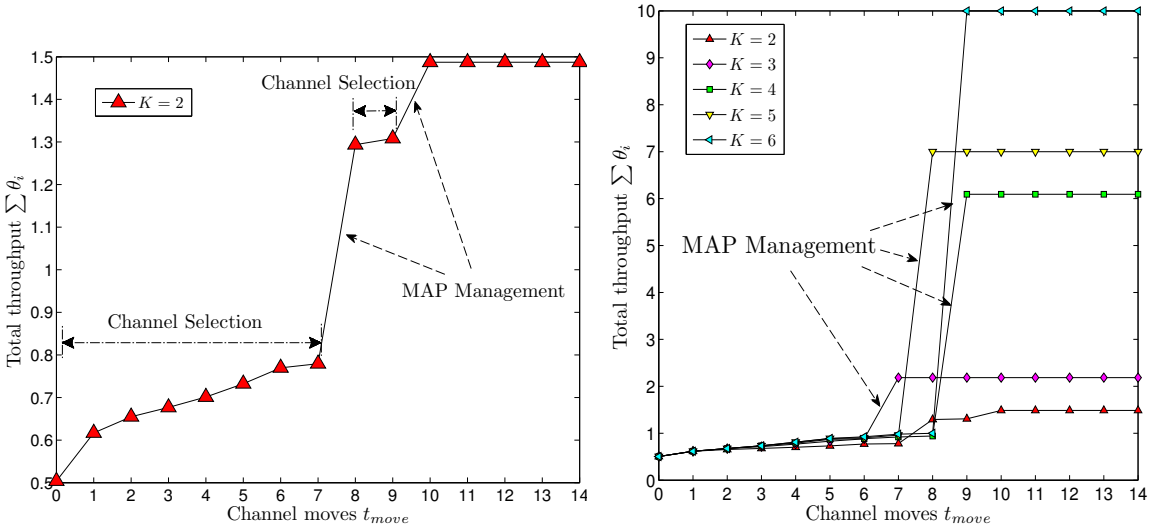

(a) $K = 2$ (b) $K = 2 \sim 6$

Figure 6.2: Improvement over Total Throughput, $N = 10, K = 2 \sim 6$

in each subnet is plotted using a bigger icon than other players. With K increasing from 1 to 6, the network is partitioned into more subnets with smaller sizes (the number of subnets G gradually increases from 1 to 10), and the total throughput of all players gradually increases as well. When $K = 6$, each player occupies a single channel without interfering other players, and the total throughput reaches 10 (each player has a throughput of 1).

6.3.2 50 Users Case

Consider a distributed network with N users, which are randomly placed in a square region of a given area. For simplicity, we assume that all the distances between any transmitter and its designated receiver are much smaller than the distances between any two transmitters, so that a Tx-Rx pair (user) can be represented by a single node in the topology. We further assume that in the single-channel case, all users have transmission range of 5 unit length, and those users who are in each other's transmission range will have significant interference on each other, and the two users are said to be connected. Based on the above assumptions, we can generate a random connected topology with 50 users in a square region of area 500 (units), as plotted in Fig. 6.3.

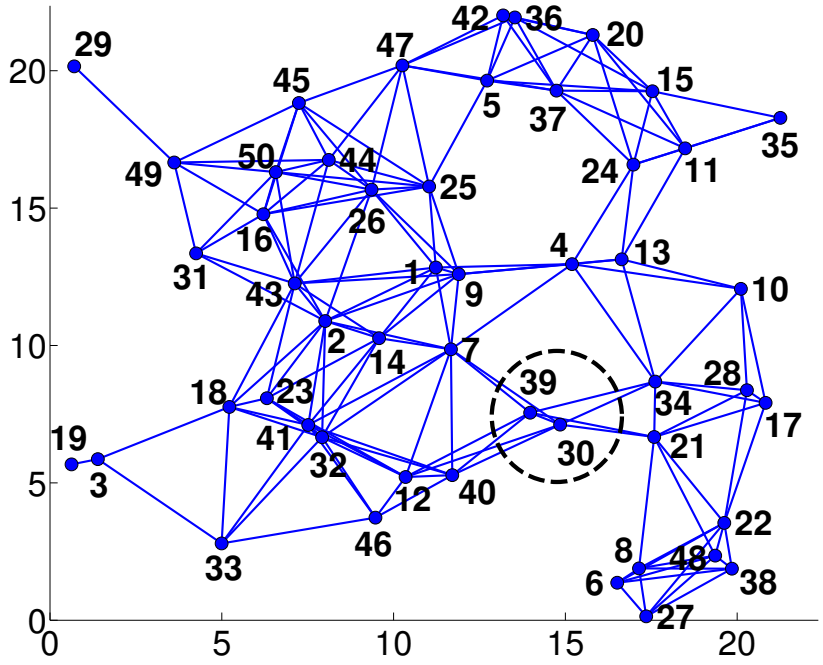

Figure 6.3: 50 Users Topology

ORM Mechanism

It happens that player 30 and player 39 in this particular topology have oscillating operating points when $K = 3$ in the MLSG game. As indicated in Fig. 6.4a, the operating points of player 30 and player 39 are $(c_{30}, q_{30}) = (1, 1/4)$ and $(c_{39}, q_{39}) = (3, 1/2)$ respectively. Given such a MAP profile, player 39 jumps from channel 3 to channel 1 since $v_{39}(1) = 1 - q_{30} = 1 - 1/4 = 3/4 > v_{39}(3) = 1 - q_{12} = 1 - 1/2 = 1/2$. After player 39 switches its channel, player 30 jumps from channel 1 to channel 3 since $v_{30}(3) = 1 - q_{12} = 1 - 1/2 = 1/2 > v_{30}(1) = (1 - q_{39})(1 - q_{34}) = (1 - 1/2)(1 -$

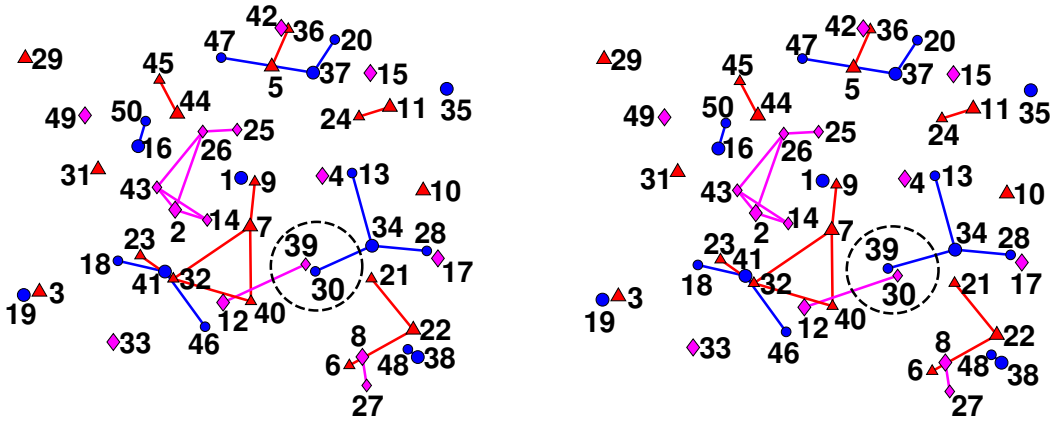

(a) N=50, K=3, State 1

(b) N=50, K=3, State 2

Figure 6.4: Oscillation States of the MLSG Game

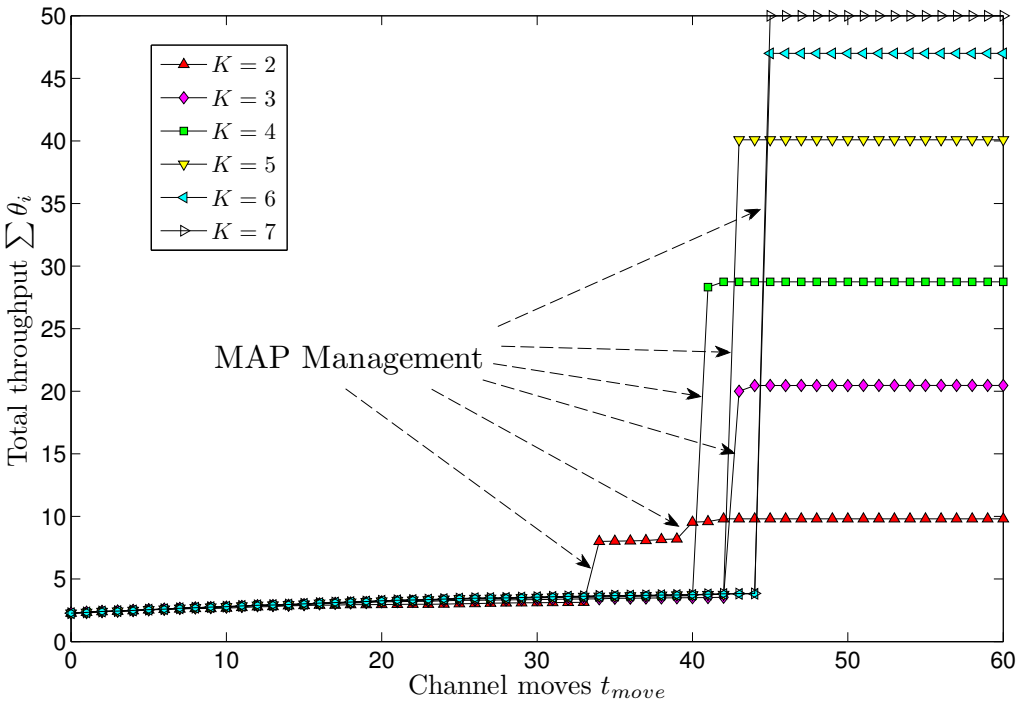

Figure 6.5: Improvement over Total Throughput, $N = 50, K = 2 \sim 7$

$1/4) = 3/8$. Then the channel selection subgame converges, with players 30 and 39 swapping their channels. After that, the MAPs of players 30 and 39 are swapped as well, as a result of the MAP management process. Now the subgame restarts with a new state as indicated in Fig. 6.4b. The only difference with Fig. 6.4a is that players 30 and 39 have swapped their operating points. In this way, there are $N_{osc} = 2$ players (players 30 and 39) whose operating points are oscillating with a period T_{osc} of 2 rounds of the MLSG game play.

Fortunately, we can apply the ORM mechanism to stabilize the network. In the above scenario, player 30 and player 39 both detect oscillation of their operating points, thus both of them freeze their operating points at the state in Fig. 6.4b, and the network is stabilized. The total number of channel moves before convergence is $t_{move} = 51$.

Improvement over total throughput

Similar to Section 6.3.1, we apply the MLSG game to the interference graph in Fig. 6.3 with more available channels. The improvement steps of total network throughput with $K = 2 \sim 7$ channels are plotted in Fig. 6.5, which shows that the MLSG game converges after $t_{move} \approx 50$ channel moves (no oscillation is detected

Table 6.1: MLSG Game ($N = 100, K = 5$)

area	D	$\Sigma\theta_i$	G	t_{move}	N_{osc}	T_{osc}
12.5	8	1.89	5	80	0	-
25	4	2.10	5	102	0	-
50	2	3.10	5	142	0	-
100	1	5.34	5	160	0	-
200	0.5	16.96	21	195	3	2
400	0.25	32.02	42	111	2	3
1000	0.1	83.50	89	81	0	-

except the $K = 3$ case, which is stabilized by ORM). Similar to the 10 users case in Fig. 6.2b, the MLSG game gradually improves the total network throughput until reaching a NE. In particular, the sudden rise(s) of the total throughput in each case is a result of the MAP management process which iteratively tunes the MAPs towards max-min throughput in each subnet. As a result, the total throughput is significantly improved under the fairness constraint.

6.3.3 100 Users with Various User Density

We define the *user density* D as the number of users per unit area. For the 50 users case above, the user density is D=50/500=0.1. Now we generate a sequence of random connected topologies with various user density, by randomly scattering 100 users in a square region of various areas. In particular, when the square region has an area of 12.5, the network becomes fully connected (the diagonal line length is equal to the transmission range of 5). We apply the MLSG games to these topologies with K=5 and summarize the results in Table 6.1.

It can be seen that the MLSG game converges after a finite number of channel moves. Oscillation is detected in two cases ($D = 0.25$ and $D = 0.5$) in the MLSG game, and the ORM mechanism is applied to stabilize the network. Table 6.1 also shows that as the user density decreases from 8 to 0.1 (from a fully connected network to a network with lower connectivity), the network is partitioned into more subnets with smaller sizes (the number of subnets G gradually increases). As a result of spatial reuse, the total throughput increases due to decreased interference from fewer neighbors experienced by each user.

6.4 Conclusions

We study the multi-channel spatial Aloha network with the objective to enable each autonomous user i to select a channel c_i and decide a MAP q_i to improve its throughput, while providing a certain degree of fairness among the users. Game theoretic approaches are applied, where each user i is a player who chooses the strategy (c_i, q_i) to improve its own throughput. To search for a NE, a MLSG game is formulated to iteratively obtain a solution on each dimension of the (c_i, q_i) strategy. An ORM mechanism is proposed to stabilize the design in some special cases where the operating points of some players in a local region would oscillate between the two dimensions of the myopic search. Compared to existing methods of pre-allocating MAPs, the MLSG game further improves the overall network throughput by iteratively tuning the MAPs toward max-min throughput in each subnet. Simulation results show that the MLSG game gradually improves the total throughput until reaching a NE, which also provides good throughput fairness for the players.

The focus of this chapter is more on the game theoretic formulation to model the selfish user behaviors in the joint channel selection and MAP tuning problem. We have only considered the case with static topology during the course of the game play. In the future we need to further investigate the non-deterministic scenarios such as topology change, time-varying channels, failure of control message passing, etc.

Chapter 7

A Stackelberg Game Model for Overlay D2D Transmission with Heterogeneous Rate Requirements

7.1 Introduction

Slotted Aloha random access has been used in the above works. In this chapter, we investigate another type of random access scheme, i.e., CSMA, under spatial reuse. We formulate the problem by applying the spectrum commons to overlay D2D communication, i.e., we assume that all D2D links use CSMA as the multiple access scheme to share a dedicated inband overlay channel.

Recall from Section 1.1.3 that a spectrum commons is characterized by the restrictions on who uses the spectrum, and when and how. The owner or controller of the spectrum commons in our settings is the cellular operator who establishes and enforces these restrictions, while the users of the spectrum commons are the D2D links who conform to these restrictions when sharing the spectrum.

Specifically, although D2D communication does not route the data traffic through the cellular network, the available network infrastructure can still be an effective means to exert light control over all the D2D links when performing resource allocation. In our model in Chapter 7, the D2D links have heterogeneous service requirements and different willingness to pay, and the central entity (e.g., eNB) [98] controls the transmission behaviors of all links by modifying the price per unit service rate [149].

Our contributions in this chapter are twofold. First of all, we propose a Stackelberg game [33] which maximizes the total throughput of the D2D links, where

these links have heterogeneous utility functions. The BS in the cellular networks will act as a Stackelberg leader to regulate the D2D link transmissions by modifying the service price, so that the payoff of each individual D2D link can be maximized while maintaining the D2D network to function within the feasible throughput region determined by the CSMA access mechanism. The problem is shown to be quasi-convex and can be solved by a sequence of equivalent convex optimization problems. The pricing strategies are designed so that the network always operates within the feasible throughput region. Secondly, each D2D link will acquire a rate based on its actual demand and willingness to pay. We explicitly model the possible selfish behaviors among the D2D links with spatial reuse. Under a given network price, the transmitter of each D2D link competes for channel usage by choosing its transmission parameters in order to maximize its own payoff. Such user dynamics are studied in the setting of non-cooperative games, and the resulting CSMA game model serves as the follower-subgame in the proposed Stackelberg game. An algorithm is proposed followed by proofs for the existence and convergence of the equilibrium solution.

The rest of the chapter is organized as follows. Based on the network model introduced in Section 2.4, the definition of feasible throughput region for a CSMA network is defined in Section 7.2, while some important properties about these feasible regions are derived. The Stackelberg game is detailed in Section 7.3. Performance of the proposed game is evaluated through simulations in Section 7.4. We conclude the chapter in Section 7.5.

The notations used in this chapter are as follows. An underscore in a random variable $\underline{\cdot}$ represents a vector, or a system state consisting of the binary status of the N links. The variable θ is used to denote the throughput from the channel access point of view, where the solution is controlled by the ICN model. On the other hand, $\tilde{\theta}$ is used to represent a desired throughput from the link layer aspect, whose value is derived from the price and link utility function. If the final solution is within the feasible throughput region, these two values should match. There are two types of equilibrium to be differentiated, the subgame equilibrium is denoted by a superscript '*' whilst for the Stackelberg game is denoted by a superscript 'opt'.

7.2 Feasible Throughput Region in Spatial CSMA Networks

The spatial CSMA network model has been introduced in Section 2.4. In this section, we state and derive the key results on ICN which are important to our proposed game theoretic framework to be presented in Section 7.3.

7.2.1 Feasible and Strictly Feasible Throughput Region

Each feasible system state $\underline{s} \in \mathcal{S}$ corresponds to a feasible scheduling vector of link transmissions. The feasible throughput region is therefore the convex hull [142, pp. 24] of $\mathcal{S}$, namely,

$$\bar{\mathcal{C}} = \{\underline{\theta} | (\underline{\theta} = \sum_{\underline{s} \in \mathcal{S}} p_{\underline{s}} \underline{s}) \wedge (p_{\underline{s}} \geq 0, \forall \underline{s}) \wedge (\sum_{\underline{s} \in \mathcal{S}} p_{\underline{s}} = 1)\}. \tag{7.1}$$

Eq.(7.1) shows that the feasible solutions are given by the convex combinations of the throughputs at these feasible states while fulfilling the probability and probability distribution constraints. The solutions are fully defined by a polytope whose vertices are the feasible system states $\underline{s} \in \mathcal{S}$.

The interior of $\bar{\mathcal{C}}$ is the *strictly feasible region*, denoted as $\mathcal{C}$:

$$\mathcal{C} = \{\underline{\theta} | (\underline{\theta} = \sum_{\underline{s} \in \mathcal{S}} p_{\underline{s}} \underline{s}) \wedge (p_{\underline{s}} > 0, \forall \underline{s}) \wedge (\sum_{\underline{s} \in \mathcal{S}} p_{\underline{s}} = 1)\}. \tag{7.2}$$

Using the contention graph in Fig. 2.1 as an example. The set of feasible system states $\mathcal{S}$ has been given in (2.3). The feasible throughput region is $\bar{\mathcal{C}}$ shown in Fig. 7.1, which is a polyhedron vertexed by the maximum throughput of these states (the region enclosed by the mesh surface and its intersections with $\theta_1 - \theta_2$, $\theta_1 - \theta_3$ and $\theta_2 - \theta_3$ planes). The strictly feasible region $\mathcal{C}$ refers to the inner region of the polyhedron only.

7.2.2 Transmission Aggressiveness

CSMA is a distributed and randomized way to schedule the transmissions among the feasible system states. It is shown in [92] using the ICN model that any throughput in the strictly feasible region can be achieved through a properly chosen Transmission Aggressiveness (TA) $\underline{r}$, which is stated in the following lemma.

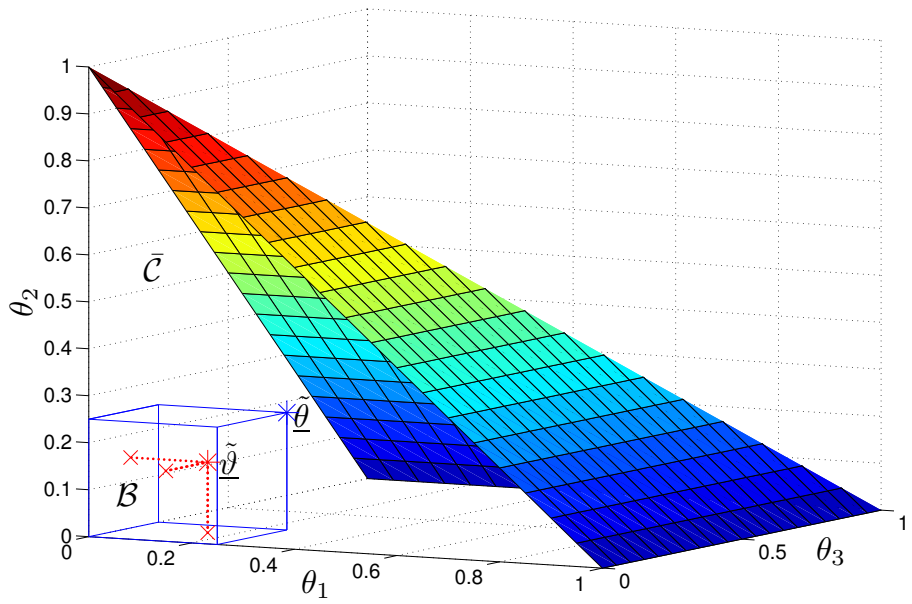

Figure 7.1: Feasible Throughput Region for the Contention Graph in Fig. 2.1

Lemma 7.1 (Lemma 8 in [150]). *In the ICN model, for any desired throughput for all the N links $\underline{\tilde{\theta}} = [\tilde{\theta}_1, \tilde{\theta}_2, \cdots, \tilde{\theta}_N] \in \mathcal{C}$ (strictly feasible region), there exists a unique finite-valued $\underline{r} = [r_1, r_2, \cdots, r_N] \in \mathbb{R}^N$ such that $\theta_i(\underline{r}) = \tilde{\theta}_i, \forall i \in \mathcal{N}$.*

A detailed proof can be found in [92] and [150]. Here we only present a sketch of the proof.

Proof: Given a $\underline{\tilde{\theta}} \in \mathcal{C}$, we use the maximum log-likelihood method to estimate the parameters $\underline{r}^*$ which result in $\underline{\theta}(\underline{r}^*) = \underline{\tilde{\theta}}$, or equivalently, result in the desired state probability distribution $\underline{p}^{\tilde{\theta}}$ such that $\underline{\tilde{\theta}} = \sum_{\underline{s} \in \mathcal{S}} p_{\underline{s}}^{\tilde{\theta}} \underline{s}$. The log-likelihood function [151] is defined as:

$$F(\underline{r}; \underline{\tilde{\theta}}) = \sum_{\underline{s} \in \mathcal{S}} p_{\underline{s}}^{\tilde{\theta}} \log_e(p_{\underline{s}}). \tag{7.3}$$

By applying $\underline{\tilde{\theta}} = \sum_{\underline{s} \in \mathcal{S}} p_{\underline{s}}^{\tilde{\theta}} \underline{s}$ and substituting the expression for $p_{\underline{s}}$ given in (2.7), and after some manipulations, we have

$$F(\underline{r}; \underline{\tilde{\theta}}) = \sum_{i=1}^{N} \tilde{\theta}_i r_i - \log_e[\sum_{\underline{s} \in \mathcal{S}} \exp(\sum_{i=1}^{N} s_i r_i)]. \tag{7.4}$$

Since $\sum_{i=1}^{N} \tilde{\theta}_i r_i$ is affine in $\underline{r}$ and $\log_e[\sum_{\underline{s} \in \mathcal{S}} \exp(\sum_{i=1}^{N} s_i r_i)]$ is a log-sum-exp function and thus is convex in $\underline{r}$, the function $F(\underline{r}; \underline{\tilde{\theta}})$ is concave in $\underline{r}$ [142, pp. 72]. Therefore, the max-log-likelihood problem below is a convex optimization problem with $\underline{r}$ as

the variables to be solved and $\underline{\tilde{\theta}}$ as the parameters:

$$\max_{\underline{r}} \quad F(\underline{r}; \underline{\tilde{\theta}}) \quad \text{(Maximize log-likelihood)}. \tag{7.5}$$

It is then shown in [92] that the max-log-likelihood problem in (7.5) is the dual problem of the max-entropy problem in (7.6), where $-\sum_{\underline{s} \in \mathcal{S}} p_{\underline{s}} \log_e p_{\underline{s}}$ is the entropy of the distribution vector $\underline{p}$, whose element $p_{\underline{s}}$ is the state probability for the state $\underline{s}, \forall \underline{s} \in \mathcal{S}$. The max-entropy problem is also a convex optimization problem, with $\underline{p}$ as the variables and $\underline{\tilde{\theta}}$ as the parameters.

$$\begin{aligned} \max_{\underline{p}} \quad & -\sum_{\underline{s} \in \mathcal{S}} p_{\underline{s}} \log_e p_{\underline{s}} \quad \text{(Maximize entropy)} \\ \text{s.t.} \quad & \begin{cases} \sum_{\underline{s} \in \mathcal{S}} s_i p_{\underline{s}} = \tilde{\theta}_i, \forall i \in \mathcal{N}, \\ p_{\underline{s}} \geq 0, \forall \underline{s} \in \mathcal{S}, \\ \sum_{\underline{s} \in \mathcal{S}} p_{\underline{s}} = 1. \end{cases} \end{aligned} \tag{7.6}$$

We are now ready to prove Lemma 7.1. We need to verify that the Slater's condition [142, pp. 226] is satisfied, so that the optimal solutions to the two convex optimization problems (7.5) (7.6) exist with zero duality gap, given that $\underline{\tilde{\theta}} \in \mathcal{C}$ (strictly feasible region).

Since all the constraints in (7.6) are linear equalities and inequalities, we only need to verify that there exists a feasible $\underline{p}$ in the relative interior [142, pp. 23] of the domain $\mathcal{D}$ of the objective function $-\sum_{\underline{s} \in \mathcal{S}} p_{\underline{s}} \log_e p_{\underline{s}}$, which is $\mathcal{D} = \{\underline{p} | p_{\underline{s}} \geq 0, \forall \underline{s} \in \mathcal{S}\}$. The relative interior of $\mathcal{D}$ is $\mathbf{relint}\mathcal{D} = \{\underline{p} | p_{\underline{s}} > 0, \forall \underline{s} \in \mathcal{S}\}$. Since $\underline{\tilde{\theta}} \in \mathcal{C}$, from (7.2) we can write $\underline{\tilde{\theta}} = \sum_{\underline{s} \in \mathcal{S}} p_{\underline{s}}^{\tilde{\theta}} \underline{s}$ where $p_{\underline{s}}^{\tilde{\theta}} > 0, \forall \underline{s} \in \mathcal{S}$ and $\sum_{\underline{s} \in \mathcal{S}} p_{\underline{s}}^{\tilde{\theta}} = 1$. By letting $\underline{p} = \underline{p}^{\tilde{\theta}} \in \mathbf{relint}\mathcal{D}$, we find a feasible $\underline{p}$ which satisfies all the constraints in (7.6). Therefore, the Slater's condition is satisfied.

As a result, the optimal solutions to the two convex optimization problems (7.5) (7.6) exist with zero duality gap. Moreover, the dual optimal value is attainable, i.e., there exists a finite $\underline{r}^*$ such that $F(\underline{r}^*; \underline{\tilde{\theta}}) = \max_{\underline{r}} F(\underline{r}; \underline{\tilde{\theta}})$. Therefore, the first order condition [142, pp. 457] of the unconstrainted differentiable convex optimization problem in (7.5) is satisfied at $\underline{r}^*$, i.e.,

$$\nabla F(\underline{r}; \underline{\tilde{\theta}}) \mid_{\underline{r} = \underline{r}^*} = \underline{0}, \tag{7.7}$$

which yields

$$\frac{\partial F(\underline{r};\underline{\tilde{\theta}})}{\partial r_i} \mid_{\underline{r}=\underline{r}^*} = \tilde{\theta}_i - \frac{\sum_{\underline{s}\in\mathcal{S}} s_i \exp(\sum_{i=1}^{N} s_i r_i^*)}{\sum_{\underline{s}\in\mathcal{S}} \exp(\sum_{i=1}^{N} s_i r_i^*)} = \tilde{\theta}_i - \sum_{\underline{s}\in\mathcal{S}} s_i p_{\underline{s}} = \tilde{\theta}_i - \theta_i^* = 0, \forall i \in \mathcal{N}. \tag{7.8}$$

Therefore, for any $\underline{\tilde{\theta}} \in \mathcal{C}$ (strictly feasible region), the log-likelihood function $F(\underline{r};\underline{\tilde{\theta}})$ attains its maximum value at a finite-valued $\underline{r} = \underline{r}^* \in \mathbb{R}^N$. At the optimal solution $\underline{r}^*$, the first-order optimality condition (7.7) is satisfied, which corresponds to $\theta_i^*(\underline{r}^*) = \tilde{\theta}_i, \forall i \in \mathcal{N}$. It is further shown in [150] that $F(\underline{r};\underline{\tilde{\theta}})$ is strictly concave in $\underline{r}$. Therefore, the optimal solution $\underline{r}^*$ is unique. ■

Lemma 7.1 suggests that, if $\underline{\tilde{\theta}} \in \mathcal{C}$, then a unique solution $\underline{r}^*$ exists such that $\theta_i^*(\underline{r}^*) = \tilde{\theta}_i, \forall i \in \mathcal{N}$. On the other hand, the above proof also suggests that we can solve for $\underline{r}^*$ by maximizing the concave function $F(\underline{r};\underline{\tilde{\theta}})$. This is useful for the design of our game iteration algorithm presented in Section 7.3.2.

7.2.3 Feasible Throughput Region Under ICN

Previously we have defined the feasible throughput region for any given set of feasible system states. The shape of the polytopes derived from the ICN model owns a property which will be discussed here.

We first introduce a binary relation "$\preceq$" between two real-valued vectors $\underline{\tilde{\vartheta}}$ and $\underline{\tilde{\theta}}$, which is defined as component-wise less than or equal to, i.e.,

$$\underline{\tilde{\vartheta}} \preceq \underline{\tilde{\theta}} \Leftrightarrow \tilde{\vartheta}_i \leq \tilde{\theta}_i, \forall i \in \mathcal{N}. \tag{7.9}$$

We now establish the following theorem which will be useful when presenting our proposed games.

Theorem 7.1. *In the ICN model, given that $\underline{\tilde{\theta}} \in \bar{\mathcal{C}}$ ($\tilde{\theta}$ is in the feasible region), then any desired throughput $\underline{\tilde{\vartheta}}$, where $\underline{0} \preceq \underline{\tilde{\vartheta}} \preceq \underline{\tilde{\theta}}$, is also in $\bar{\mathcal{C}}$.*

Proof: A first glance at Fig. 7.1 may lead to the thought that the theorem is trivial, but this is not true. Fig. 7.2a shows a convex set $\mathcal{A}_1$ in the two-dimensional space. For a $\underline{\tilde{\theta}} \in \mathcal{A}_1$ as shown in Fig. 7.2a, it is easy to find a point $\underline{\tilde{\vartheta}}$ such that $\underline{\tilde{\vartheta}} \preceq \underline{\tilde{\theta}}$ and yet $\underline{\tilde{\vartheta}}$ is not within the convex region $\mathcal{A}_1$. On the other hand, it is not difficult to figure out that the convex set $\mathcal{A}_2$ in Fig. 7.2b owns the property stated in Theorem 7.1.

In the ICN model, for a target throughput vector $\underline{\tilde{\theta}}$ where $\underline{\tilde{\theta}} \in \bar{\mathcal{C}}$, there exists a probability distribution $\underline{p}^{\tilde{\theta}} = \{p_{\underline{s}}^{\tilde{\theta}}, \forall \underline{s} \in \mathcal{S}\}$ where $\underline{\tilde{\theta}} = \sum_{\underline{s}\in\mathcal{S}} p_{\underline{s}}^{\tilde{\theta}} \underline{s}$ according to (7.1).

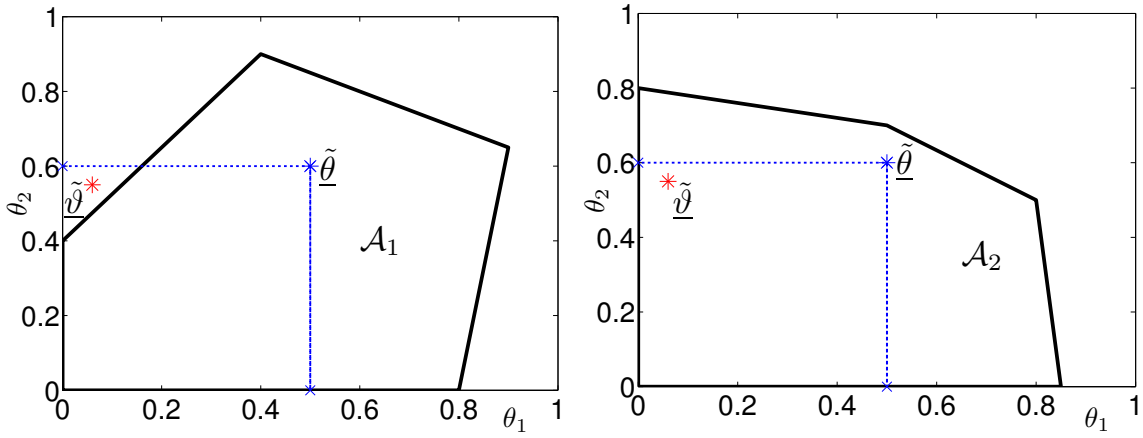

(a) Convex Polytope $\mathcal{A}_1$ without Property in Theorem 7.1

(b) Convex Polytope $\mathcal{A}_2$ with Property in Theorem 7.1

Figure 7.2: Examples of 2-Dimensional Convex "Polytopes"

To prove that $\tilde{\underline{\vartheta}} \preceq \tilde{\underline{\theta}} \in \bar{\mathcal{C}}$, we need to similarly show that there exists another probability distribution $\underline{p}^{\tilde{\vartheta}} = \{p_{\underline{s}}^{\tilde{\vartheta}}, \forall \underline{s} \in \mathcal{S}\}$ such that it fulfills (7.1). However, it is difficult to obtain the distribution $\underline{p}^{\tilde{\vartheta}}$ directly from $\underline{p}^{\tilde{\theta}}$ since it depends on the underlying link topology.

Our approach is to define an orthotope $\mathcal{B}$ whose "vertices" are obtained by projecting $\tilde{\underline{\theta}}$ on all the coordinate planes. An example for the 3-dimensional illustration is shown in Fig. 7.1. The problem is now becoming equivalent to showing that all the "vertices" of $\mathcal{B}$ are in $\bar{\mathcal{C}}$. Finally, because $\tilde{\underline{\vartheta}} \preceq \tilde{\underline{\theta}}$, $\tilde{\underline{\vartheta}}$ is within the cuboid and hence within $\bar{\mathcal{C}}$.

We first perform a projection parallel to the i-th axis. Consider a throughput vector $\tilde{\underline{\psi}}$, with the setting of $\tilde{\psi}_i = 0, \tilde{\psi}_j = \tilde{\theta}_j, \forall j \neq i$, i.e., the i-th link has zero throughput. It is intuitive that $\tilde{\underline{\psi}}$ is one of the "vertices" of $\mathcal{B}$. In order to show that $\tilde{\underline{\psi}}$ is in $\bar{\mathcal{C}}$, we need to show that we are able to obtain its state probability distribution $\{\underline{p}^{\tilde{\psi}}\}$ from $\{\underline{p}^{\tilde{\theta}}\}$, and $\tilde{\underline{\psi}}$ can be expressed in the form as in (7.1). This can be done in the following way.

For $\tilde{\underline{\theta}} \in \bar{\mathcal{C}}$, its state distribution $\underline{p}^{\tilde{\theta}}$ satisfies $\tilde{\underline{\theta}} = \sum_{\underline{s} \in \mathcal{S}} p_{\underline{s}}^{\tilde{\theta}} \underline{s}$, $p_{\underline{s}}^{\tilde{\theta}} \geq 0, \forall \underline{s} \in \mathcal{S}$ and $\sum_{\underline{s} \in \mathcal{S}} p_{\underline{s}}^{\tilde{\theta}} = 1$. We next describe how to construct the state distribution $\underline{p}^{\tilde{\psi}}$ for $\tilde{\underline{\psi}}$. For those states in $\mathcal{S}$ with $s_i = 1$, choose $p_{\underline{s}}^{\tilde{\psi}} = 0$ and $p_{\underline{s}-\underline{e}_i}^{\tilde{\psi}} = p_{\underline{s}-\underline{e}_i}^{\tilde{\theta}} + p_{\underline{s}}^{\tilde{\theta}}$. For the remaining states, choose $p_{\underline{s}}^{\tilde{\psi}} = p_{\underline{s}}^{\tilde{\theta}}$. In other words, those states $\underline{s}$ with $s_i = 1$ should now have state probability $p_{\underline{s}}^{\tilde{\psi}} = 0$. The "removed" state probability $p_{\underline{s}}^{\tilde{\psi}}$ should now be attributed to the state $\underline{s} - \underline{e}_i$. It is not difficult to verify that, by doing so, the total probability remains one and the throughputs of all unaffected links remain the same as before. This state probability distribution $p_{\underline{s}}^{\tilde{\psi}}$ clearly satisfies (7.1), hence

we conclude that the vertex $\underline{\tilde{\psi}}$ is within $\bar{\mathcal{C}}$ and so are other vertexes of $\mathcal{B}$.

It is not difficult to verify this by using the example shown in Fig. 2.3. Assume that we have a throughput $\underline{\tilde{\theta}} = [\tilde{\theta}_1, \tilde{\theta}_2, \tilde{\theta}_3] \in \bar{\mathcal{C}}$. We now show that $\underline{\tilde{\psi}} = [\tilde{\psi}_1, \tilde{\psi}_2, \tilde{\psi}_3] = [0, \tilde{\theta}_2, \tilde{\theta}_3]$ is also in $\bar{\mathcal{C}}$. Note that the throughput $\underline{\tilde{\psi}}$ is equivalent to the case in which link 1 powers off and stops transmitting. In such a case, there are only three feasible system states left: 000, 010, 001. In other words, the states 100 and 101 disappear and are merged into the states 000 and 001 respectively, since link 1 is no longer transmitting. State 010 remains unchanged. Merging the state probability p_{101} with p_{001} will ensure the throughput for link 3 remains the same, since $\tilde{\theta}_3 = p_{001} + p_{101}$. Merging the state probability p_{100} with p_{000} will not affect the throughput of any remaining links. Since the total probability still sums up to be one, link 1 will not be transmitting and both link 2 and link 3 transmit as before. Therefore, the throughput $\underline{\tilde{\psi}}$ resulting from the above state merging operations is still in $\bar{\mathcal{C}}$.

Other vertices of $\mathcal{B}$ can also be similarly shown to be in $\bar{\mathcal{C}}$. Since $\bar{\mathcal{C}}$ is a convex set and the convex combination of these "vertices" are all in $\bar{\mathcal{C}}$, we have $\mathcal{B} \subset \bar{\mathcal{C}}$. Since $\underline{\tilde{\vartheta}} \preceq \underline{\tilde{\theta}}$ is enclosed in the hyperrectangle (N-orthotope), $\underline{\tilde{\vartheta}}$ should also be in $\bar{\mathcal{C}}$. ■

A remark to make is that Theorem 7.1 is not generally true for any convex set. It is true since the values of s_i are chosen from 0 and 1 only; and the subset of feasible states induced by a maximal independent set is a complete partially ordered set [2] based on how ICN is modelled. For the example in Fig. 2.3, the maximal independent set $\{1, 3\}$ induces the subset of feasible states $\mathcal{Q} = \{[0, 0, 0], [1, 0, 0], [0, 0, 1], [1, 0, 1]\}$, which is a complete partially ordered set, with the least element $[0, 0, 0]$ and the largest element $[1, 0, 1]$ under the partial order "$\preceq$". Hence the use of the theorem needs to be carefully dealt with.

Theorem 7.1 will be used in Section 7.3.3 to show that the pricing problem is a valid quasi-convex optimization problem.

7.2.4 D2D Network Model

The discussion in this subsection is on how to efficiently model the resulting D2D network if the CSMA channel access mechanism is adopted by all D2D links. If the objective of the network is to maximize the sum-rate of all transmitting links, and the BS gives no control on the admission and transmission of links, then [92] has successfully solved this problem. The solution is computed in a completely distributed manner. However, as pointed out earlier in Section 1.4.3, such a fully

cooperative model is too idealistic and there is no consideration on the utility heterogeneity and selfish behaviors of the links. It may be better to build a pricing framework so that each link tries to maximize its payoff function when competing for resources, rather than someone tries to take advantage when the network is in operation and drive the network to unstable states. Furthermore, maximizing the sum-rate may not distribute the resources according to demand because links with low demand may be assigned to transmit at higher rates due to its spatial location.

In this chapter, we feel that the BS can take a more proactive role to assist in D2D transmission. In fact, the problem can be formulated separately in terms of the objectives of the D2D links and the BS. The objective of the BS is to maximize the sum-rate while satisfying the physical layer constraints:

$$\begin{aligned} &\max \quad \textstyle\sum_{i=1}^{N} \tilde{\theta}_i \\ &\text{s.t.} \quad \underline{\tilde{\theta}} \in \mathcal{C}, \end{aligned} \tag{7.10}$$

where $\tilde{\theta}_i$ is the target rate the network has to support link i, and the solution must fulfill the CSMA channel access constraint, i.e., the final rates to support all D2D links must be in the strictly feasible throughput region defined in (7.2).

Each link is a player of a non-cooperative game. Each player tries to maximize its payoff $v_i(\theta_i, \theta_{-i})$ while satisfying the physical layer constraints.

$$\begin{aligned} &\max \quad v_i(\theta_i, \theta_{-i}), \forall i \\ &\text{s.t.} \quad \underline{\theta} \in \mathcal{C}. \end{aligned} \tag{7.11}$$

In (7.10), $\tilde{\theta}_i$ is used to represent the rate demand from the utility point of view and should be differentiated from θ_i in (7.11) or (2.11) used in the ICN model as a result of competing for channel access. At the equilibrium state, these two quantities have to be the same and the pricing mechanism aims to achieve this objective.

There are two challenges in the formulation. The above two optimization problems both involve the constraint defined by the strictly feasible throughput region $\mathcal{C}$. From Lemma 7.1 we know that, for any desired throughput $\underline{\tilde{\theta}}$ in the strictly feasible region $\mathcal{C}$, there exists an operating point $\underline{r}$ such that $\underline{\theta}(\underline{r}) = \underline{\tilde{\theta}}$. However, in order to obtain $\mathcal{C}$ as in (7.2), we need to know all the feasible system states, which correspond to all the independent sets [86] in the contention graph. As is shown in [86], to compute all the independent sets (include the maximal independent sets) is a NP-hard problem. Hence it is practically difficult to obtain $\mathcal{C}$. The second

challenge is how to align the solution of (7.10) with the involvement of (7.11).

Our approach is to develop a simple mechanism which does not require a-prior knowledge of $\mathcal{C}$ and yet the radio resource can be allocated to the heterogeneous D2D links efficiently while satisfying the objectives of both the BS and D2D links. A pricing mechanism is introduced to achieve this purpose. The payoff function of each link is made to be dependent on the resource price. The BS will broadcast the resource price and use it to control the transmission behavior of each link. Mathematically, the leader solves the following optimization problem:

$$\max_{M \geq 0} \quad g(M) := \sum_{i=1}^{N} \tilde{\theta}_i(M) \tag{7.12}$$

where $\tilde{\theta}_i(M)$ is the target rate of D2D link i under the service price M, which will be presented in (7.13). The D2D links are the followers in the overall Stackelberg game, each of which chooses its transmission strategy so that their individual payoff is maximized under the service price chosen by the BS, i.e., the Stackelberg leader.

In the next section, we describe how our proposed Stackelberg game model can achieve the above purposes.

7.3 Stackelberg Games for Non-Cooperative D2D Links

Stackelberg games [33] are a class of non-cooperative games in which a leader, who makes the first move in the game, anticipates the actions of the followers based on a model of how the followers would respond to its actions. We propose a Stackelberg game, in which the BS in the cellular network acts as a Stackelberg leader to regulate the transmission behaviors of all the D2D links by broadcasting a proper service price M. The D2D links are the followers, each of which responds to the price M by choosing its transmission strategy in an attempt to maximize its individual payoff.

In Section 7.3.1, we first define the utility functions for the D2D links, each of which characterizes the individual service requirements and willingness to pay. In Section 7.3.2, we study the non-cooperative behaviors of the D2D links under a given network price M, which defines the follower-subgame in the Stackelberg game. The Stackelberg game is analyzed in Section 7.3.3. Based on the analysis, the pricing strategies of the Stackelberg leader are proposed in Section 7.3.4.

7.3.1 D2D Link Utility Function

We modify the traffic model used in [60] to our system. Suppose D2D link i has a target rate $\tilde{\theta}_i$ in the range of $[\gamma_i, \pi_i]$, where $\gamma_i \leq \tilde{\theta}_i \leq \pi_i$. If $\tilde{\theta}_i \leq \gamma_i$, link i achieves zero utility, and each link has no intention to go beyond $\tilde{\theta}_i \geq \pi_i$. The exact target rate value $\tilde{\theta}_i$ is controlled by the service price M through the following relationship

$$\tilde{\theta}_i(M) = \begin{cases} 0, & M > m_i, \\ \min\{\gamma_i - b_i(M - m_i), \pi_i\}, & 0 \leq M \leq m_i, \end{cases} \tag{7.13}$$

where γ_i, π_i and m_i together decide how link i is willing to pay for the transmission. For simplicity, we have adopted a monotonically decreasing linear function for $\tilde{\theta}_i(M)$ in the range $\gamma_i \leq \tilde{\theta}_i \leq \pi_i$, where b_i is a positive coefficient and $-b_i$ is the slope.

Eq. (7.13) is interpreted as follows. The parameter m_i is the highest price that link i is willing to pay for its transmission. When $M = m_i$, link i will only desire a minimum throughput of γ_i. When the price is too high (i.e., $M > m_i$), link i chooses not to transmit, and thus its target rate drops to zero, i.e., $\tilde{\theta}_i(M) = 0$. Over the range $0 \leq M \leq m_i$, link i is willing to pay for its transmission, and the lower the price M, the higher throughput it desires, unless it has already reached its maximum desired throughput π_i. In this range, we have used a linear function to simplify the above monotonic relationship. Other function forms such as hyperbolic, parabolic, cubic $\cdots$ can also be used, as long as the monotonic relationship is preserved. As a result, the relationship in (7.13) is a piecewise linear function. In the special case where the minimum desired throughput is $\gamma_i = 0$ and the maximum desired throughput $\pi_i \geq b_i m_i$, the piecewise linear relationship in (7.13) simply reduces to a linear relationship. A smooth monotonic curve can be similarly obtained when other function forms are adopted. Note that our algorithm works if only the monotonic function property holds.

The utility function is designed to provide differentiated treatment for the links based on their actual demand and willingness to pay for the desired transmission rate. For the example given in Fig. 7.3a, D2D link 1 and link 3 have the same range in their target rates, i.e., $\pi_1 = \pi_3$ and $\gamma_1 = \gamma_3$, and link 3 has a higher willingness to pay, i.e., $m_3 > m_1$. When the price M continually decreases from a large value until zero, link 3 will be admitted into the system first.

From the game theoretic perspective, link i will try to choose its target rate $\tilde{\theta}_i$ in order to maximize its own payoff $v_i(\theta_i) = U_i(\theta_i) - M\theta_i$ (utility minus cost). To be compatible with such an incentive, we can reversely derive the utility function of

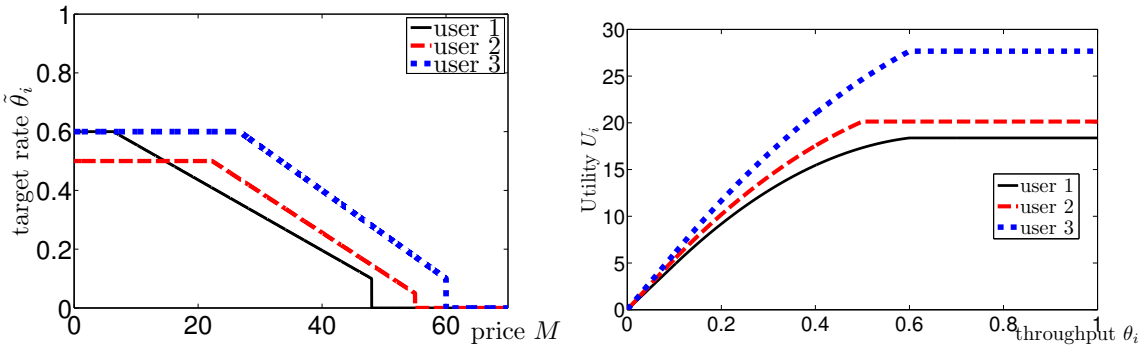

(a) Target Rates of the CSMA Users under the Price M

(b) Utility Functions of the Three CSMA Users

Figure 7.3: Target Rates and Utility Functions of the CSMA Users

D2D link i as follows. If the utility function $U_i(\theta_i)$ is concave, then the θ_i value that maximizes $v_i(\theta_i)$ is given by the first-order condition $v_i'(\theta_i) = 0$, i.e., $\tilde{\theta}_i = (U_i')^{-1}(M)$. Equating with the example of (7.13) and we can reversely derive the utility function for D2D link i:

$$U_i(\theta_i) = \begin{cases} m_i\theta_i, & 0 \le \theta_i < \gamma_i, \\ m_i\theta_i - \frac{(\theta_i-\gamma_i)^2}{2b_i}, & \gamma_i \le \theta_i < \pi_i, \\ m_i\pi_i - \frac{(\pi_i-\gamma_i)^2}{2b_i}, & \pi_i \le \theta_i \le 1. \end{cases} \tag{7.14}$$

The utility functions for the three links' example in Fig. 7.3a are plotted in Fig. 7.3b. If we take the derivative of $U_i(\theta_i)$ on θ_i in (7.14), it can be seen that a higher m_i value corresponds to a steeper slope, which suggests a higher willingness to pay. This can be seen from Fig. 7.3b, in which the utility function of link 3 has a steeper slope than that of link 1.

7.3.2 A Subgame of Noncooperative CSMA Users

The Stackelberg game at the l-th iteration begins with the BS broadcasting a price $M^{(l)}$. Each D2D link i ($i \in \mathcal{N}$) aims to maximize its payoff $v_i(\theta_i) = U(\theta_i) - M^{(l)}\theta_i$. According to the analysis in Section 7.3.1, link i's objective is equivalent to attaining a target rate $\tilde{\theta}_i^{(l)}$ under the service price $M^{(l)}$, as given in (7.13). Whether these target rates are achievable still depends on whether the underlying CSMA mechanism can support these transmissions. The D2D links therefore play a CSMA game among themselves to determine their individual TAs to make the throughput θ_i as close to $\tilde{\theta}_i^{(l)}$ as possible. This CSMA game is therefore the follower-subgame in the Stackelberg game. To avoid the links from transmitting too aggressively and

driving the network to unstable states as a result of congestion, a simple approach is to let M begin with a large value and then gradually decrease.

We formally state the CSMA subgame as follows:

Players: Distributed Tx-Rx pairs (D2D links), $i \in \mathcal{N}$, who compete to transmit in the ideal CSMA network.

Strategies: Each player i chooses its TA $r_i \in \mathbb{R}$, $\forall i \in \mathcal{N}$.

Objectives: Each player i ($i \in \mathcal{N}$) aims to achieve its target rate $\tilde{\theta}_i^{(l)}$ set by maximizing its payoff

$$v_i(\theta_i) = U(\theta_i) - M^{(l)}\theta_i \tag{7.15}$$

under the given service price $M^{(l)}$.

Note that the throughput θ_i that player i can achieve is determined by its own TA r_i and the TAs of all the other players r_{-i} based on the relationships in (2.11). The equilibrium solution of the CSMA subgame is a NE [33], which is defined as a strategy profile $\underline{r}^* = [r_1^*, \cdots, r_N^*])$ in which player i's strategy r_i^* is a best response to the strategies of all the other players r_{-i}^* , i.e.,

$$r_i^* = \arg \min_{r_i \in (-\infty, +\infty)} |\tilde{\theta}_i^{(l)} - \theta_i(r_i, r_{-i}^*)|, \forall i \in \mathcal{N}, \tag{7.16}$$

where $\theta_i(\underline{r})$ is the achieved throughput of D2D link i in the ICN model, as given in (2.11).

It is clear that the objective of the subgame is to find the equilibrium TAs for all D2D links so that every link achieves throughputs that are as close to what are desired. According to Lemma 7.1, if the target rate $\underline{\tilde{\theta}}$ is in $\mathcal{C}$, i.e., it is achievable, then there exists a unique TA $\underline{r}^*$ such that $\theta_i^*(\underline{r}^*) = \tilde{\theta}_i^{(l)}, \forall i \in \mathcal{N}$. On the other hand, if the target rate $\underline{\tilde{\theta}}$ is beyond $\mathcal{C}$, during the myopic best response updates, all players will eventually achieve $r_i^* = +\infty, \forall i$ if there is no further control taken, i.e., all links transmit aggressively and result in undesired network congestion. The existence and uniqueness of the NE in the CSMA subgame can then be established in the following proposition.

Proposition 7.1. *For the target rate $\underline{\tilde{\theta}} \in \mathcal{C}$ (strictly feasible region), there exists a unique finite-valued NE $\underline{r}^* \in \mathbb{R}^N$ in the CSMA subgame. Moreover, the target rate $\underline{\tilde{\theta}}$ is achieved at the NE, i.e., $\underline{\theta}^*(\underline{r}^*) = \underline{\tilde{\theta}}$.*

Proof: From Lemma 7.1, if the target rate $\underline{\tilde{\theta}} \in \mathcal{C}$ (strictly feasible region), then there exists a unique finite-valued $\underline{r}^* \in \mathbb{R}^N$ such that $\underline{\theta}^*(\underline{r}^*) = \underline{\tilde{\theta}}$. As can be seen from (7.16), there exists a unique NE $\underline{r}^*$, since the payoff of each player is

maximized when $\underline{\theta}^*(\underline{r}^*) = \underline{\tilde{\theta}}$ and no player has the incentive to deviate from this NE unilaterally. ■

In practice, the strategies of all the other players r_{-i} are usually not known by player i if we assume that there is no explicit information exchange among the players. We therefore design some distributed updating method for the players to arrive at the NE. Let each player update its strategy by measuring its own local statistics, e.g., measured throughput $\hat{\theta}_i$. For the k-th measurement period $\tau(k)$, player i keeps a record of the accumulated transmission time, $T_i(k)$, and obtains the empirical average throughput as

$$\hat{\theta}_i(k) = T_i(k)/\tau(k), \forall i \in \mathcal{N}. \tag{7.17}$$

A distributed way for player i to update its strategy can be

$$r_i(k+1) = r_i(k) + \alpha \cdot (\tilde{\theta}_i^{(l)} - \hat{\theta}_i(k)), \forall i \in \mathcal{N}, \tag{7.18}$$

where α is a small positive step size. The conditions for the convergence of the NE in the CSMA subgame are summarized in the following proposition.

Proposition 7.2. *For the target rate $\underline{\tilde{\theta}} \in \mathcal{C}$ (strictly feasible region), the iteration dynamics in (7.18) with a small enough step size α and a long enough measurement period τ will always converge to the NE $\underline{r}^* \in \mathbb{R}^N$ in the CSMA subgame.*

Proof: We apply the same idea used when proving Lemma 7.1. Given a $\underline{\tilde{\theta}} \in \mathcal{C}$, we use the maximum log-likelihood method to estimate the parameters $\underline{r}^*$ which result in $\underline{\theta}(\underline{r}^*) = \underline{\tilde{\theta}}$, or equivalently, result in the desired state probability distribution $\underline{p}^{\tilde{\theta}}$ such that $\underline{\tilde{\theta}} = \sum_{\underline{s} \in \mathcal{S}} p_{\underline{s}}^{\tilde{\theta}} \underline{s}$. The log-likelihood function $F(\underline{r}; \underline{\tilde{\theta}})$ is given in (7.4). It has been shown in Section 7.2.2 that $F(\underline{r}; \underline{\tilde{\theta}})$ is a strictly concave function in $\underline{r}$ and attains its maximum when $\underline{\theta}(\underline{r}^*) = \underline{\tilde{\theta}}$. Therefore, we can use the subgradient method [152] to obtain the optimal solution $\underline{r}^*$, where $\tilde{\theta}_i^{(l)} - \hat{\theta}_i(k)$ is an estimation of the gradient $\frac{\partial F(\underline{r}; \underline{\tilde{\theta}})}{\partial r_i}$ (see (7.8)) in the k-th measurement period. Since the objective function $F(\underline{r}; \underline{\tilde{\theta}})$ is differentiable and concave in $\underline{r}$, the subgradient method with constant step size α yields convergence to the optimal value, provided the step size α is small enough and the measurement period is long enough [152]. In summary, the above proposition follows. ■

As mentioned above, under the myopic best response update approach, if the target rate $\underline{\tilde{\theta}}$ is beyond $\mathcal{C}$, all players will eventually achieve $r_i^* = +\infty, \forall i$, and the network will be pushed into the totally congested situation. To overcome this prob-

lem, we impose a upper limit r_{max} on $r_i, \forall i \in \mathcal{N}$ as an implementation constraint. The iteration dynamics in (7.18) then become:

$$r_i(k+1) = \min\{r_i(k) + \alpha \cdot (\tilde{\theta}_i^{(l)} - \hat{\theta}_i(k)), r_{max}\}, \forall i \in \mathcal{N}. \tag{7.19}$$

The physical meaning of imposing the r_{max} constraint is to refrain the D2D links from transmitting too aggressively, so that the local congestion at some links will not affect the whole network. The outcome of introducing such a restriction is that the feasible throughput region will shrink into a subset of the original one. Hence the solution obtained with this constraint imposed is always ensured to be within $\mathcal{C}$. During the myopic play, if any link arrives at r_{max}, the BS will be informed. Then the price M is frozen and the whole D2D network functions at the boundary of the "shrunken" feasible throughput region. If this happens, not all users are able to achieve their desired rates or even admitted, as the network is in "congestion".

7.3.3 Analysis of the Stackelberg Game

In this subsection we analyze the game structure of the Stackelberg game. From Proposition 7.1 and Proposition 7.2, to satisfy $\underline{\tilde{\theta}} \in \mathcal{C}$, it is equivalent to checking that the CSMA subgame converges to the unique subgame NE $\underline{r}^*$ defined in (7.16) under the given service price M. Therefore, the leader problem in (7.12) is equivalent to the following optimization problem:

$$\begin{aligned} \max_{M \geq 0} \quad & g(M) \\ \text{s.t.} \quad & \begin{cases} \text{equality constraint (7.13)}, \forall i \in \mathcal{N}, \\ \text{equality constraint (7.16)}, \\ r_i^* < r_{max}, \forall i \in \mathcal{N}, \end{cases} \end{aligned} \tag{7.20}$$

where r_i^* is the TA of D2D link i at the NE of the CSMA subgame, as given in (7.16). The constraint $r_i^* < r_{max}, \forall i \in \mathcal{N}$ implies that the target rate $\underline{\tilde{\theta}}$ as given in (7.13) is strictly feasible at the subgame NE, i.e., the throughput will converge to $\underline{\theta}^*(\underline{r}^*) = \underline{\tilde{\theta}}$ in the CSMA subgame.

To distinguish from the NE $\underline{r}^*$ in the CSMA subgame, we call the equilibrium solution $(M^{opt}, \underline{r}^{opt})$ of the Stackelberg game as the Stackelberg Equilibrium (SE) [153], where M^{opt} is the optimal solution to (7.20) and $\underline{r}^{opt}$ is the subgame NE under the price M^{opt}.

The problem in (7.20) is non-convex [142, pp. 136] since the objective function

$g(M) = \sum_{i=1}^{N} \tilde{\theta}_i(M)$ is non-concave in M and the equality constraints (7.13) and (7.16) are nonlinear. Fortunately, the problem can be converted into a quasi-convex optimization problem [142, pp. 144] and the solution can be iteratively evaluated by solving a sequence of convex optimization problems. It can be interpreted in the following way. Since the target rate $\tilde{\theta}_i(M)$ of each D2D link i is non-increasing with the price M, the chain of prices $M^{(0)} > M^{(1)} > \cdots > M^{(l)} > M^{(l+1)}$ induces a chain of target rates $\underline{\tilde{\theta}}^{(0)} \preceq \underline{\tilde{\theta}}^{(1)} \preceq \cdots \preceq \underline{\tilde{\theta}}^{(l)} \preceq \underline{\tilde{\theta}}^{(l+1)}$. Therefore, the objective function $g(M) = \sum_{i=1}^{N} \tilde{\theta}_i(M)$ is also non-increasing with M, and hence is quasi-concave in M. Regarding the constraints in (7.20), from Lemma 7.1, if the target rate $\underline{\tilde{\theta}}^{(l)} \in \mathcal{C}$ (strictly feasible throughput region, which is the interior of the feasible throughput region $\bar{\mathcal{C}}$), then it is achievable with finite-valued TAs $\underline{r}^*$. On the other hand, from Theorem 7.1, if the target rate $\underline{\tilde{\theta}}^{(l)} \notin \bar{\mathcal{C}}$, then any target rate $\underline{\tilde{\theta}}^{(l+1)} \succeq \underline{\tilde{\theta}}^{(l)}$ is not in $\bar{\mathcal{C}}$, i.e., it is not achievable and the constraints in (7.20) are not satisfied. The crossing from within $\bar{\mathcal{C}}$ to beyond can be detected by the use of r_{max}. Therefore, the superlevel set $\{M|g(M) \geq G\}$ is convex, which is equivalent to the line segment $\{M|g^{-1}(\sup g) \leq M \leq g^{-1}(G)\}$, where G is a constant, g^{-1} is the inverse function of $g(M)$, and $\sup g$ is the optimal value of (7.20).

In summary, the problem in (7.20) is quasi-convex [142, pp. 144], since the objective function $g(M)$ to be maximized is quasi-concave, and the superlevel set $\{M|g(M) \geq G\}$ is convex. As a result, the problem in (7.20) can be reduced into a sequence of feasibility problems:

$$\begin{aligned} \text{find} \quad & M \\ \text{s.t.} \quad & \begin{cases} g(M) \geq G, \\ \text{equality constraint (7.13)}, \forall i \in \mathcal{N}, \\ \text{equality constraint (7.16)}, \\ r_i^* < r_{max}, \forall i \in \mathcal{N}. \end{cases} \end{aligned} \tag{7.21}$$

If the problem (7.21) is feasible, then the maximum total throughput $\sup g$ is not less than G. Conversely, if the problem (7.21) is infeasible, then we can conclude $\sup g < G$. In order to find the optimal value $\sup g$ to the problem (7.20), we can test different superlevels G in the feasibility problem (7.21).

For each superlevel G, from the proof of Proposition 7.2, the feasibility problem

in (7.21) is equivalent to the following max-log-likelihood problem:

$$\begin{aligned} \max_{\underline{r}} \quad & F(\underline{r};\underline{\tilde{\theta}}) \\ \text{s.t.} \quad & \begin{cases} \text{equality constraint (7.13)}, \forall i \in \mathcal{N}, \\ M = g^{-1}(G), \\ r_i < r_{max}, \forall i \in \mathcal{N}, \end{cases} \end{aligned} \tag{7.22}$$

where $F(\underline{r};\underline{\tilde{\theta}})$ is the log-likelihood function defined in (7.4). In other words, if the problem (7.21) is feasible, then there exists a price $M = g^{-1}(G)$, such that the target rate $\underline{\tilde{\theta}}(M)$ is achievable with finite TA $r_i < r_{max}, \forall i \in \mathcal{N}$. Therefore, we can use the max-log-likelihood method to estimate the parameters $\underline{r}$ which achieve the target rate $\underline{\tilde{\theta}}(M)|_{M=g^{-1}(G)}$, as given in (7.13). Notice that given the constant G, the price M and the target rate $\underline{\tilde{\theta}}$ become constant values as well. Moreover, as shown in the proof of Proposition 7.2, the log-likelihood function is concave in $\underline{r}$. As a result, the max-log-likelihood problem in (7.22) is a convex optimization problem, and can be solved by the subgradient updating method in (7.19).

If the iteration dynamics converge to a subgame NE with $r_i^* < r_{max}, \forall i \in \mathcal{N}$, then the optimal solution to (7.22) exists, i.e., the problem (7.21) is feasible. Otherwise, if the iteration dynamics in (7.19) converge to a subgame NE with $r_i^* = r_{max}$ and $\theta_i^* < \tilde{\theta}_i$ for some D2D link i, then the optimal solution to (7.22) does not exist and the problem (7.21) is infeasible, i.e., not all D2D links' target rates are being achieved.

In summary, the problem in (7.20) can be reduced into a sequence of convex optimization problems. A simple bisection method can be used to choose the superlevels G (or equivalently, the price $M = g^{-1}(G)$) and test the feasibility problem (7.21). Alternatively, we can borrow ideas from the feasible direction method [154, Chap. 10] which avoids testing in the infeasible region, and design the pricing strategies so as to keep the network operating in the feasible region while tuning the price M.

7.3.4 Pricing Strategies of the Stackelberg Leader

We call each round of CSMA subgame under a certain price M as a *stage* in the Stackelberg game. In each stage, the leader needs the feedback from each D2D link i about its target rate $\tilde{\theta}_i$, and the converged TA r_i^* and throughput θ_i^*. Notice that the leader only has knowledge about the monotonicity of the D2D link's target rate with the price M and no information about (7.13) of all links is required.

Under some low load situations, all links achieve their maximum desired through-

put $\pi_i, \forall i \in \mathcal{N}$, if for all links $i \in \mathcal{N}$, the target rate $\tilde{\theta}_i > 0$ and remains unchanged between two consecutive prices $M^{(l)}$ and $M^{(l+1)}$. Under heavy load situations, the pricing strategies of the Stackelberg leader need to be carefully designed to converge to the optimal price M^{opt}.

To detect convergence, we define $\Delta_i = r_{max} - r_i^*$ as the "margin" of transmission aggressiveness for each D2D link $i \in \mathcal{N}$. When the achieved target rates are close to the capacity boundary, the leader can make use of $\Delta_{min} = \min\{\Delta_i, \forall i \in \mathcal{N}\}$ as an indication of how close the current throughput $\underline{\theta}^*$ is to the boundary of $\mathcal{C}$. Since the total throughput $g(M)$ is non-increasing with the price M, the leader can gradually decrease M to increase $g(M)$ until the constraint $r_i^* < r_{max}$ is "critically" satisfied for some D2D link says i, i.e., $\Delta_{min} \leq \epsilon$, where ϵ is a small positive threshold.

The algorithm at the BS works as follows. In the 0-th stage, the leader can start with a large price $M^{(0)}$ so that the network starts with low load. Similar to the Newton method [142, pp. 488] which applies line search to narrow down the searching region before using Newtonian steps to refine the optimal solution, the adjustment of our price strategies consist of two phases as well. In the first phase the leader uses a relatively large decrement step ϕ to decrease price M until $\Delta_{min} \leq \eta$, where $\eta > \epsilon$ is a threshold before entering the second phase. In the second phase, the decrement steps are refined using Δ_{min} since Δ_{min} is getting smaller as the target rates are approaching the boundary of the feasible throughput region.

In summary, the leader can update its price M based on Δ_{min} at the end of the l-th stage as follows:

$$M^{(l+1)} = \begin{cases} M^{(l)} - \phi, & \Delta_{min} > \eta, \\ \max\{M^{(l)} - \beta \cdot \Delta_{min}, M_{lower}\}, & \Delta_{min} \leq \eta, \end{cases} \tag{7.23}$$

where ϕ is a positive constant, β is a positive parameter. M_{lower} is initially set at 0 and is updated to take the value of current $M^{(l)}$ once it is detected that the solution for the target rate $\underline{\tilde{\theta}}$ is outside the feasible region. Its purpose is to ensure that subsequent $M^{(l+1)}, \cdots$ should not go below this value. The parameter β can be chosen to be small enough so that the price gradually decreases until $\Delta_{min} \leq \epsilon$. However, for faster convergence, it might happen that the initially chosen β is too large such that the new price $M^{(l+1)}$ pushes the target rate $\underline{\tilde{\theta}}$ to be outside the feasible region, i.e., $r_i^* = r_{max}$ but $\theta_i^* < \tilde{\theta}_i$ for some D2D link i. In such cases, the leader stores the current unachievable price as the new lower bound M_{lower}, resets the price to the previously found achievable price M_{prev}, and reduces β by a discount factor σ, e.g., $\sigma = 0.9$.

The pricing strategies of the leader and the CSMA subgame are summarized in Algorithm 7.1. Through Algorithm 7.1, the Stackelberg game is guaranteed to gradually converge to the optimal price M^{opt} under which the total throughput of the CSMA users are maximized while their heterogeneous target rates can all be satisfied.

Algorithm 7.1 Iteration Process of the Stackelberg Game

Initialize:
The BS chooses the initial price $M = M^{(0)}$ and informs the D2D links in the control plane;
Each D2D link $i \in \mathcal{N}$ chooses the initial TA $r_i(0)$;

repeat:
    In the l-th stage:
    for $i = 1, \cdots, N$ D2D links **do**:
        Set the target rate $\tilde{\theta}_i^{(l)}$ based on the price $M^{(l)}$, as in (7.13);
    end for

    repeat:
        In the k-th measurement period:
        for $i = 1, \cdots, N$ users **do**:
            Estimate the empirical throughput $\hat{\theta}_i(k)$, as in (7.17);
            Update the TA $r_i(k+1)$, as in (7.19);
        end for
        $k \leftarrow k + 1$;
    until $\underline{r}$ converges to the subgame NE $\underline{r}^*$.
    Each user $i \in \mathcal{N}$ informs the BS about $\tilde{\theta}_i^{(l)}$, r_i^* and θ_i^*;

    At the BS:
    $\Delta_{min} = \min_{i \in \mathcal{N}} \Delta_i = \min_{i \in \mathcal{N}} (r_{max} - r_i^*)$;
    if $\Delta_{min} > \epsilon$ **then**:
        set $M^{(l+1)}$ as in (7.23); $M_{prev} = M^{(l)}$; $\Delta_{prev} = \Delta_{min}$.
    else if $0 < \Delta_{min} \leq \epsilon$ or ($\underline{\tilde{\theta}}^{(l)} \succ \underline{0}$ and $\underline{\tilde{\theta}}^{(l)} = \underline{\tilde{\theta}}^{(l-1)}$) **then**:
        The Stackelberg game converges with $M^{opt} = M^{(l)}$; go to **END**.
    else if $r_i^* = r_{max}$ but $\theta_i^* < \tilde{\theta}_i$ for some user i **then**:
        $M_{lower} = M^{(l)}$; $\beta \leftarrow \sigma \cdot \beta$; $M^{(l+1)} = \max\{M_{prev} - \beta \cdot \Delta_{prev}, M_{lower}\}$.
    end if
    $l \leftarrow l + 1$;
until The Stackelberg game converges. **END**.

An important side-information which can be provided by the proposed algorithm is the identification of the bottleneck link in the heterogeneous D2D networks. Upon convergence of the Stackelberg game, the D2D link $L = \arg\min\{\Delta_i, \forall i \in \mathcal{N}\} = \arg\min\{r_{max} - r_i^{opt}, \forall i \in \mathcal{N}\}$ is the bottleneck link to the network since any further decrease on the price M^{opt} would drive the target rate $\underline{\tilde{\theta}}$ to be outside the capacity

region and link L can no longer achieve its target rate. The identification of such bottleneck links can be of valuable information, for example, in data offloading, to re-assign these links back to the cellular network when necessary. A possible way to improve system performance is to remove the bottleneck link L in the D2D network and port link L's traffic towards the conventional cellular mode. How to achieve optimal trade-off remains as interesting future work.

7.3.5 Complexity of Algorithm 7.1

Algorithm 7.1 consists of two loops. In the outer loop, the BS chooses a service price $M^{(l)}$ at the l-th stage according to the pricing strategies in Section 7.3.4. In the inner loop, for each given service price $M^{(l)}$, the D2D links play the CSMA subgame distributively and iteratively until converging to their respective target rates. We analyze the complexity in terms of the number of iterations required, first for the CSMA subgame, then for setting the pricing strategies.

For the CSMA subgame, assume that the target rate $\underline{\tilde{\theta}}$ under the given service price $M^{(l)}$ is in the strictly feasible region $\mathcal{C}$. According to Proposition 7.1 and Proposition 7.2, the distributed strategy updates of the CSMA users in (7.18) are equivalent to the gradient method in maximizing the log-likelihood function $F(\underline{r};\underline{\tilde{\theta}})$ which is differentiable and strictly concave in $\underline{r}$. In particular, the gradient of $F(\underline{r};\underline{\tilde{\theta}})$ is $\nabla F(\underline{r};\underline{\tilde{\theta}}) = \underline{\tilde{\theta}} - \underline{\theta}(\underline{r})$, as shown in (7.8). Since the maximum value of $F(\underline{r};\underline{\tilde{\theta}})$ is finite and attained at $\underline{r}^*$, hence $\underline{\theta}^*(\underline{r}^*) = \underline{\tilde{\theta}}$ can be solved by setting the gradient $\nabla F(\underline{r}^*;\underline{\tilde{\theta}}) = \underline{0}$.

Since the norms of the throughput $\underline{\theta}(\underline{r})$ and its gradient $\nabla\underline{\theta}(\underline{r})$ are both bounded, it can be shown that $\nabla F(\underline{r};\underline{\tilde{\theta}})$ is Lipschitz continuous [155] in $\underline{r}$, i.e., $\|\nabla F(\underline{r}_a;\underline{\tilde{\theta}}) - \nabla F(\underline{r}_b;\underline{\tilde{\theta}})\| = \|\underline{\theta}(\underline{r}_a) - \underline{\theta}(\underline{r}_b)\| \leq H\|\underline{r}_a - \underline{r}_b\|$, $\forall \underline{r}_a, \underline{r}_b \in \mathbb{R}^N$, where H is a positive constant. According to Theorem 1 in [155, Section 1.4] and Theorem 2.1.14 in [156, Section 2.1.5], for small enough step size α ($0 < \alpha \leq 1/H$), the number of iterations to reach $\|\nabla F(\underline{r};\underline{\tilde{\theta}})\| = \|\underline{\tilde{\theta}} - \underline{\theta}(\underline{r})\| < \xi$ is $O(1/\xi)$ (i.e., no more than a fixed multiple of $1/\xi$).

It is worth to mention that although this complexity $O(1/\xi)$ on the number of required iterations is independent on the number of users, we have inherently assumed that the measurement period τ is long enough to provide an accurate estimation of throughputs. In fact, the choice of τ depends on the number of users and the underlying topology. The purpose of choosing a large τ is to ensure that the Markov chain corresponding to the updated $\underline{r}$ reaches its stationary distribution

to allow for an accurate estimation of throughputs. In general, a larger number of users requires a larger value of τ. More comparisons and discussions on how to choose τ for a given number of users and different topologies can be found in [150].

We now briefly discuss how to estimate the number of pricing stages required in the outer loop. This analysis is complicated by the fact that the step sizes for M are changing each time. Assume that the maximum value of the price is M_{max}. In phase 1 of the price setting, since the price is decreasing at a large constant step ϕ, the number of pricing stages in phase 1 is capped by $\lceil M_{max}/\phi \rceil$, or $\lceil M_{max}/\phi \rceil/2$ on average. In phase 2, the TA margin $\Delta_{min} \leq \eta$, and the price is already close to the optimal. In the algorithm, we refine the price change $\delta M^{(l+1)} = M^{(l+1)} - M^{(l)}$ at stage l according to $\delta M^{(l+1)} = -\beta \Delta_{min}^{(l)}$ progressively until the TA margin gradually approaches the required precision ϵ, i.e., $\Delta_{min} \leq \epsilon$. Assume that the interval $\epsilon < \Delta_{min} \leq \eta$ is small, through simulations we find that the relationship between the TA margin $\Delta_{min}^{(l+1)}$ and the price change $\delta M^{(l+1)}$ can be approximated by $\Delta_{min}^{(l+1)} = \Delta_{min}^{(l)} + B \cdot \delta M^{(l+1)}$, where B is a positive constant. Since we set $\delta M^{(l+1)} = -\beta \Delta_{min}^{(l)}$, hence $\Delta_{min}^{(l+1)} = \Delta_{min}^{(l)} + B \cdot (-\beta \Delta_{min}^{(l)}) = (1 - \beta B)\Delta_{min}^{(l)}$. The TA margin then follows a geometric progression and we can estimate the value of h, so that $\delta M^{(l+h)} \leq \epsilon$. Hence it can be easily shown that the number of stages for Δ_{min} to decrease from η to ϵ is approximately $\frac{\log_{10} \eta/\epsilon}{\log_{10} 1/(1-\beta B)}$, or $O(d \log_{10}(\eta/\epsilon))$ for some suitable choices of β and B ($0 < \beta B < 1$), where $d = \frac{1}{\log_{10} 1/(1-\beta B)}$. Note that β can be chosen according to the value of B, but B is topology and utility dependent. As a result, the total number of stages required for convergence is $O(1/\phi) + O(d \log_{10}(\eta/\epsilon))$.

In summary, the number of iterations required for convergence in the proposed game is given by the number of iterations per stage multiplied by the required number of stages, i.e., $O(1/\xi) \cdot (O(1/\phi) + O(d \log_{10}(\eta/\epsilon)))$.

7.4 Simulation Study

In this section we demonstrate the Stackelberg game via an example. Consider the 8 D2D links' contention graph in Fig. 7.4a. Assume that the relationships between the links' target rates and the price M are given as in Fig. 7.4b. In the ICN model, we assume that the links' transmission time is uniformly distributed with mean of 1 ms in the range $[0.5, 1.5]$ ms. Further assume that link i's backoff time is uniformly distributed with mean of $1/\exp(r_i)$ ms in the range $[0, 2/\exp(r_i)]$ ms.

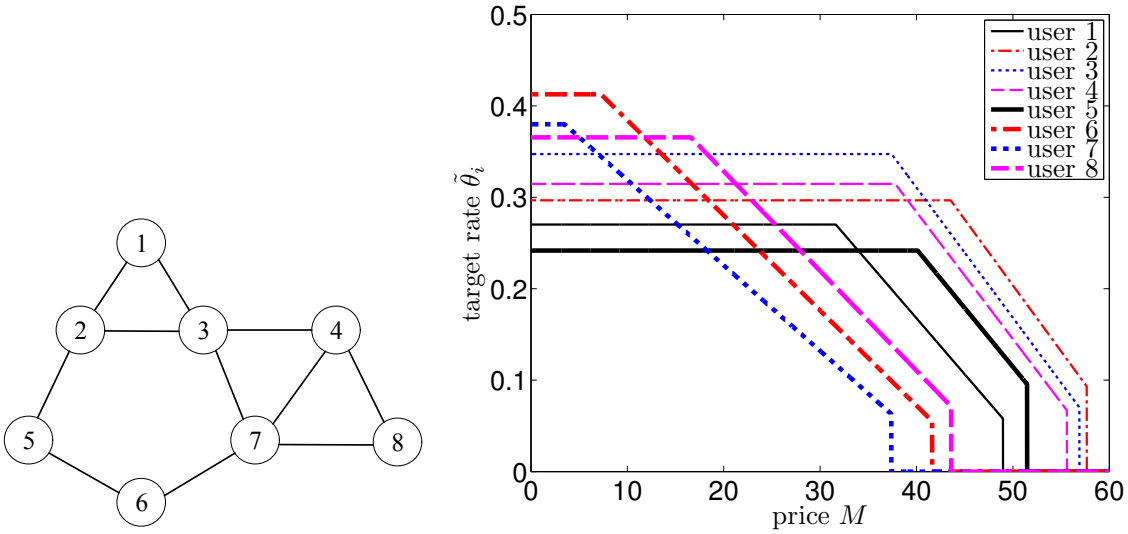

(a) contention Graph (b) Target Rates under Price M

Figure 7.4: Topology and Target Rates of 8 D2D Links

7.4.1 CSMA Subgame

Assume that the current price $M = 30$, then from Fig. 7.4b we know that the D2D links' target rates are $\underline{\tilde{\theta}} = [0.270, 0.297, 0.347, 0.315, 0.242, 0.176, 0.132, 0.220]$. Assume that the initial TAs $r_i = -2, \forall i \in \mathcal{N}$. The CSMA subgame is then played according to Lines 10 to 17 in Algorithm 7.1. In the k-th measurement period, we apply a simple averaging filter to smooth the measured throughput as:

$$\hat{\theta}_i(k) = (1 - \delta) \cdot \hat{\theta}_i(k-1) + \delta \cdot T_i(k)/\tau, \forall i \in \mathcal{N}, \tag{7.24}$$

where δ is the weight of the new measurement. In our simulations, we choose $\delta = 0.05$ and the measurement time $\tau = 200$ ms. A smaller value of δ makes the measured throughput more smooth, but also increases the convergence time. To update TAs as in (7.19), we choose the step size $\alpha = 0.4$ and the maximum allowable TA $r_{max} = 3$. Note that a smaller value of α guarantees the convergence of the CSMA subgame, but also increases the convergence time. The iteration process of the CSMA subgame is then plotted in Fig. 7.5. The CSMA subgame converges to 99% of the target rates ($\xi = 1\%$) in around 150 iterations. According to the complexity analysis in Section 7.3.5, the number of required iterations is $O(1/\xi)$, i.e., in the order of a fixed multiple of $1/\xi = 100$. Thus our simulation result is in the same order as the above prediction.

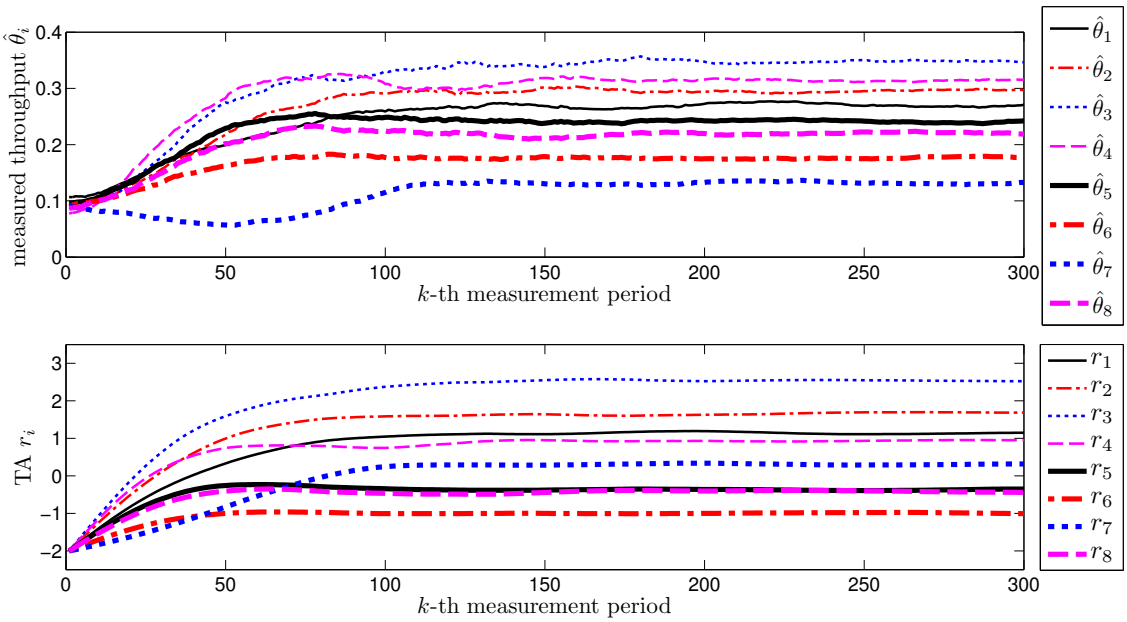

Figure 7.5: CSMA Subgame of the 8 D2D links under $M = 30$

7.4.2 Stackelberg Game

Assume that the initial price $M^{(0)} = 55$, $\phi = 5$, $\beta = 5$, $\eta = 1$, $\epsilon = 0.1$, $\sigma = 0.9$, and the rest of the parameters are the same as in Section 7.4.1. The iteration process of the Stackelberg game is shown in Fig. 7.6. The game converges after 11 stages, in which $\Delta_{min} = r_{max} - r_3 = 3 - r_3$ and gradually approaches 0. The first 6 stages undergo a constant price decrement ($\phi = 5$), i.e., $M = 55, 50, 45, 40, 35, 30$ until $\Delta_{min} \leq \eta = 1$ is detected. After the CSMA subgame converges under the price $M = 30$, we have $\Delta_{min} = r_{max} - r_3^* = 3 - 2.4 = 0.6$ and hence $0.1 = \epsilon < \Delta_{min} < \eta$. Therefore, the Stackelberg game enters the second pricing phase, which consists of 5 stages ($M = 27.10, 25.00, 23.68, 22.73, 22.12$), according to (7.23). We consider the game converged when $\Delta_{min} \approx 0.08 < \epsilon$ and the optimal price is $M^{opt} = 22.12$. After convergence, the average error of the measured throughputs as compared to the target rates is around $\xi = 1\%$. Notice that we cannot decrease M any further since the network is already close to the capacity boundary ($r_3^* = 2.92 \approx r_{max} = 3$). In other words, any further decrease on M would drive the target rate $\vec{\tilde{\theta}}$ to be outside the capacity region and some D2D links (e.g., link 3) can no longer achieve their target rates. In summary, the proposed Stackelberg game is able to maximize the total throughput of the CSMA users while the target rates of the heterogeneous users can all be satisfied.

The number of required stages before convergence is consistent with the analysis in Section 7.3.5. In the above simulations, the maximum value of the price is

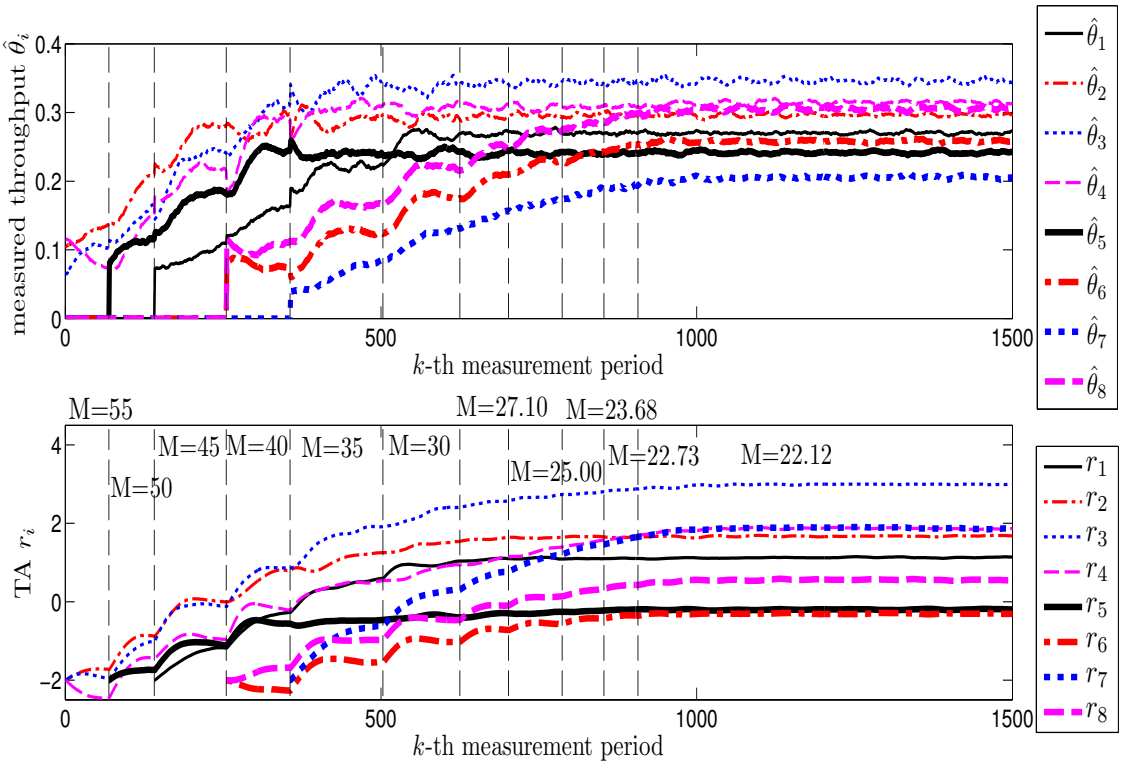

Figure 7.6: Stackelberg Games of the 8 D2D Links

$M_{max} = 60$, and the constant step $\phi = 5$. Therefore, the maximum number of stages in phase 1 is $\lceil M_{max}/\phi \rceil = 12$, or 6 on average. In the simulations, phase 1 actually consists of 6 stages before entering phase 2. In phase 2, the required precision $\epsilon = 0.1, \eta = 1$ and the required number of stages is $O(d \log_{10}(\eta/\epsilon))$, where $d = \frac{1}{\log_{10} 1/(1-\beta B)}$. The value of B can be estimated by using $(\Delta_{min}^{(l+1)} - \Delta_{min}^{(l)})/(M^{(l+1)} - M^{(l)})$, which is approximately 0.07 in the small interval $\epsilon < \Delta_{min} \leq \eta$. Since we have chosen $\beta = 5$, hence $0 < \beta B = 0.35 < 1$ and $d = \frac{1}{\log_{10} 1/(1-\beta B)} = 5.3$, and the required stages in phase 2 is in the order of a fixed multiple of $d \log_{10}(\eta/\epsilon) = 5.3$. In the simulations, phase 1 actually consists of 5 stages before convergence. Note that a smaller β could be used to guarantee $\beta B < 1$, however, it also increases d and hence requires more stages for convergence. Finally, the total number of iterations required in the Stackelberg game is $O(1/\xi) \cdot (O(1/\phi) + O(d \log_{10}(\eta/\epsilon)))$, which is in the order of $100 \cdot (6 + 5.3) = 1130$. In the simulations, the Stackelberg game actually converges in around 1000 iterations, which is in the same order as the above prediction.

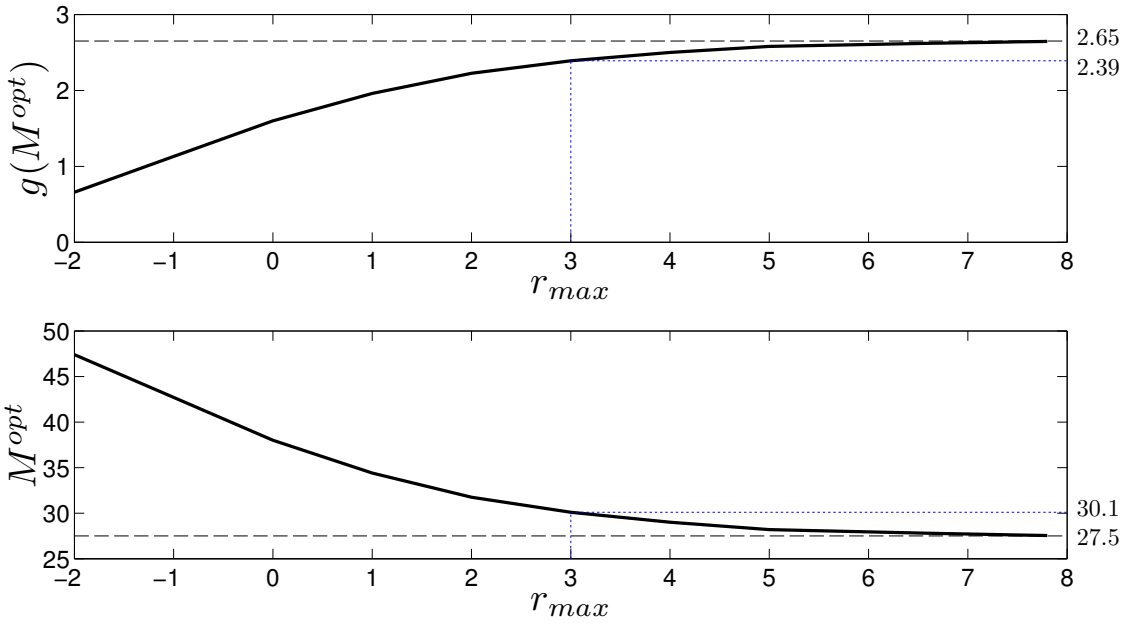

Figure 7.7: Effect of Parameter r_{max}

7.4.3 Effect of Parameter r_{max}

In the above simulations, we have used the parameter $r_{max} = 3$, and obtained the optimal price M^{opt} that maximizes the total throughput $g(M)$ for the 8 users in Fig. 7.4 with heterogeneous rate requirements. As is discussed at the end of Section 7.3.2, by introducing the r_{max} constraint, the feasible throughput region will shrink into a subset of the original one. In this subsection, we apply different values of r_{max} to the network and obtain the optimal price M^{opt} that maximizes the total throughput $g(M)$ for the 8 users in Fig. 7.4a. To see the effect of parameter r_{max} only, we assume that the 8 users are homogeneous in their rate requirements, i.e., $\gamma_i = 0.05, \pi_i = 0.55, b_i = 0.0125, m_i = 50, \forall i \in \mathcal{N}$.

The optimal price M^{opt} and the corresponding total throughput $g(M^{opt})$ under each value of the parameter r_{max} are plotted in Fig. 7.7. From Fig. 7.7 we can see that, as the value of r_{max} increases, the achievable total throughput $g(M^{opt})$ also increases, moreover, the rate of increase gradually slows down. In particular, when $r_{max} = 3$, the achievable total throughput is 2.39. For $r_{max} > 3$, the total throughput curve becomes almost flat and approaches the upper bound 2.65 when r_{max} tends to infinity, under which the shrunken capacity region stretches back to the original feasible throughput region $\bar{\mathcal{C}}$. The corresponding bound on the optimal price is $M^{opt} = 27.5$. In other words, we cannot further reduce the price M below 27.5 to increase the target rate $\underline{\tilde{\theta}}$, as it is already on the boundary of the feasible

throughput region $\bar{\mathcal{C}}$.

It is observed from Fig. 7.7 that a larger r_{max} value leads to a larger capacity region, but this also allows for longer transmission durations. However, the transmission duration should not be too long in practice, otherwise it would lead to large access delay (where the access delay refers to the time between the onset of two consecutive successful transmissions of a link) and large variations of the delay. The readers are referred to [95, Sec. IV] for more discussions. As a result of the above observations, we have adopted $r_{max} = 3$ in the above two subsections.

7.4.4 Performance Comparison with Generalized Aloha Game under BS Pricing

We have studied the generalized Aloha game in Chapter 3. Here we compare the performance with the Stackelberg game for spatial CSMA under the same setup.

In the CSMA setting the BS assists in the resource allocation by controlling the service price of the D2D users. If slotted Aloha is used by the D2D users under the same pricing framework, we can compare the performance difference of these two techniques. Here we assume that the BS does not know the contention graph and cannot predict the optimal price by centralized computation. Instead, the BS receives feedback from the users about the convergence results of the CSMA subgame or slotted Aloha subgame (i.e., the generalized Aloha game with a profile of target rates controlled by the service price), and then tunes the price to maximize the total D2D throughput.

For the 8 users' example in Fig. 7.4a, to focus on the performance comparison, we assume that the users have the same target rate requirements, as given in Section 7.4.3. The results in Fig. 7.7 plot the maximum total throughput in the CSMA setting under different r_{max} parameter values. In particular, when $r_{max} = 8$, the maximum total throughput approaches the upper bound 2.65. The corresponding optimal price is $M^{opt} = 27.5$.

In the slotted Aloha setting, to achieve the target rate $\underline{y}$ under a given network price M, the users play the generalized Aloha game in Chapter 3. Recall that the MAP of player i in the $(m+1)$-th iteration is given in (3.3), where y_i is the target rate:

$$q_i^{(m+1)} = \min\{\frac{y_i}{\prod_{a_{ij}=1}(1-q_j^{(m)})}, 1\}, \quad \forall i \in \mathcal{N}. \tag{7.25}$$

Since in the CSMA subgame each player updates its transmission parameter TA

based on measured throughput, we also update the MAP in the generalized Aloha game based on measured throughput. Suppose each iteration in the generalized Aloha game consists of 2000 slots and each slot takes 0.1ms. Then each iteration takes 200ms, which is the same as in the CSMA subgame. In the m-th iteration, each Aloha player i counts the number of successful packets and estimates its throughput $\hat{\theta}_i^{(m)}$. Then the channel idle rate in the m-th iteration can be estimated as:

$$x_i^{(m)} := \prod_{a_{ij}=1} (1 - q_j^{(m)}) \approx \hat{\theta}_i^{(m)} / q_i^{(m)}, \quad \forall i \in \mathcal{N}. \tag{7.26}$$

Then the iteration dynamics in (7.25) becomes:

$$q_i^{(m+1)} = \min\{\frac{y_i}{\prod_{a_{ij}=1}(1 - q_j^{(m)})}, 1\} = \min\{\frac{y_i}{x_i^{(m)}}, 1\}, \quad \forall i \in \mathcal{N}. \tag{7.27}$$

If the target rate $\underline{y}$ under a given network price M is within the feasible target rate region of the generalized Aloha game, then the generalized Aloha game will converge to a throughput equal to the target rate $\underline{y}$. To detect whether the game has converged, each player needs to analyze the characteristics of its measured throughput. First, it applies a simple averaging filter to obtain a smoothed version $\bar{\theta}_i^{(m)}$ of the measured throughput $\hat{\theta}_i^{(m)}$:

$$\bar{\theta}_i^{(m)} = 0.95 \cdot \bar{\theta}_i^{(m-1)} + 0.05 \cdot \hat{\theta}_i^{(m)}, \quad \forall i \in \mathcal{N}. \tag{7.28}$$

Then player i keeps a record of $\bar{\theta}_i^{(m)}$ in the recent 40 iterations. If the average value and standard deviation of these $\bar{\theta}_i^{(m)}$ values are below a certain threshold respectively, then it suggests that the game converges. On the other hand, if all players are dead-locked in a situation with $\underline{q} = \underline{1}$, then the game diverges.

The BS can then tune the price M to maximize the total throughput of all players. Such a price tuning process along with the generalized Aloha game as a subgame can be seen as a Stackelberg game similar to that in this chapter. Here we demonstrate a simple pricing strategy. We can start with a high price (e.g., $M = 50$) so that the network starts with low load. Then we gradually decrease the price by a constant step size $\delta M = 1$ until the generalized Aloha game cannot achieve the corresponding target rate and diverges to $\underline{q} = \underline{1}$. Then we reset the price M to previously feasible price M and gradually decrease the price by a smaller step size $\delta M = 0.1$ until the refined price is no longer achievable. We can continue to refine the optimal price by using even smaller step size. For illustration purpose,

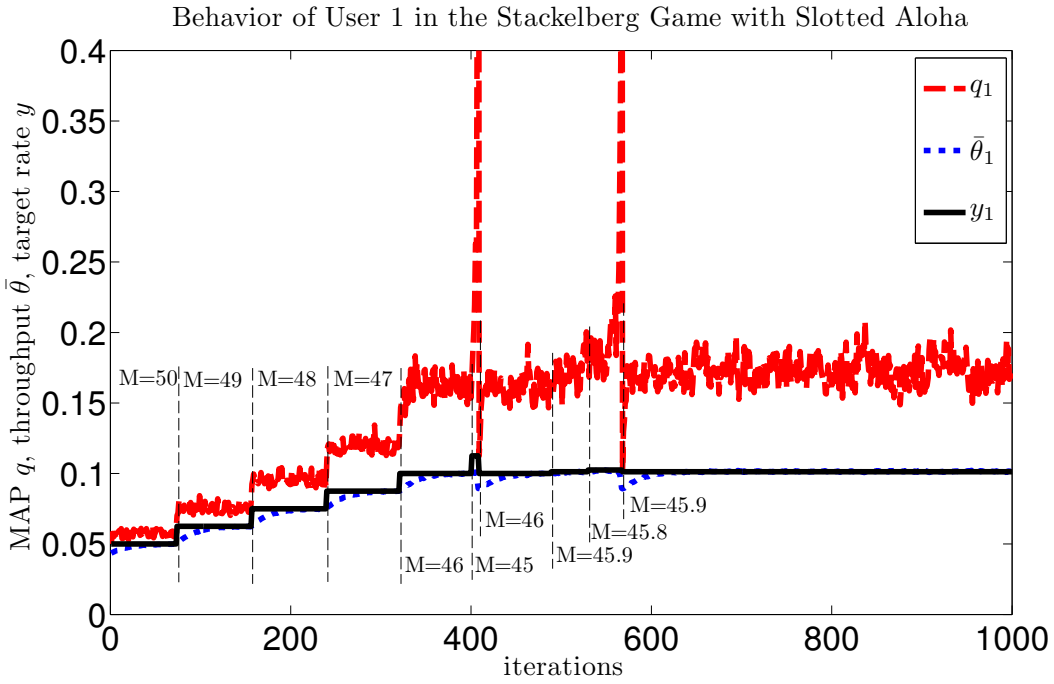

Figure 7.8: Behavior of User 1 in the Stackelberg Game with Slotted Aloha

we refine the price up to the precision of $\delta M = 0.1$.

The Stackelberg game with spatial Aloha converges in around 600 iterations, shown in Fig. 7.8. There are 10 pricing stages (M= 50, 49, 48, 47, 46, 45, 46, 45.9, 45.8, 45.9) until the optimal price $M^{opt} = 45.9$ is found. The maximum total throughput achieved is 0.81. The distance to Pareto front is $d_{Pareto} = 1.01$, suggesting that achieved target rate is very close to the Pareto front (the residue is due to the step size of pricing and the effect of estimation errors on the stability). The throughput ratio between Stackelberg game with slotted Aloha and Stackelberg game with CSMA is $0.81/2.65 \approx 0.305$.

7.5 Conclusions

We study a group of D2D links which share a dedicated inband overlay channel via CSMA. The ICN model is leveraged on to analyze their behaviors and interactions under spatial reuse. We further assume that the D2D links have heterogeneous rate requirements and different willingness to pay, and they act non-altruistically to achieve their target rates and maximize their own payoffs. To manage such non-cooperative user dynamics, we propose a Stackelberg game in which the BS in the cellular network acts as a Stackelberg leader to regulate the D2D link transmissions by modifying the service price, so that the total throughput is maximized while

the heterogeneous target rates of the D2D links can all be satisfied. The problem is shown to be quasi-convex and can be solved by a sequence of equivalent convex optimization problems. The pricing strategies are designed so that the network always operates within the capacity region. The results are verified by simulations. The joint optimization of D2D link scheduling and cellular data off-loading is our future work.

Chapter 8

Conclusions and Future Work

8.1 Conclusions of the Thesis

This thesis focuses on the spectrum sharing problems among a group of spatially distributed Tx-Rx user pairs in a spectrum commons. The users are equipped with built-in intelligence and are able to make intelligent decisions on choosing transmission parameters by learning the spectrum dynamics and their competitors' decisions. As a result of their autonomous interactions, stability issues arise concerning whether the whole network would converge to an equilibrium solution. We therefore study how to manage the spectrum access problem for such autonomous and spatially distributed Tx-Rx pairs with the objective to achieve efficient spectrum sharing with fairness and scalability.

As an initial attempt to solve these challenges, we first investigate slotted-Aloha-type random access with spatial reuse. We propose the generalized Aloha games and obtain the stability conditions for the unique NE in terms of MAPs. Based on the stability conditions, we first develop a fully autonomous algorithm for the distributed users to heuristically search for a fair and close-to-Pareto-front operating point. Then we further design a control theoretic scheme to approach global optimization of network throughput through limited local information and yet can achieve quick convergence and operational stability. After investigating the single-channel scenario, we then extend to multi-channel spatial Aloha networks and propose a multi-leader Stackelberg game to solve the joint MAP tuning and spatial channel selection problem. Finally, we leverage on the ICN model in the context of overlay D2D communications, and investigate how the commons spectrum can be efficiently and fairly shared among the self-interested spatial CSMA users with heterogeneous rate requirements.

In summary, this thesis provides theoretical guidance for managing the shared access to a spectrum commons, with insights into how the spatially distributed Tx-Rx pairs can share the commons spectrum with stability, efficiency, fairness and scalability.

8.2 Future Work

8.2.1 Apply PI Controller in Multi-Channel Spatial Aloha

In the single channel case, the PI controller is used to control the MAPs of the Aloha users, which is more ready for implementation since the users stay on the same channel and can exchange local information with neighbors via piggy-backing with low overhead. The addition dimension of channel selection in the multi-channel case makes the problem more challenging. The control theoretic approach has the potential to be applied in the multi-channel case. In this thesis we first look for an efficient and reliable mechanism to search for a stable solution, which is the focus of Chapter 6. The use of control theoretic approach is an implementation issue. While it will still work at each of the updates, the controlling process is a two-parameter adjusting process and the approach might not be so direct and requires future investigations.

8.2.2 Exact Characterization of Throughput in Spatial CSMA Networks

Due to the simplicity of slotted Aloha, the throughput performance of spatial Aloha networks can be exactly characterized by the MAPs of the users, as given in (2.1). The major challenges lie in the modeling of the self-interested strategic interactions among the heterogeneous users, and the investigation of the properties of the equilibrium solutions, e.g., existence, uniqueness, convergence, stability, efficiency, fairness, etc. Moreover, since the users are spatially distributed and have only local information, it is worth designing distributed algorithms to approach global optimization of network throughput through limited spread of local information and realize the model's quick convergence and stability.

However, in the presence of spatial reuse, it is extremely difficult to exactly characterize the throughput performance of CSMA users. We have adopted the ICN model in Chapter 7 to compute the user throughputs. Although the ICN

model captures the essence of CSMA and indeed yields good approximation of the user throughputs, an exact throughput characterization for spatial CSMA is still lacking. The idealized assumption made in ICN is that the backoff countdown process is in "continuous-time" and carrier sensing is instantaneous. As a result, there is no collision in ICN. In practical CSMA protocols such as IEEE 802.11, the users count down in "mini-timeslot" and the process is hence a "discrete-time" process. In [94], Kai and Liew proposed a generalized ICN model for a perturbation analysis that tries to capture the effects of backoff collisions. However, they still rely on some strong assumptions, e.g., the transmission time is of the same fixed length for all users. Therefore, the exact characterization of user throughputs in spatial CSMA networks still awaits future work.

8.2.3 Non-Saturated Throughput

In the system model in Section 2.1, we have assumed that every user's transmission queue is continuously backlogged, i.e., the transmitter of every user always has a packet to transmit to its designated receiver. In other words, we have only considered the saturated throughput performance, which well models the behavior of links that always have traffic to send, e.g., Transmission Control Protocol (TCP) traffic arising from long-lasting peer-to-peer (P2P) file downloads.

For networks with unsaturated links, there are two possible extremes. The first is the bursty traffic case in which each link becomes saturated and idle alternatively, with the saturated and idle periods each lasting a long time. This case can be viewed as one in which the network topology changes dynamically. At any instance, the network consists only those links with saturated traffic. As time progresses, there is a sequence of effective network topologies. The second is the intermittent traffic case in which the input traffic of links (i.e., their offered load) is below their saturated throughputs, but the traffic arrives to the links intermittently. This case is more challenging, particularly if we are interested in not just the access delay, but also the overall queuing delay which includes the buffer delay at a link. These challenging issues would require further investigations.

8.2.4 Quality of Service

In this thesis we have mainly focused on throughput as the performance metric. Future work could consider other Quality-of-Service (QoS) metrics such as packet loss, delay, jitter, retry rates, etc.

In particular, for spatial CSMA, beyond the throughput optimality, designing a CSMA algorithm which is optimal in both throughput and delay remains quite open. In [157], the authors show that the task is very difficult for arbitrary interference topology. However, the interference topology arising in practice is not arbitrary, but has certain geometric properties [158] or bounded degrees [159]. Therefore, designing and analyzing CSMA algorithms toward delay optimality is still a challenging subject to be further investigated.

Based on future improvements of design and analysis on the medium access characterizations, we can further consider the incorporation of the QoS requirements into the users' utility functions to provide service differentiation and better contention control. A proper utility function should take system parameters into account, including QoS requirements, user's priority, user's queues status, channel conditions, power limitations, priorities of packets, etc. Therefore, it is still a challenging issue to propose a general framework to design utility and cost functions for the heterogeneous users, which are convergent toward optimal equilibrium point that meets different users' QoS requirements.

8.2.5 Implementation Issues

Theories depend on a mathematical crystallization of the engineering system under study. For the mathematical tractability, we have made simplifying assumptions in the system models, which in turn deserve a closer look during implementation.

In this thesis, we have not considered detailed physical channel conditions, such as ambient noise or time-varying channels. In particular, time-varying channels would cause perturbations to the interference relationship among the wireless links. Time-varying channels also generate packet loss induced by channel degradation, which is not considered by the current theory. Stability issues of perturbations caused by ambient noise, measurement errors or time-varying channels are important in practice and will be the subject of future study.

In the system models, we have assumed that both link channel conditions and link interference relationship are symmetric and fixed. However, wireless links are often asymmetric in practice because signals propagate differently between two links. Furthermore, link asymmetry can be also time-varying. These issues would need to be further investigated.

Other implementation issues also deserve a closer look, such as asynchronism of device operations, overhead within the protocol stacks, retry limit and retrans-

mission schemes, packet designs, etc. Implementation studies should also bridge the gap between theory and practice, and bring a sharper understanding of what theory has assumed away or analyzed only loosely so far, e.g., granularity of control parameters, convergence speed, transient behavior like queue buildup, etc.

Bibliography

[1] Q. Zhao and B. Sadler, "A Survey of Dynamic Spectrum Access," *IEEE Signal Process. Mag.*, vol. 24, no. 3, pp. 79–89, May 2007.

[2] J. Lyu, Y. H. Chew, and W.-C. Wong, "Aloha Games with Spatial Reuse," *IEEE Trans. Wireless Commun.*, vol. 12, no. 8, pp. 3932–3941, 2013.

[3] S. Haykin, "Cognitive radio: brain-empowered wireless communications," *IEEE J. Sel. Areas Commun.*, vol. 23, no. 2, pp. 201–220, 2005.

[4] D. Hatfield and P. Weiser, "Property rights in spectrum: taking the next step," in *IEEE Int. Symp. New Frontiers in Dynamic Spectrum Access Networks (DySPAN)*, 2005, pp. 43–55.

[5] L. Xu, R. Tonjes, T. Paila, W. Hansmann, M. Frank, and M. Albrecht, "Driveing to the internet: Dynamic radio for ip services in vehicular environments," in *IEEE Conf. Local Computer Networks (LCN)*, 2000, pp. 281–289.

[6] I. F. Akyildiz, W.-Y. Lee, M. C. Vuran, and S. Mohanty, "Next generation/dynamic spectrum access/cognitive radio wireless networks: A survey," *Computer Networks*, vol. 50, no. 13, pp. 2127 – 2159, 2006.

[7] L. B. Le and E. Hossain, "Resource allocation for spectrum underlay in cognitive radio networks," *IEEE Trans. Wireless Commun.*, vol. 7, no. 12, pp. 5306–5315, 2008.

[8] S. Roy, J. Foerster, V. Somayazulu, and D. Leeper, "Ultrawideband radio design: the promise of high-speed, short-range wireless connectivity," *IEEE Proc.*, vol. 92, no. 2, pp. 295–311, 2004.

[9] Y. Benkler, "Overcoming agoraphobia: building the commons of the digitally networked environment," *Harv. JL & Tech.*, vol. 11, p. 287, 1997.

[10] B. Eli Noam, "Spectrum auctions: Yesterday's heresy, today's orthodoxy, tomorrow's anachronism. taking the next step to open spectrum access," *Journal of Law and Economics*, vol. 41, no. S2, pp. pp. 765–790, 1998.

[11] K. Werbach, "Open spectrum: The new wireless paradigm," *New America Foundation Spectrum Policy Program*, 2002.

[12] D. P. Reed, "How wireless networks scale: the illusion of spectrum scarcity," in *International Symposium on Advanced Radio Technology, Boulder, Colorado*, 2002.

[13] W. Lehr and J. Crowcroft, "Managing shared access to a spectrum commons," in *IEEE Int. Symp. New Frontiers in Dynamic Spectrum Access Networks (DySPAN)*, 2005, pp. 420–444.

[14] A. S. Tanenbaum and D. J. Wetherall, "The Medium Access Control," in *Computer Networks, Fifth International Edition.* Prentice Hall, 2011, ch. 4.

[15] G. Hardin, "The tragedy of the commons," *Science*, vol. 162, no. 3859, pp. 1243–1248, 1968. [Online]. Available: http://www.sciencemag.org/content/162/3859/1243.abstract

[16] J. Brito, "The spectrum commons in theory and practice," *Stanford Technology Law Review*, 2006.

[17] R. V. Andelson, *Commons without tragedy.* Shepheard-Walwyn, 1991.

[18] R. Etkin, A. Parekh, and D. Tse, "Spectrum sharing for unlicensed bands," in *IEEE Int. Symp. New Frontiers in Dynamic Spectrum Access Networks (DySPAN)*, 2005, pp. 251–258.

[19] M. J. Osborne and A. Rubinstein, "Terminology and Notation," in *A Course in Game Theory.* The MIT Press, 1994, ch. 1.7.

[20] X. Wang and K. Kar, "Distributed algorithms for max-min fair rate allocation in aloha networks," in *Annual Allerton Conf. Communication, Control, and Computing (Allerton)*, 2004.

[21] K. Kar, S. Sarkar, and L. Tassiulas, "Achieving proportional fairness using local information in aloha networks," *IEEE Trans. Autom. Control*, vol. 49, no. 10, pp. 1858–1863, 2004.

[22] C. Raman, R. Yates, and N. B. Mandayam, "Scheduling variable rate links via a spectrum server," in *IEEE Int. Symp. New Frontiers in Dynamic Spectrum Access Networks (DySPAN)*, 2005, pp. 110–118.

[23] O. Ileri, D. Samardzija, and N. Mandayam, "Demand responsive pricing and competitive spectrum allocation via a spectrum server," in *IEEE Int. Symp. New Frontiers in Dynamic Spectrum Access Networks (DySPAN)*, 2005, pp. 194–202.

[24] S. T. Chung, S.-J. Kim, J. Lee, and J. Cioffi, "A game-theoretic approach to power allocation in frequency-selective gaussian interference channels," in *IEEE Int. Symp. Information Theory*, 2003, pp. 316–316.

[25] J. Huang, R. Berry, and M. Honig, "Spectrum sharing with distributed interference compensation," in *IEEE Int. Symp. New Frontiers in Dynamic Spectrum Access Networks (DySPAN)*, 2005, pp. 88–93.

[26] Y. Wu, B. Wang, K. J. R. Liu, and T. Clancy, "Repeated open spectrum sharing game with cheat-proof strategies," *IEEE Trans. Wireless Commun.*, vol. 8, no. 4, pp. 1922–1933, 2009.

[27] X. Chen and J. Huang, "Evolutionarily stable open spectrum access in a many-users regime," in *IEEE Global Telecommunications Conference (GLOBECOM)*, 2011, pp. 1–5.

[28] Z. Ji and K. J. R. Liu, "Cognitive radios for dynamic spectrum access - dynamic spectrum sharing: A game theoretical overview," *IEEE Commun. Mag.*, vol. 45, no. 5, pp. 88–94, 2007.

[29] M. Wooldridge, *An Introduction to Multiagent Systems*. John Wiley and Sons, Ltd, 2002.

[30] Y. Shoham and K. L. Brown, *Multiagent Systems: Algorithmic, Game-Theoretic, and Logical Foundations*. Cambridge University Press, 2008.

[31] X. Wang, K. Kar, and J.-S. Pang, "Lexicographic max–min fairness in a wireless ad-hoc network with random access," in *IEEE Conf. Decision and Control (CDC)*. Citeseer, 2006.

[32] A. Nedic and A. Ozdaglar, "Cooperative distributed multi-agent optimization," in *Convex Optimization in Signal Processing and Communications*. Cambridge University Press, 2010, ch. 10.

[33] D. Fudenberg and J. Tirole, *Game Theory*. The MIT Press, 1993.

[34] J. Nash, "Non-Cooperative Games," *Annals of Mathematics*, 1951.

[35] M. L. Puterman, *Markov Decision Processes: Discrete Stochastic Dynamic Programming*. John Wiley and Sons, Inc., 2005.

[36] S. Meyn and R. L. Tweedie, *Markov Chains and Stochastic Stability, second edition*. Cambridge University Press, 2009.

[37] L. S. Shapley, "Stochastic games," *Proceedings of the National Academy of Sciences of the United States of America*, vol. 39, no. 10, pp. 1095–1100, 1953.

[38] A. MacKenzie and S. Wicker, "Selfish users in Aloha: a game-theoretic approach," in *IEEE Vehicular Technology Conference (VTC)*, vol. 3, 2001.

[39] A. MacKenzie and S. Wicker, "Game theory and the design of self-configuring, adaptive wireless networks," *IEEE Commun. Mag.*, vol. 39, no. 11, pp. 126–131, Nov 2001.

[40] I. L. Glicksberg, "A further generalization of the kakutani fixed point theorem, with application to nash equilibrium points," *Proceedings of the American Mathematical Society*, vol. 3, no. 1, pp. 170–174, 1952.

[41] K. Fan, "Fixed-point and minimax theorems in locally convex topological linear spaces," *Proceedings of the National Academy of Sciences of the United States of America*, vol. 38, no. 2, pp. 121–126, 1952.

[42] A. MacKenzie and S. Wicker, "Stability of multipacket slotted Aloha with selfish users and perfect information," in *IEEE Conf. Computer and Communications (INFOCOM)*, vol. 2, April 2003.

[43] H. K. Khalil, "Lyapunov Stability," in *Nonlinear Systems, Third Edition.* Upper Saddle River, NJ 07458: Prentice Hall, 2002, ch. 4, p. 122.

[44] J.-J. E. Slotine and W. Li, "Fundamentals of Lyapunov Theory," in *Applied Nonlinear Control.* Prentice Hall, 1991, ch. 3, pp. 83–87.

[45] T. Cui, L. Chen, and S. Low, "A game-theoretic framework for medium access control," *IEEE J. Sel. Areas Commun.*, vol. 26, no. 7, pp. 1116–1127, 2008.

[46] D. Topkis, "Equilibrium points in nonzero-sum n-person submodular games," *SIAM Journal on Control and Optimization*, vol. 17, no. 6, pp. 773–787, 1979.

[47] S. D. FLM, "Equilibrium, evolutionary stability and gradient dynamics," *International Game Theory Review*, vol. 04, no. 04, pp. 357–370, 2002.

[48] R. La and V. Anantharam, "Charge-sensitive TCP and rate control in the Internet," in *IEEE Conf. Computer and Communications (INFOCOM)*, vol. 3, mar 2000, pp. 1166 –1175 vol.3.

[49] Y. Jin and G. Kesidis, "Equilibria of a noncooperative game for heterogeneous users of an ALOHA network," *IEEE Commun. Lett.*, vol. 6, no. 7, pp. 282–284, 2002.

[50] K. Akkarajitsakul, E. Hossain, D. Niyato, and D. I. Kim, "Game Theoretic Approaches for Multiple Access in Wireless Networks: A Survey," *IEEE Commun. Surv. Tut.*, vol. 13, no. 3, 2011.

[51] Q. Du and X. Zhang, "Game-theoretic approach for QoS-aware resource competition in wireless networks," in *IEEE Military Communications Conference (MILCOM)*, Oct 2009, pp. 1–7.

[52] A. T. Hoang and Y.-C. Liang, "Dynamic spectrum allocation with second-price auctions: When time is money," in *Int. Conf. Cognitive Radio Oriented Wireless Networks and Communications (CrownCom)*, May 2008, pp. 1–6.

[53] J. Sun, E. Modiano, and L. Zheng, "Wireless channel allocation using an auction algorithm," *IEEE J. Sel. Areas Commun.*, vol. 24, no. 5, pp. 1085–1096, May 2006.

[54] F. Wu, S. Zhong, and C. Qiao, "Globally Optimal Channel Assignment for Non-Cooperative Wireless Networks," in *IEEE Conf. Computer and Communications (INFOCOM)*, April 2008, pp. –.

[55] Z. Han, Z. Ji, and K. Liu, "Non-cooperative resource competition game by virtual referee in multi-cell OFDMA networks," *IEEE J. Sel. Areas Commun.*, vol. 25, no. 6, pp. 1079–1090, August 2007.

[56] H. Kwon and B. G. Lee, "Distributed Resource Allocation through Noncooperative Game Approach in Multi-cell OFDMA Systems," in *IEEE Int. Conf. Communications (ICC)*, vol. 9, June 2006, pp. 4345–4350.

[57] F. Meshkati, M. Chiang, H. Poor, and S. Schwartz, "A game-theoretic approach to energy-efficient power control in multicarrier CDMA systems," *IEEE J. Sel. Areas Commun.*, vol. 24, no. 6, pp. 1115–1129, June 2006.

[58] C. St Jean and B. Jabbari, "Bayesian game-theoretic modeling of transmit power determination in a self-organizing CDMA wireless network," in *IEEE Vehicular Technology Conference (VTC)*, vol. 5, Sept 2004, pp. 3496–3500.

[59] S. Koskie and Z. Gajic, "A nash game algorithm for SIR-based power control in 3G wireless CDMA networks," *IEEE/ACM Trans. Netw.*, vol. 13, no. 5, pp. 1017–1026, Oct 2005.

[60] Y. Jin and G. Kesidis, "A pricing strategy for an ALOHA network of heterogeneous users with inelastic bandwidth requirements," in *Proc. CISS 2002, Princeton*, March 2002.

[61] G. Kesidis, Y. Jin, A. Azad, and E. Altman, "Stable Nash equilibria of ALOHA medium access games under symmetric, socially altruistic behavior," in *IEEE Conf. Decision and Control (CDC)*, dec. 2010.

[62] Y. Jin and G. Kesidis, "Nash equilibria of a generic networking game with applications to circuit-switched networks," in *IEEE Conf. Computer and Communications (INFOCOM)*, vol. 2, March 2003, pp. 1242–1249.

[63] I. Menache and N. Shimkin, "Rate-Based Equilibria in Collision Channels with Fading," *IEEE J. Sel. Areas Commun.*, vol. 26, no. 7, pp. 1070 –1077, september 2008.

[64] K. Son, S. Chong, and G. Veciana, "Dynamic association for load balancing and interference avoidance in multi-cell networks," *IEEE Trans. Wireless Commun.*, vol. 8, no. 7, pp. 3566 –3576, july 2009.

[65] D. Lopez-Perez, I. Guvenc, G. de la Roche, M. Kountouris, T. Quek, and J. Zhang, "Enhanced intercell interference coordination challenges in heterogeneous networks," *IEEE Wireless Commun.*, vol. 18, no. 3, pp. 22 –30, june 2011.

[66] G. Xingang, S. Roy, and W. Conner, "Spatial reuse in wireless ad-hoc networks," in *IEEE Vehicular Technology Conference (VTC)*, vol. 3, oct. 2003, pp. 1437 – 1442.

[67] F. Ye, S. Yi, and B. Sikdar, "Improving spatial reuse of IEEE 802.11 based ad hoc networks," in *IEEE Global Telecommunications Conference (GLOBECOM)*, vol. 2, dec. 2003, pp. 1013 – 1017.

[68] A. Hasan and J. Andrews, "The Guard Zone in Wireless Ad hoc Networks," *IEEE Trans. Wireless Commun.*, vol. 6, no. 3, pp. 897 –906, march 2007.

[69] P. Li, Q. Shen, Y. Fang, and H. Zhang, "Power controlled network protocols for Multi-Rate ad hoc networks," *IEEE Trans. Wireless Commun.*, vol. 8, no. 4, pp. 2142 –2149, april 2009.

[70] X. Chen and J. Huang, "Distributed Spectrum Access with Spatial Reuse," *IEEE J. Sel. Areas Commun.*, vol. 31, no. 3, pp. 593–603, March 2013.

[71] D. Monderer and L. S. Shapley, "Potential Games," *Games and Economic Behavior*, vol. 14, no. 1, pp. 124 – 143, 1996.

[72] W. H. Sandholm, "Potential games with continuous player sets," *Journal of Economic Theory*, vol. 97, no. 1, pp. 81–108, 2001.

[73] K. Cohen, A. Leshem, and E. Zehavi, "Game Theoretic Aspects of the Multi-Channel ALOHA Protocol in Cognitive Radio Networks," *IEEE J. Sel. Areas Commun.*, vol. 31, no. 11, November 2013.

[74] H. D. Sherali, "A Multiple Leader Stackelberg Model and Analysis," *Operations Research*, vol. 32, no. 2, pp. 390–404, 1984.

[75] M. Ghazvini, N. Movahedinia, K. Jamshidi, and N. Moghim, "Game Theory Applications in CSMA Methods," *IEEE Commun. Surv. Tut.*, vol. 15, no. 3, pp. 1062–1087, Third 2013.

[76] N. BenAmmar and J. S. Baras, "Incentive Compatible Medium Access Control in Wireless Networks," in *Proc. Game Theory for Communications and Networks (GameNets)*. New York, NY, USA: ACM, 2006.

[77] J.-W. Lee, M. Chiang, and A. Calderbank, "Utility-Optimal Medium Access Control: Reverse and Forward Engineering," in *IEEE Conf. Computer and Communications (INFOCOM)*, April 2006, pp. 1–13.

[78] J.-W. Lee, A. Tang, J. Huang, M. Chiang, and A. Calderbank, "Reverse-Engineering MAC: A Non-Cooperative Game Model," *IEEE J. Sel. Areas Commun.*, vol. 25, no. 6, pp. 1135–1147, August 2007.

[79] Y. Xiao, X. Shan, and Y. Ren, "Game theory models for IEEE 802.11 DCF in wireless ad hoc networks," *IEEE Commun. Mag.*, vol. 43, no. 3, pp. S22–S26, March 2005.

[80] "IEEE Standard for Information Technology- Telecommunications and Information Exchange Between Systems- Local and Metropolitan Area Networks-Specific Requirements- Part 11: Wireless LAN Medium Access Control (MAC) and Physical Layer (PHY) Specifications," *ANSI/IEEE Std 802.11, 1999 Edition (R2003)*, pp. i–513, 2003.

[81] L. Chen, S. Low, and J. Doyle, "Contention control: A game-theoretic approach," in *IEEE Conf. Decision and Control (CDC)*, Dec 2007, pp. 3428–3434.

[82] L. Chen, S. Low, and J. Doyle, "Random access game and medium access control design," *IEEE/ACM Trans. Netw.*, vol. 18, no. 4, pp. 1303–1316, Aug 2010.

[83] L. Chen and J. Leneutre, "Efficient medium access control design for autonomous wireless networks - a game theoretic approach," in *IEEE Conf. Local Computer Networks (LCN)*, Oct 2009, pp. 376–383.

[84] Y. Jin and G. Kesidis, "Distributed Contention Window Control for Selfish Users in IEEE 802.11 Wireless LANs," *IEEE J. Sel. Areas Commun.*, vol. 25, no. 6, pp. 1113–1123, August 2007.

[85] G. Bianchi, "Performance analysis of the IEEE 802.11 distributed coordination function," *IEEE J. Sel. Areas Commun.*, vol. 18, no. 3, pp. 535–547, March 2000.

[86] S.-C. Liew, C. H. Kai, H. C. Leung, and P. Wong, "Back-of-the-Envelope Computation of Throughput Distributions in CSMA Wireless Networks," *IEEE Trans. Mobile Comput.*, vol. 9, no. 9, pp. 1319–1331, Sept 2010.

[87] K. Ghaboosi, B. H. Khalaj, Y. Xiao, and M. Latva-aho, "Modeling IEEE 802.11 DCF Using Parallel Space-Time Markov Chain," *IEEE Trans. Veh. Technol.*, vol. 57, no. 4, pp. 2404–2413, July 2008.

[88] P. Venkata Krishna, S. Misra, M. Obaidat, and V. Saritha, "Virtual Backoff Algorithm: An Enhancement to 802.11 Medium-Access Control to Improve the Performance of Wireless Networks," *IEEE Trans. Veh. Technol.*, vol. 59, no. 3, pp. 1068–1075, March 2010.

[89] I. Tinnirello, G. Bianchi, and Y. Xiao, "Refinements on IEEE 802.11 Distributed Coordination Function Modeling Approaches," *IEEE Trans. Veh. Technol.*, vol. 59, no. 3, pp. 1055–1067, March 2010.

[90] R. Boorstyn, A. Kershenbaum, B. Maglaris, and V. Sahin, "Throughput Analysis in Multihop CSMA Packet Radio Networks," *IEEE Trans. Commun.*, vol. 35, no. 3, pp. 267–274, Mar 1987.

[91] X. Wang and K. Kar, "Throughput modelling and fairness issues in CSMA/CA based ad-hoc networks," in *IEEE Conf. Computer and Communications (INFOCOM)*, vol. 1, March 2005, pp. 23–34.

[92] L. Jiang and J. Walrand, "A Distributed CSMA Algorithm for Throughput and Utility Maximization in Wireless Networks," *IEEE/ACM Trans. Netw.*, vol. 18, no. 3, pp. 960–972, June 2010.

[93] C. Kai and S.-C. Liew, "Applications of Belief Propagation in CSMA Wireless Networks," *IEEE/ACM Trans. Netw.*, vol. 20, no. 4, pp. 1276–1289, Aug 2012.

[94] C. Kai and S. C. Liew, "Throughput computation in CSMA wireless networks with collision effects," *CoRR*, vol. abs/1107.1633, 2011. [Online]. Available: http://arxiv.org/abs/1107.1633

[95] L. Jiang and J. Walrand, "Approaching Throughput-Optimality in Distributed CSMA Scheduling Algorithms With Collisions," *IEEE/ACM Trans. Netw.*, vol. 19, no. 3, pp. 816–829, June 2011.

[96] M. Cagalj, S. Ganeriwal, I. Aad, and J.-P. Hubaux, "On selfish behavior in CSMA/CA networks," in *IEEE Conf. Computer and Communications (INFOCOM)*, vol. 4, March 2005, pp. 2513–2524.

[97] D. Kuptsov, B. Nechaev, A. Lukyanenko, and A. Gurtov, "How penalty leads to improvement: A measurement study of wireless backoff in IEEE 802.11 networks," *Computer Networks*, vol. 75, Part A, no. 0, pp. 37 – 57, 2014.

[98] A. Asadi, Q. Wang, and V. Mancuso, "A Survey on Device-to-Device Communication in Cellular Networks," *CoRR*, vol. abs/1310.0720, 2013.

[99] X. Lin, J. Andrews, and A. Ghosh, "Spectrum sharing for device-to-device communication in cellular networks," *IEEE Trans. Wireless Commun.*, vol. 13, no. 12, pp. 6727–6740, Dec 2014.

[100] L. Song, D. Niyato, Z. Han, and E. Hossain, "Game-theoretic resource allocation methods for device-to-device communication," *IEEE Wireless Commun.*, vol. 21, no. 3, pp. 136–144, June 2014.

[101] Y. Cai, H. Chen, D. Wu, W. Yang, and L. Zhou, "A distributed resource management scheme for D2D communications based on coalition formation game," in *IEEE Int. Conf. Communications (ICC)*, June 2014, pp. 355–359.

[102] D. Wu, J. Wang, R. Hu, Y. Cai, and L. Zhou, "Energy-efficient resource sharing for mobile device-to-device multimedia communications," *IEEE Trans. Veh. Technol.*, vol. 63, no. 5, pp. 2093–2103, Jun 2014.

[103] S. Basagni, M. Conti, S. Giordano, and I. Stojmenovic, *Mobile ad hoc networking*. John Wiley & Sons, 2004.

[104] P. Thulasiraman, J. Chen, and X. Shen, "Multipath Routing and Max-Min Fair QoS Provisioning under Interference Constraints in Wireless Multihop Networks," *IEEE Trans. Parallel Distrib. Syst.*, vol. 22, no. 5, pp. 716–728, May 2011.

[105] W. Xu, J. Chen, Y. Zhang, Y. Xiao, and Y. Sun, "Optimal Rate Routing in Wireless Sensor Networks with Guaranteed Lifetime," in *IEEE Global Telecommunications Conference (GLOBECOM)*, Nov 2008, pp. 1–5.

[106] P. Gupta and P. Kumar, "The capacity of wireless networks," *IEEE Trans. Inf. Theory*, vol. 46, no. 2, pp. 388–404, Mar 2000.

[107] Y. Shi, Y. Hou, S. Kompella, and H. Sherali, "Maximizing capacity in multihop cognitive radio networks under the sinr model," *IEEE Trans. Mobile Comput.*, vol. 10, no. 7, pp. 954–967, July 2011.

[108] Y. Zhang, S. He, and J. Chen, "Data gathering optimization by dynamic sensing and routing in rechargeable sensor networks," in *Annual IEEE Conf. Sensor, Mesh and Ad Hoc Communications and Networks (SECON)*, June 2013, pp. 273–281.

[109] Y. Zhang, S. He, and J. Chen, "Data gathering optimization by dynamic sensing and routing in rechargeable sensor networks," *IEEE/ACM Trans. Netw.*, to appear.

[110] J. Chen, Q. Yu, P. Cheng, Y. Sun, Y. Fan, and X. Shen, "Game theoretical approach for channel allocation in wireless sensor and actuator networks," *IEEE Trans. Autom. Control*, vol. 56, no. 10, pp. 2332–2344, Oct 2011.

[111] J. Chen, Q. Yu, B. Chai, Y. Sun, Y. Fan, and X. Shen, "Dynamic channel assignment for wireless sensor networks: A regret matching based approach," *IEEE Trans. Parallel Distrib. Syst.*, vol. 26, no. 1, pp. 95–106, Jan 2015.

[112] Y. Shi and Y. Hou, "Optimal power control for multi-hop software defined radio networks," in *IEEE Conf. Computer and Communications (INFOCOM)*, May 2007, pp. 1694–1702.

[113] Y. Shi, Y. Hou, and H. Zhou, "Per-node based optimal power control for multi-hop cognitive radio networks," *IEEE Trans. Wireless Commun.*, vol. 8, no. 10, pp. 5290–5299, October 2009.

[114] Y. Shi, Y. T. Hou, J. Liu, and S. Kompella, "How to correctly use the protocol interference model for multi-hop wireless networks," in *Proc. ACM Int. Symp. on Mobile Ad Hoc Networking and Computing (MobiHoc)*. New York, NY, USA: ACM, 2009, pp. 239–248.

[115] Y. Shi, Y. Hou, J. Liu, and S. Kompella, "Bridging the gap between protocol and physical models for wireless networks," *IEEE Trans. Mobile Comput.*, vol. 12, no. 7, pp. 1404–1416, July 2013.

[116] L. Yang, L. Cao, and H. Zheng, "Physical interference driven dynamic spectrum management," in *IEEE Int. Symp. New Frontiers in Dynamic Spectrum Access Networks (DySPAN)*, Oct 2008, pp. 1–12.

[117] J. Lyu, Y. H. Chew, and W.-C. Wong, "An Autonomous Pareto Optimality Achieving Algorithm beyond Aloha Games with Spatial Reuse," in *IEEE Int. Symp. Personal Indoor and Mobile Radio Communications (PIMRC)*, 2013, pp. 2689–2693.

[118] X. Zhou, Z. Zhang, G. Wang, X. Yu, B. Y. Zhao, and H. Zheng, "Practical Conflict Graphs for Dynamic Spectrum Distribution," *SIGMETRICS Perform. Eval. Rev.*, vol. 41, no. 1, pp. 5–16, Jun. 2013.

[119] L. B. Jiang and S. C. Liew, "Hidden-Node Removal and Its Application in Cellular WiFi Networks," *IEEE Trans. Veh. Technol.*, vol. 56, no. 5, pp. 2641–2654, Sept 2007.

[120] L. Fu, S. C. Liew, and J. Huang, "Effective Carrier Sensing in CSMA Networks under Cumulative Interference," *IEEE Trans. Mobile Comput.*, vol. 12, no. 4, pp. 748–760, 2013.

[121] A. Granas and J. Dugundji, "Theorems of Brouwer and Borsuk," in *Fixed Point Theory.* Springer, 2003, ch. 5, p. 95.

[122] A. Baranga, "The contraction principle as a particular case of kleene's fixed point theorem," *Discrete Mathematics*, vol. 98, no. 1, pp. 75 – 79, 1991.

[123] P. Hitzler and A. K. Seda, "Multivalued Mappings, Fixed-Point Theorems and Disjunctive Databases," in *Proc. Irish Workshop on Formal Methods (IWFM'99), Electronic Workshops in Computing, British Computer Society*, May 1999.

[124] R. A. Horn and C. R. Johnson, "Positive definite matrices," in *Matrix Analysis.* Cambridge University Press, 1990, ch. 7, pp. 396–405.

[125] Y. A. Kuznetsov, "One-Parameter Bifurcations of Equilibria in Continuous-Time Dynamical Systems," in *Elements of Applied Bifurcation Theory, 2nd Edition.* Springer-Verlag New York, Inc, 1998, ch. 3, 5, pp. 80–86, 157–160.

[126] F. Baccelli, B. Blaszczyszyn, and P. Muhlethaler, "Stochastic analysis of spatial and opportunistic Aloha," *IEEE J. Sel. Areas Commun.*, vol. 27, no. 7, pp. 1105–1119, 2009.

[127] J. Yu and P. Chong, "A survey of clustering schemes for mobile ad hoc networks," *IEEE Commun. Surv. Tut.*, vol. 7, no. 1, pp. 32–48, First 2005.

[128] S. Mehta, P. Sharma, and K. Kotecha, "A survey on various cluster head election algorithms for manet," in *Nirma University Int. Conf. on Engineering (NUiCONE)*, Dec 2011, pp. 1–6.

[129] A. A. Abbasi and M. Younis, "A survey on clustering algorithms for wireless sensor networks," *Computer Communications*, vol. 30, no. 1415, pp. 2826 – 2841, 2007.

[130] S. Sen, D. Dorsey, R. Guerin, and M. Chiang, "Analysis of slotted aloha with multipacket messages in clustered surveillance networks," in *IEEE Military Communications Conference (MILCOM)*, Oct 2012, pp. 1–6.

[131] J. Hoydis, M. Petrova, and P. Mahonen, "Effects of topology on local throughput-capacity of ad hoc networks," in *IEEE Int. Symp. Personal Indoor and Mobile Radio Communications (PIMRC)*, Sept 2008, pp. 1–5.

[132] P. Patras, A. Banchs, P. Serrano, and A. Azcorra, "A Control-Theoretic Approach to Distributed Optimal Configuration of 802.11 WLANs," *IEEE Trans. Mobile Comput.*, vol. 10, no. 6, pp. 897–910, 2011.

[133] A. Garcia-Saavedra, A. Banchs, P. Serrano, and J. Widmer, "Distributed opportunistic scheduling: A control theoretic approach," in *IEEE Conf. Computer and Communications (INFOCOM)*, March 2012, pp. 540–548.

[134] A. Banchs, A. Garcia-Saavedra, P. Serrano, and J. Widmer, "A game-theoretic approach to distributed opportunistic scheduling," *IEEE/ACM Trans. Netw.*, vol. 21, no. 5, pp. 1553–1566, Oct 2013.

[135] J. Chen, Q. Yu, Y. Zhang, H.-H. Chen, and Y. Sun, "Feedback-based clock synchronization in wireless sensor networks: A control theoretic approach," *IEEE Trans. Veh. Technol.*, vol. 59, no. 6, pp. 2963–2973, July 2010.

[136] J. Lyu, Y. H. Chew, and W.-C. Wong, "Efficient and Scalable Distributed Autonomous Spatial Aloha Networks via Local Leader Election," *IEEE Trans. Veh. Technol.*, accepted with minor revision as a paper.

[137] V. I. Arnold, S. M. Gusein-Zade, and A. N. Varchenko, "Critical points and critical values of smooth maps," in *Singularities of Differentiable Maps*. Birkhauser Boston, 1985, vol. I, ch. 1.2, p. 5.

[138] N. Abramson, "The Throughput of Packet Broadcasting Channels," *IEEE Trans. Commun.*, vol. 25, no. 1, pp. 117–128, 1977.

[139] R. Diestel, *Graph theory, 4th edition*. Springer-Verlag, 2010.

[140] K. J. Åström and R. M. Murray, *Feedback Systems*. Princeton University Press, 2008.

[141] H. K. Khalil, *Nonlinear Systems, Third Edition*. Prentice Hall, 2002.

[142] S. Boyd and L. Vandenberghe, *Convex Optimization*. New York, NY, USA: Cambridge University Press, 2004.

[143] T. Glad and L. Ljung, *Control Theory: Multivariable and Nonlinear Methods*. Taylor and Francis, 2000.

[144] K. J. Åström and B. Wittenmark, *Computer-controlled systems: theory and design, 3rd ed.* Prentice Hall, 1997.

[145] Wolfram Research Inc., *Mathematica 9.0 Student Edition*. Wolfram Research, Inc., Champaign, Illinois, 2012.

[146] C. Kissling, "On the stability of contention resolution diversity slotted aloha (crdsa)," in *IEEE Global Telecommunications Conference (GLOBECOM)*, Dec 2011, pp. 1–6.

[147] R. Jain, D.-M. Chiu, and W. R. Hawe, "A quantitative measure of fairness and discrimination for resource allocation in shared computer system," *DEC Research Report TR-301*, 1984.

[148] J. Lyu, Y. H. Chew, and W.-C. Wong, "Multi-Leader Stackelberg Games in Multi-Channel Spatial Aloha Networks," in *IEEE Vehicular Technology Conference (VTC Spring)*, May 2015, pp. 1–6.

[149] J. Lyu, Y. H. Chew, and W.-C. Wong, "A Stackelberg Game Model for Overlay D2D Transmission with Heterogeneous Rate Requirements," *IEEE Trans. Veh. Technol.*, accepted with minor revision as a paper.

[150] L. Jiang, D. Shah, J. Shin, and J. Walrand, "Distributed random access algorithm: Scheduling and congestion control," *IEEE Trans. Inf. Theory*, vol. 56, no. 12, pp. 6182–6207, Dec 2010.

[151] M. J. Wainwright and M. I. Jordan, "Graphical models, exponential families, and variational inference," *Found. Trends Mach. Learn.*, vol. 1, no. 1-2, pp. 1–305, Jan. 2008.

[152] S. Boyd, L. Xiao, and A. Mutapcic, "Subgradient methods," *lecture notes of EE392o, Stanford University, Autumn Quarter*, 2003.

[153] R. Amir and I. Grilo, "Stackelberg versus cournot equilibrium," *Games and Economic Behavior*, vol. 26, no. 1, pp. 1–21, 1999.

[154] M. S. Bazaraa, H. D. Sherali, and C. M. Shetty, *Nonlinear Programming: Theory And Algorithms*. Wiley-Interscience, May 2006.

[155] B. T. Polyak, *Introduction to optimization*. Optimization Software New York, 1987.

[156] Y. Nesterov, *Introductory lectures on convex optimization*. Springer Science & Business Media, 2004.

[157] D. Shah, D. Tse, and J. Tsitsiklis, "Hardness of Low Delay Network Scheduling," *IEEE Trans. Inf. Theory*, vol. 57, no. 12, pp. 7810–7817, Dec 2011.

[158] M. Lotfinezhad and P. Marbach, "Throughput-optimal random access with order-optimal delay," in *IEEE Conf. Computer and Communications (INFOCOM)*, April 2011, pp. 2867–2875.

[159] L. Jiang, M. Leconte, J. Ni, R. Srikant, and J. Walrand, "Fast Mixing of Parallel Glauber Dynamics and Low-Delay CSMA Scheduling," *IEEE Trans. Inf. Theory*, vol. 58, no. 10, pp. 6541–6555, Oct 2012.

List of Publications

Journal papers:

1. Jiangbin Lyu, Yong Huat Chew, Wai-Choong Wong, "A Stackelberg Game Model for Overlay D2D Transmission with Heterogeneous Rate Requirements", submitted to *IEEE Transactions on Vehicular Technology*, accepted with minor revision as a paper.

2. Jiangbin Lyu, Yong Huat Chew, Wai-Choong Wong, "Efficient and Scalable Distributed Autonomous Spatial Aloha Networks via Local Leader Election", submitted to *IEEE Transactions on Vehicular Technology*, accepted with minor revision as a paper.

3. Jiangbin Lyu; Yong Huat Chew; Wai-Choong Wong, "Aloha Games with Spatial Reuse," *IEEE Transactions on Wireless Communications*, vol.12, no.8, pp.3932,3941, August 2013.

Conference papers:

1. Jiangbin Lyu, Yong Huat Chew, Wai-Choong Wong, "Multi-Leader Stackelberg Games in Multi-Channel Spatial Aloha Networks", in 2015 IEEE 81st *Vehicular Technology Conference (VTC2015-Spring)*, May 2015, Glasgow, Scotland.

2. Jiangbin Lyu, Yong Huat Chew, Wai-Choong Wong, "[Poster Presentation] Efficient and Scalable Distributed Autonomous Spatial Aloha Networks via Local Leader Election", **Best Paper Award** in 2014 Singapore-Japan International Workshop on *Smart Wireless Communications (SmartCom 2014)*, Oct 2014, Singapore.

3. Jiangbin Lyu, Yong Huat Chew, Wai-Choong Wong, "An Autonomous Pareto Optimality Achieving Algorithm beyond Aloha Games with Spatial Reuse", in *Personal Indoor and Mobile Radio Communications (PIMRC)*, 2013 IEEE 24th International Symposium on, Sep 2013, London, UK.